POLITECNICO DI MILANO

Department of Civil and Environmental Engineering

Doctoral Programme in Structural, Seismic and Geotechnical Engineering
XXXI Cycle

POLITECNICO
MILANO 1863

PhD Thesis

ON THE ROLE OF MATERIALS PROPERTIES AND STRUCTURAL CONTEXT IN REINFORCED CONCRETE MEMBERS EXPOSED TO NATURAL FIRES

Supervisor:
Prof. PATRICK BAMONTE

PhD Candidate:
NATAŠA KALABA

Tutor:
Prof. ANNA PANDOLFI

Co-ordinator of the Doctoral Programme:
Prof. UMBERTO PEREGO

ACADEMICAL YEAR 2018-2019

On the role of materials properties and structural context in reinforced concrete members exposed to natural fires

PhD thesis by Nataša Kalaba
Supervisor: Prof. Patrick Bamonte

July 2019

Doctoral Programme in Structural, Seismic and Geotechnical Engineering
Department of Civil and Environmental Engineering
Politecnico di Milano

XXXI Cycle - 2015-2019

Faculty:

Prof. Umberto	Perego (Co-ordinator)
Prof. Raffele	Ardito
Prof. Patrick	Bamonte
Prof. Gabriella	Bolzon
Prof. Fabio	Biondini
Prof. Claudia	Comi
Prof. Matteo	Bruggi
Prof. Alberto	Corigliano
Prof. Dario	Coronelli
Prof. Marco	di Prisco
Prof. Piergiorgio	Malerba
Prof. Gabriele	Della Vecchia
Prof. Claudio	Di Prisco
Prof. Roberto	Fedele
Prof. Roberto	Felicetti
Prof. Liberato	Ferrara
Prof. Attilio	Frangi
Prof. Aldo	Ghisi
Prof. Cristina	Jommi
Prof. Maurizio	Lualdi
Prof. Stefano	Mariani
Prof. Luca	Martinelli
Prof. Roberto	Paolucci
Prof. Lorenza	Petrini
Prof. Gianpaolo	Rosati

To my thesis supervisor, prof. Patrick Bamonte - your unique approach, guidance and valuable suggestions were of utmost importance for the development of this thesis. I am very grateful for the teaching of the last five years and above all - for the understanding and support, in all the moments of uncertainty and self-doubt. You were a great mentor and I hope we will continue to collaborate in the future.

To prof. Venkatesh Kodur and Ankit Agrawal - thank you for hosting me during my five-months stay at Michigan State University. It was a very fruitful experience, that encouraged both my professional and personal growth.

To all my PhD colleagues - you enriched my life and I am really overwhelmed by the amount of emotions and wonderful moments that we shared and lived together. To Gianluca, Giovanna, Mariagrazia, Elisa, Maria and Martina - you were my family far from home and I am very proud of the strong bonds that we created. Our friendship and all the memories, I will carry forever with me.

To Francesco - I feel so blessed for having you by my side. It was not always easy, but your patience and support were fundamental in overcoming all the big and small obstacles. I can not wait to see what the future will bring and I hope this harmony we live in now will remain our source of happiness in the years to come.

Finally, to my family - I am forever grateful for everything that you gave to me. For the life, for the freedom to make decisions and choices, for all the support along the way. Thank you for making me feel the most loved daughter and sister, for always believing in me and for being there for me throughout all the good and bad days. Every day I try and will keep trying my best to make you proud. To you I dedicate this thesis.

Milan, July 2019

Nataša Kalaba

Summary

Fire is one of the most severe hazards that a structure can experience during its service life. When dealing with reinforced concrete members, fire can cause significant damage to the structure, but a complete collapse of a building is definitely rare, thanks to concrete incombustibility and favourable thermal properties. Given that the most of the RC structures are able to survive the full heating-cooling phase, investigating the residual behaviour and suffered damage during fire becomes the priority.
Still, the current design practice focuses only on the heating phase, giving very little indication on the behaviour during cooling and in the residual phase. Nowadays, there is a tendency to shift from a traditional approach, based on standard fire, to performance-based design, which requires more accurate representation of the reality (i.e. a realistic fire scenario), in order to reach more effective and cost-effective solutions.
Most of the knowledge on the structural behaviour of RC members in fire comes from standard testing; therefore most of the studies available in the literature are focused on the structural behaviour in the heating phase. Though several authors did research on the residual behaviour, there is no clear common background for performing analyses as regards fires involving heating and cooling.
This thesis deals with the structural analysis of typical reinforced and prestressed concrete beams and columns, on the basis of three different modeling approaches: sectional analysis, finite element analysis via beam elements and finite element analysis via 3D elements. The

aim of this thesis is twofold: (a) to investigate the role of materials properties in the cooling phase on the structural behaviour; (b) to give an overview on the possible modeling strategies, highlighting the particular aspects of the cooling phase. The obtained results showed that increasing the complexity of the numerical model does not necessarily lead to a more accurate prediction of the structural response. The focus should rather be put on the realistic definition of the fire scenario and the materials' mechanical properties in cooling.

Contents

List of Figures

List of Tables

Chapter 1

Introduction

1.1 Background

Fire is one of the most severe conditions that a structure can possibly experience during its service life. High temperatures that can be reached in the structural member affect and alter its characteristics, at every level - from material to structural.
Generally, reinforced concrete (RC) structures behave well at elevated temperatures, thanks to concrete incombustibility and favourable thermal properties. Low thermal diffusivity of concrete delays the penetration of high temperatures towards the inner layers of the section/member. Inherent fire resistance of concrete gives it an edge over some other construction materials (e.g. steel, timber etc.). This favourable behaviour of concrete is determined by the behaviour of its constituents- cement paste and aggregate. As for the behaviour of the hardened cement paste, water content (both evaporable water in gel and capillary pores as well as chemically bound water in cement hydrates) is governing the response. Changes in cement paste are taking place at relatively low temperatures - for instance, if a temperature of 100°C is sustained over some period of time, all the evaporable water will be lost, causing shrinkage of the cement paste, and concrete, as most of the aggregates are fully stable at that temperature. On the

other hand, aggregate behaviour is intrinsically different- most of the aggregates commonly used in RC and PC members are thermally stable at temperatures up to 350°C. Nonetheless, any thermal damage to the aggregates has a pronounced effect on concrete properties, given the fact that aggregates are a major constituent of concrete. Aggregate response to elevated temperature is strongly dependent on the aggregate type, more specifically, on its silica content.
Differently from concrete where the steep thermal gradients develop within the section, the temperature in the steel rebars tends to uniformity, due to the high thermal conductivity of steel. Reinforcing bars retain their yield strength almost completely until around 400°C, while strength and stiffness loss of prestressing steel begins at temperatures as low as 100°C, and at a higher rate. In design for fire resistance of RC and PC members, one of the main requirements is to protect the renforcing bars from reaching severe temperatures and to minimize the decay of mechanical properties. Given that concrete protects the steel bars from reaching high temperatures, it is clear that adequate concrete cover plays an important role, especially in flexural members whose behaviour is governed by the steel. The critical temperature that steel should be prevented from reaching in order to avoid significant loss of strength and stiffness can be found from some experimental studies (e.g. Felicetti et al., 2009, Neves et al., 1996). Critical temperatures for prestressing steel (around 350°C) is lower than for reinforcing steel (around 550°C), due to the higher sensitivity to high temperatures of the former.

1.2 Natural fire in view of current design practice

In the design of structures exposed to fire, there are three stages of fire that should be taken into account. The first stage is the heating phase, when the temperatures in the fire compartment and structural member are monotonically increasing. This stage is followed by the

cooling phase, where the temperatures in the compartment and in the structural member are decreasing down to ambient. Finally, the third stage is the residual phase, when the structural members are back to ambient temperature.
The current design practice focuses only at the first stage of fire exposure - heating phase, while very little attention is given to the cooling and residual phase. The fire performance of structures exposed to fire is indicated through a Fire Resistance Rating, which is a duration (in minutes) during which a structural member fulfils some specified criteria:the resistance, or for the members that are able to ensure compartmentation- also integrity and insulation. Generally, fire ratings are measured in standard tests, where the member is loaded and then exposed to a prescribed temperature-time curve (e.g. ISO834, ASTM E-119 and other). Therefore, fire resistance of an RC member is usually determined following a prescriptive approach or using simplified methods, such as for example tabulated data, that rely on satisfying requirements on the minimum member dimensions and the minimum concrete cover to the steel. This approach, though generally conservative, does not allow to take into account many important parameters that characterize the thermal and mechanical behaviour of RC members exposed to fire, such as geometrical configuration, load level, restraint conditions, evolution of materials properties with temperature, local behaviour (cracking and tension stiffening), acceptable failure criteria and so on (Kodur and Dwaikat (2007)). In addition, most of the currently available research works, both numerical and experimental, deals with standard fires, so not considering the behaviour of the structural member during or right after cooling phase. It is clear that a fire defined by the monotonic increase in temperature with time implies that the fire fuel is inexhaustible (Elingwood and Lin, 1988), which is surely not a realistic hypothesis. In fact, this unrealistic definition of the fire scenario, without cooling phase, is a significant shortcoming. In addition, as it is the case in seismic design, a holistic approach to the fire safety implies that adequate load bearing capacity of the structural members is guaranteed not only for the

maximum temperature reached within the required time, but also for the full burnout phase. Within this context, in the design phase it may be advantageous from the economic point of view to resort to more realistic - natural (or parametric) fires, which account for the actual geometry of the compartment and on the available fire load (among other significant factors). As a matter of fact, EN 1991-1-2 allows resorting to performance-based design through the use of natural fires, taking as many significant parameters as possible into consideration, so as to eventually yield more accurate representation of the actual behaviour, and thus achieve more effective and cost-effective solutions. Within this framework, it is clear that the structural behaviour of reinforced and prestressed concrete members exposed to natural fires is definitely of interest for the designer.

Modelling the cooling phase certainly brings up many difficulties, but it also allows to cover a wider range of situations of practical interest, in comparison to standard fires. It allows to investigate the possibility of the failure in the cooling phase (so-called "delayed" failure) (Gernay, 2019), like the one that took place in Switzerland in 2004, when the Gretzenbach underground parking collapsed, leading to the death of seven firefighters. Thus, the question of delayed failure is of utmost importance when talking about safety of firefighter brigades and people involved in the first inspection after fire. Delayed temperature increase in concrete even after the maximum gas temperature is reached and the damage in the material that takes place during cooling are two peculiar factors governing the problem. With increase in temperature, the decay of the mechanical properties becomes more pronounced. Therefore, the load bearing capacity of the member decreases as long as the temperature is increasing, typically even after the maximum gas temperature is reached and the cooling phase has started. Minimum load capacity corresponds to the maximum reached temperature; this is then followed by a total or partial recovery of the material strength and stiffness, and thus of a bearing capacity (Gernay and Franssen, 2015).

Besides the delayed failure, the realistic fire scenario opens up the

possibility to study the residual behaviour, for the structures that survive the full heating-cooling cycle. Given the thermal properties of concrete and more specifically its high insulating power, failure is generally not the main concern, except for thin and sizably loaded sections, or whenever second order effects play a significant role. Still, RC structures can suffer a sizable damage, and extent of the suffered damage will depend on the severity of the fire scenario. This is very significant in view of the structural post-fire assessment, since it can help answering a crucial question: is a structure that survived a fire safe or not? Should it be repaired or demolition is inevitable? Indications on the residual behaviour could be obtained by looking at the residual deformations/deflections, as general indicators of the damage in the member; this information is also a fundamental prerequisite to perform meaningful numerical simulations to evaluate the residual bearing capacity and thus choose between demolition and repair.

The switch from prescriptive to performance-based fire safety design requires tools for the accurate fire resistance analysis of reinforced concrete members (or structural systems), something that paved the way for the development of numerical simulation tools with the desired capability (Gao et al., 2013). Generally, a three-steps analysis consisting of (a) fire scenario analysis, followed by (b) heat transfer analysis, to obtain the temperature at each time instant in the section/member, and (c) eventually a mechanical analysis, to work out stresses and strains or displacements is performed.

To date, no simplified methods are available for assessing the fire resistance of reinforced concrete members exposed to natural fires. EN 1992-1-2 (European Committee for Standardization, 2005b) indicates the possibility of using the 500°C isotherm method, but only if the thermal profiles inside the member are similar to those caused by the standard fire: this is certainly not the case in the cooling phase, when the superficial layers undergo cooling while the inner layers are still hot. As a matter of fact, the numerical studies carried out so far on concrete members all took advantage of advanced calculation me-

thods, and mainly by using commercial softwares or performing demanding 3D thermo-mechanical analyses (Gernay and Dimia, 2012, Kodur and Agrawal, 2016). This leads to the conclusion that simple approaches are thus needed, in order for practitioners to take advantage of the possibilities offered by the use of natural fires, without the need of computationally-demanding analyses, even in the case of members with simple structural layout, that form the basis for current code provisions.

1.3 Motivation for the research

As already pointed out, most of the studies available in the literature are focused on the structural behaviour in the heating phase only basically because the tests used for validation or comparison are carried out under standard fires. Though this approach proved to be very useful for practical applications over the last decades, paving the way for the widespread use of advanced calculation methods, its main disadvantage/limitation lies in the fact that it does not give any indication on the effects that cooling has structural response (Gernay, 2019). Nevertheless, in view of the aforementioned need to resort to more advanced, sophisticated and above all more realistic analyses, there were several researchers dealing with heating and cooling (i.e. natural fires) in the last years. It is difficult to say whether there were more experimental or numerical researches. Nevertheless, the cross-examination of the literature points to the fact that several authors did research on the topic, although with different approaches, different assumptions concerning the materials and still, no clear common background for performing analyses as regards heating and cooling, as in the case of natural/parametric fires.
Moreover, even in the Standards there are slightly contradictory provisions, as for example in the current versions of EN 1992-1-2 (European Committee for Standardization, 2005b and EN 1994-1-2 (European Committee for Standardization, 2005a). There are different in-

dications concerning the strength of concrete in the cooling phase. In more detail, EN 1992-1-2 in Section 3.2.2.1 states *"Possible strength gain of concrete in the cooling phase should not be taken into account."*. This sentence could be interpreted in different ways, but in any case it does not give clear indications on what to do in the cooling phase. On the contrary, in EN 1994-1-2 Section it is stated: *"As concrete, which has cooled down after having been heated, does not recover its initial compressive strength, the proposal of informative Annex C may be used in an advanced calculation model"* giving a clear equation for evaluating the compressive strength in the cooling phase, as a function of maximum temperature and the temperature in the cooling branch. Moreover, EN 1992-1-2 states that for thermal actions in accordance with EN 1991-1-2 Section 3 (i.e. when dealing with parametric fires), particularly when considering the descending temperature branch, the mathematical model for stress-strain relationships of concrete provided should be modified, without however giving more precise indications.
To give an overview on the possible strategies concerning the computational aspects of heating and cooling and also to investigate the role of materials properties in the cooling phase in view of the structural performance, this thesis deals with the structural analysis of typical reinforced and prestressed concrete beams and columns, on the basis of three different modelling approaches: sectional analysis, finite element analysis via beam elements and finite element analysis via three-dimensional elements.

1.4 Thesis Outline

The work presented in this thesis is organized into six Chapters.

Starting with the introductory **Chapter 1**, the aim was to give the background for what motivated this research. The critical limitation(s) of the current design guidelines are highlighted. The main shortcoming lies in the fact that cooling phase is neglected in most

of the experimental and numerical researches, in line with the traditional approach to fire safety, which still forms the basis for the design. Tendency to move to a more realistic, performance based design, in order to achieve more cost-effective solutions is present and calls for a more accurate definition of the fire scenario. Including the cooling phase allows studying the structural behaviour and checking the safety of the structure until complete burnout. Such an advanced calculation certainly brings up many questions, some of which are still open, given that the clear approach for the structural analysis of members exposed to natural fires is not yet clearly defined.

In **Chapter 2**, a comprehensive review of the literature is given. First part of the Chapter deals with materials properties - thermal and mechanical - of concrete and steel. Some of the most significant findings from high temperature tests at the material level are recalled. Besides the properties in ”hot” conditions, the residual properties are reviewed, as they are fundamental to understand the material behaviour during cooling and the extent of the suffered damage - the latter having great implication on the overall structural response. Second part of the chapter deals with the structural behaviour, and some of the most important experimental and numerical studies performed so far are dealt with. Most of the experimental studies available in the literature deal with standard testing, and in this thesis only few of those were mentioned, given that the objective was to study the residual behaviour and to focus on the tests/numerical studies that include the cooling phase. The tests were divided on the basis of the structural member investigated (i.e. reinforced and prestressed concrete beams and reinforced concrete columns) and the type of study (experimental or numerical study). The available data from the reviewed experiments were used as a reliable database for validating the numerical models developed and presented in the chapters that follow.
In this thesis, the structural behaviour of members exposed to natural fire was studied using three modelling approaches, characterized by increasing accuracy but also computational effort: from the simple (but fundamental) sectional analysis of statically determined mem-

bers to the 1D "frame-based" approach using beam finite elements and finally, finite element analysis with 3D elements. **Chapter 3** is dedicated to sectional analysis, which is the simplest method and lays the fundaments for more general and more complex structural analysis methods. Structural analysis based on the most stressed section of the member has a great practical significance, given that it serves as a basis for code prescriptions and provisions given to the designer and also for the simplified calculation method, used in everyday practice. Despite being the simplest method available, it can still cover a wide range of important structural elements. The principles of sectional analysis in fire conditions will be addressed, after what the general procedure for performing the sequentially coupled thermo-mechanical analysis through a purposely developed *VisualBasic* code will be given. After validating the code against well-documented tests taken from the literature, two typical prestressed concrete beam sections, as well as several reinforced concrete beams tested in heating and cooling, are analysed. The influence of several parameters on the global behaviour was studied, and also the role played by some modelling assumptions concerning the materials behaviour has been investigated. In order to tackle also the analysis of columns, with the decisive role played by second order effects, the method based on nominal curvature (Annex B3 method in EN 1992-1-2), where the structural behaviour of the member as a whole comes down to just one (the most stressed) section, was used to simulate a number of tests on columns featuring heating and cooling phase. When it comes to studying simple structural members, sectional analysis has many advantages in comparison to more complex methods. Its simplified assumptions, however, put some limitations on its field of application. Some of these limitations can be overcome by resorting to more complex methods. **Chapter 4** is dedicated nonlinear structural analysis based on RC beam finite elements. The code used for the sectional analysis was suitably integrated within an updated numerical tool (also developed in Visual Basic), based on the classic theoretical framework of finite element analysis with linear Euler-Bernoulli

finite elements. This new code offers a more general, yet not too complex, approach. Some intrinsic limitations of the sectional analysis can be overcome and the members that cannot be analysed with sectional analysis, or at least not accurately enough, were analysed. Both material and geometrical nonlinearity are taken into account, the latter aspect being particularly significant, as it was proven that second-order effects can be treated with the sectional analysis only in a simplified, and very conservative, manner. The columns available from several standard and residual tests were simulated, and the model has been successfully validated.
When more complex structural members (such as ceilings, walls and tunnel linings) are considered, 2D or 3D finite elements analyses must be carried out, thus requiring the definition of concrete behaviour for multiaxial states of stresses. Moreover, 3D finite element based models are a very efficient tool to analyse structural members when local behaviour is of concern - for instance, localized heating, bond modelling, localized spalling, just to name a few. Nowadays, the availability of numerous commercial softwares lead to many researchers using complex 3D models, even when dealing with simple structural members that could be more effectively studied with more simple methods. Therefore, 3D models definitely deserve attention, and particularly when it comes to accurate definition of the material properties and the damage that takes place during cooling - a feature that is, in general, not embedded in the finite element software by default but can be resolved, for example, through the use of user subroutines. 3D Finite element analysis procedure in ABAQUS software was the topic of **Chapter 5**. Special attention was put on the stress-strain law and material properties definition in cooling, on the basis of the available literature and also of the findings of the previous chapters. Several reinforced concrete beams were modelled, as well as columns recently tested at University of Edinburgh (MacLean, 2018). Finally, the results from the simulations using the three mentioned methods (sectional, beam element and 3D element analysis) on several beams and columns will be confronted and discussed.

The last Chapter of this thesis, **Chapter 6**, provides a summary of the findings of this thesis and outlines the key conclusions. In addition, some recommendations for possible further developments and improvements are given.

Chapter 2

Literature Review

The inherent heterogeneity of concrete makes it a very complex material, with a strongly nonlinear behaviour. Different constituents (i.e. aggregate and cement paste) have different thermal and mechanical properties and respond to elevated temperature in a different way. Complex interactions at the aggregate-cement paste interface affect the behaviour of the whole mix. Moreover, temperature-dependent thermal and mechanical properties, transient creep strain, spalling and tensile cracking affect concrete behaviour and load-bearing capacity of reinforced concrete members both during exposure to high temperatures as well as in residual and post-fire conditions. This chapter deals with two main topics. First, an overview of material properties of concrete and steel will be given. Some words will be dedicated on the thermal and mechanical properties of concrete and steel at elevated temperatures and in residual conditions. The latter is particularly important - as this work is dealing with reinforced concrete structures exposed to natural fires. The definition of the material behaviour during cooling phase is crucial, as it is well-known that the residual properties are different from the so-called ”hot” properties. Following, the most significant experimental and numerical studies on the structural behaviour of prestressed and reinforced concrete structures exposed in residual conditions will be reviewed. Most

of the reviewed experimental studies served as a solid database for the validation of the numerical models developed in this work. The available studies are reviewed and grouped according to the structural member typology: prestressed concrete members, reinforced concrete beams and columns, as those three member types were studied in this work. Several of the quite a few available experimental findings coming from standard fire tests were cited - though they do not contain cooling phase, they still provided a solid base for validation of the models' abilities to, for example, predict the failure time under continuous heating or to account for the second order effects etc.

2.1 Material properties of concrete at elevated temperatures

Properties of concrete that affect its response at elevated temperatures are thermal, mechanical and deformation properties.

2.1.1 Thermal properties

Thermal properties of concrete are the conductivity and specific heat. They are nonlinear, temperature dependent and they govern the thermal field inside the concrete member. Measuring thermal properties in experimental conditions gives rise to a lot of difficulties, related to the presence of moisture in the concrete, non-homogeneity and to the experimental set-up itself - separating the thermal from other effects (change of physical composition, storage of the latent heat during phase changes, the porosity etc.) can be difficult (Harmathy, 1968, Harmathy and Allen, 1973). Eurocode (2004) (European Committee for Standardization, 2005b) and ASCE Committee on Fire Protection (1992)) propose a model for concrete thermal properties, and these two models are most commonly used in engineering applications.

Thermal conductivity

Thermal conductivity is the ability of the material to transfer heat. It directly influences the temperature rise inside the element. It is measured in W/mK and can be measured by means of steady-state or transient tests. Thermal conductivity of concrete is found to greatly vary depending on the type and amount of aggregate in the concrete mix (ASCE Committee on Fire Protection, 1992, RILEM, 1985). This consideration is taken into account in ASCE proposal, while it is not in the model proposed by Eurocode 2. In general, thermal conductivity decreases with the increase in temperature. Some researchers suggest that the thermal conductivity of concrete is not reversible during cooling and as such were considered in the respective numerical studies (Wu et al., 2010, Gernay and Dimia, 2012). For thermal conductivity in the cooling phase, few data are available. Yet, as a major factor in concrete conductivity is the moisture content and given that there is no re-condensation of the water during cooling, it is reasonable to assume that the thermal conductivity is not reversible either.

Specific heat and Density

Specific heat is defined as the amount of heat per unit mass required to change the temperature of the unit mass by one degree. In SI units it is measured in J/kgK. At constant pressure, the specific heat, indicated with c_p can be evaluated by means of the following expression given in Harmathy and Allen (1973):

$$c_p = \frac{\partial H}{\partial T}_p \tag{2.1}$$

where H is the enthalpy, T is the temperature and p is the pressure. At ambient temperature, the values of specific heat are in the range between 500 and 900 J/kgK. The product of specific heat and density is called heat capacity. According to Eurocode 2, specific heat of

concrete varies in a broad range, depending mostly on the moisture content. The specific heat nonlinearly increases with temperature, with a peak between 100°C and 200°C, to implicitly account for water evaporation during heating.
Density is primarily influenced by water loss, and decreases only slightly with temperature. On the other hand, due to different processes occurring in siliceous and calcareous (or carbonate) concrete: up to 600°C siliceous concrete exhibits a steeper decay of density in comparison carbonate concrete, but above 600°C and up to 800°C, density rapidly decreases in carbonate concrete, due to the calcination which results in a significant increase of the porosity RILEM, 1985. Given that this density variation is mostly due to moisture losses during heating, it is irreversible during cooling (Schneider, 1988).

2.1.2 Mechanical properties

Mechanical properties that govern the constitutive behaviour of concrete at elevated temperatures are compressive and tensile strength, as well as elastic modulus. Measurement of the material's mechanical properties is closely related to the specific test method employed. The three parameters governing the test modality are heating, application of the load and control of strain (RILEM, 1985). Two types of tests can be performed, namely steady-state and transient tests. In Steady-State tests, concrete is subjected to heating until a pre-defined temperature is reached and then loaded, while the temperature is kept constant (RILEM, 2000). By applying a monotonically increasing load (or displacement) until and beyond the material strength is reached, the stress-strain curve (having both ascending and descending branch) for the corresponding temperature can be obtained. This type of test is useful for determining the aforementioned mechanical properties at high temperature. On the other hand, in transient tests the specimen is first loaded and then uniformly heated at constant load (RILEM, 1998). The results obtained are often expressed in terms of strain developed during heating as a function of temperature,

for different load levels. In comparison to steady-state tests, transient tests are somewhat more complicated to perform, though they better represent the actual conditions of structural members, where the exposure to fire follows the application of the external loads.

Compressive strength

The main factors influencing concrete strength in compression at ambient temperature are:

- cement type and aggregate type and size
- cement-aggregate interface
- curing conditions
- mix design
- stress level during heating

As summarized in (RILEM, 1985), some conclusions regarding the compressive strength at elevated temperatures can be drawn. While factors such as concrete strength in virgin conditions, water/cement ratio, cement type, maximum aggregate size, heating rate (as long as temperature gradients are limited) have little or no effect on strength-temperature characteristics, factors such as aggregate/cement ratio and especially aggregate type have significant effects on strength-temperature characteristics. Knowing that most aggregates are thermally stable up to 350°C, it is clear that the interaction between cement paste and aggregate plays a major role. Aggregate and cement paste behave in an opposite way upon heating: cement paste shrinks due to water evaporation while aggregate expands. This may cause cracking on their interface, which can lead to significant decay of the compressive strength. Sustained stress during heating certainly has an influence on the shape of the strength-temperature relationship. Compressive strength of stressed specimens shows a less pronounced decay with temperature than that of unstressed specimens.

A very important factor that influences the compressive strength of concrete at elevated temperatures is the level of pre-loading. The larger the preload, the smaller the influence of temperature on the compressive strength and elastic modulus, as pre-loaded specimens are confined during heating and internal cracking is prevented (or at least limited). (Abrams, 1971; Khoury et al., 1985). Results from the tests on compressive strength, for varying aggregate type, performed by Abrams (1971) are reported in ASCE Committee on Fire Protection (1992). Influence of load was investigated: specimens heated to the reference temperatures with no superimposed load are denoted as "unstressed", specimens heated while stressed to 40% of their 28-day compressive strength and then tested are "stressed to 0.4f'c" and finally, "unstressed residual" stands for specimens heated to the reference temperature, cooled down, stored at 75% of relative humidity for 6 days and then tested in compression. Results are plotted as a function of temperature in Figure 2.1. As it can be observed from the plots, stressed specimens perform better in terms of degradation of strength - it is evident that up to 600°C for carbonate aggregate and 400°C for siliceous aggregate, compressive strength remained unaffected. Unstressed specimens exhibited a more pronounced decay, which started at low temperatures. Carbonate aggregate concrete performed better than siliceous on the whole, especially at higher temperatures. Residual testing on unstressed specimen revealed that concrete does not recover its initial strength upon cooling, moreover, degradation continues even during cooling, leading to values of the residual strength lower than those of the hot strength.

Tensile strength

Being a quasi-brittle material, concrete is characterized by low values of the tensile strength, something that facilitates crack development and propagation. At elevated temperature, concrete is prone to loss of its tensile strength. Reduction coefficients are proposed in EC2 (European Committee for Standardization, 2005b). Concrete retains

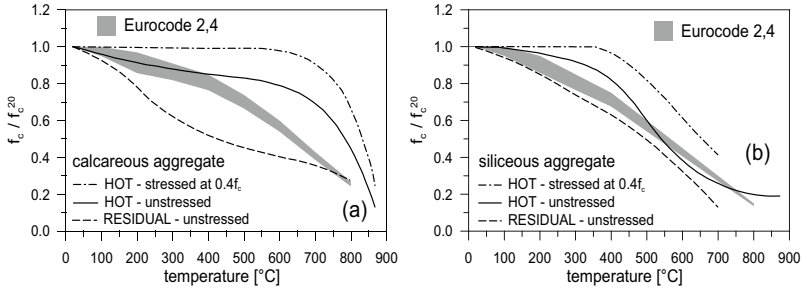

(a) (b)

FIGURE 2.1: Provisions by ASCE-ACI (based on the tests by Abrams (1971)) and EC2-EC4 for concrete with (a) calcareous aggregates; (b) siliceous aggregate (dark gray area refers to the provisions by EC2 and EC4), adapted from Bamonte and Gambarova (2015).

its tensile strength at temperatures T¡= 100°C; at higher temperatures decay is assumed linear and at temperatures of 600°C, concrete eventually loses its tensile strength. The prescriptions provided in EN 1992-1-2 testify that there is a strong decay of tensile strength with temperature. It is worth noting, however, that these prescriptions may be over-conservative and meant for design purposes, as experimental evidence points that tensile strength of concrete is not lost completely at 600°C (Bamonte and Felicetti, 2012).

In most of the applications concerning bending and normal force, a common assumption is to neglect tensile strength, therefore the particular law that is assumed for tensile strength does not play a big role. It is only there relevant where, for example, finite elements analyses are performed and certain toughness has to be provided to the material in tension, in order to make the material more strain-tolerant from the computation point of view. This is a common feature of several commercial softwares.

Elastic modulus

At ambient temperature, elastic modulus is affected by the same factors that affect compressive strength, such as the aggregate type (the stiffer the aggregate, the higher the modulus of elasticity), cement type, water/cement ratio (high w/c ratio reduces Young modulus), age of concrete and stress conditions. At elevated temperatures, aggregate type and sustained stress during heating (RILEM, 1985), together with the maximum temperature experienced, have the most significant effects on the elastic modulus. As summarized in (Naus, 2005), results from the experiments performed by researchers from PR of China showed that the elastic modulus decreases monotonically with temperature. The residual elastic modulus was lower than the elastic modulus at high temperature and the decay proved to be more related to the maximum temperature experienced during heating than to the heating-cooling cycle. Moreover, the factors that proved to sizably affect elastic modulus at elevated temperature are: aggregate type/content (quartzitic aggregate brings in the worst performance compared to other aggregate types; carbonate performs better than siliceous up to 500-550°C whereas lightweight aggregate suffers the least decay in elastic modulus) and presence of sustained stress during heating (lower decreases in modulus are observed in the presence of a pre-load). When high temperatures and fire are at issue, concept of the elastic modulus becomes less meaningful, given that the linear-elastic phase is practically non-existent and that the tests to measure modulus of elasticity in ”hot” conditions are almost never carried out in the way they are carried out at 20°C (i.e. cycles of loading-unloading, to stabilize the response, under increasing levels of maximum stress). Rather than elastic modulus, the attention could be paid at concrete deformability, which is a concept that surely is more meaningful when high temperature and fire are at issue. Next section will therefore be dedicated to the concrete deformability at elevated temperatures.

Stress-strain response

The stress-strain response of concrete at elevated temperatures is highly nonlinear. Several researchers (Anderberg and Thelandersson, 1976, Lie and Lin, Kodur et al., Terro, Chang et al., Scheinder etc.) have proposed different stress-strain models. A widely used stress-strain model for concrete at elevated temperatures is the one available in EC2. The stress-strain law is described by three variables: compressive strength $f_{c,\theta}$, peak strain $\varepsilon_{c_1,\theta}$ and ultimate strain $\varepsilon_{cu_1,\theta}$, all of which are temperature dependent, through the coefficients proposed in EN1992-1-2. Temperature is, therefore, the main factor governing the shape of the stress-strain curve; for each temperature, a unique curve can be defined. Compressive strength is deteriorating while peak strain and ultimate strain are mainly increasing with temperature. This leads the initial slope of the curve to decrease with temperature and the concrete becomes more strain-tolerant.
Besides temperature, aggregate type plays a major role in defining the shape of the stress-strain curve, given that EC2 defines all the mechanical properties at elevated temperature as dependent on aggregate type. Concretes made with hard aggregates (siliceous, basaltic) generally have a steeper decrease of the initial slope than softer aggregates concretes (e.g. limestone). Factors such as virgin concrete strength, water/cement ratio and type of cement proved to have little or no influence on the stress-strain response at elevated temperatures (RILEM, 1985). Ultimate and peak strains are temperature dependent but not aggregate dependent, hence the aggregate type used in the concrete mix has little or no impact on the deformability.

2.1.3 Deformation properties

Four strain components are traditionally used to describe concrete response in compression at elevated temperatures: mechanical, thermal, creep and transient strain. It is a very difficult task to define each of these strain components in an accurate and unique way, due

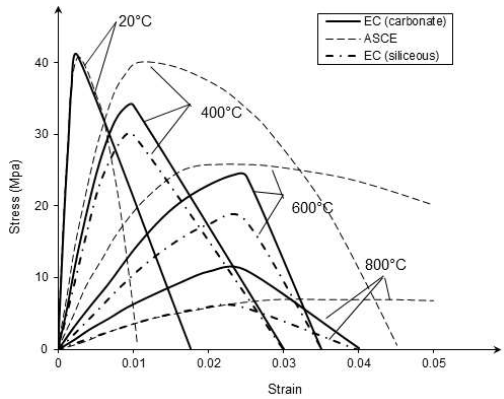

FIGURE 2.2: Stress-strain curves for concrete at high temperatures (adapted from EN 1992-1-2 and ASCE Committee on Fire Protection (1992)).

to all the complex interactions and interdependencies between them, especially in fire conditions. Moreover, performing tests that allow to isolate each strain components from the others is rather demanding from the practical point of view. As summarized in (Anderberg and Thelandersson, 1973), several parameters affect the magnitude of the different strain components:

- concrete mix proportions and physical nature of its constituents
- age and curing conditions of concrete prior to heating and loading
- moisture loss from the specimen during the test
- heating procedure (e.g. temperature level, temperature history, rate and duration of heating, presence of temperature gradients inside the specimen)

- external loading (magnitude and duration of loading, stress history in relation to temperature history)

Thermal strain

Thermal strain represents an expansion of the material in the absence of external loads/stresses and is defined as the expansion of a unit length of material when the temperature is raised by one degree. Temperature variation with the ensuing dilations can produce significant stresses in structural members, especially if in the presence of restraints (Naus, 2005). Thermal expansion is a very complex phenomenon due to concrete heterogeneity- its main constituents have fundamentally different behaviour when heated. Aggregates and cement paste are characterized by different coefficients of thermal expansion- aggregates tend to expand upon heating while cement paste shrinks, at temperatures above 100°C, due to moisture loss. Given the thermal incompatibility between the aforementioned two main constituents of concrete, it is clear that cement/aggregate ratio affects the thermal strain of concrete. However, aggregate is the major constituent of concrete, therefore the resultant coefficient of thermal expansion is more influenced by the aggregate rather than by the cement paste. Influence of the aggregate type on the thermal expansion can be seen in (Figure 2.4). Anderberg and Thelandersson (1973) suggested that there is a sizable influence of the load level during heating on the coefficient of thermal expansion (Figure 2.3). If the specimen is loaded during heating, thermal expansion will be reduced and internal damage will be prevented. On the other hand, heating an unloaded specimen will result in greater expansion, which can then cause the cracking and sizable damage. Naturally, this has significant influence on the stress-strain response. EN1992-1-2 proposes a set of expressions to evaluate thermal elongation, with siliceous concretes having larger thermal expansion than carbonate concretes. Thermal strain is monotonically increasing with temperature, up to 700°C for siliceous and 805°C for carbonate aggregate, after that the values are

set as constant.

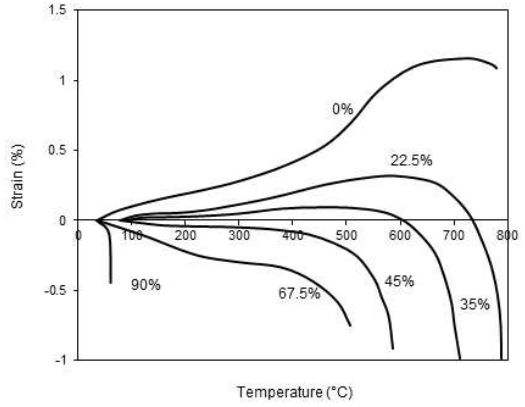

FIGURE 2.3: Thermal expansion as a function of load level (adapted from ASCE 1992, according to experimental results from Anderberg and Thelandersson (1973)).

Transient creep strain

In concrete subjected to high temperatures, a particular phenomenon appears, the so-called transient creep. Transient creep is a difference in strain between concrete that is heated under load and concrete that is loaded at elevated temperature (Anderberg and Thelandersson, 1976). Transient creep strain develops during first time heating of the concrete specimen under compressive load, and it is irrecoverable upon cooling. If the material is re-heated under sustained load, no significant transient creep will develop for temperature levels lower than the maximum experienced temperature during first heating (Mindeguia et al., 2013, Khoury et al., 1986, Colina and Sercombe, 2004, Hassen and Colina, 2006).

An extensive literature (and critical) review on the experimentally demonstrated characteristics of transient creep strain, main factors that

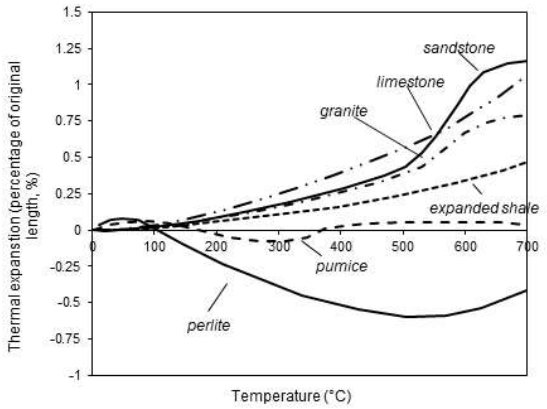

FIGURE 2.4: Thermal expansion for different aggregate type (adapted from ASCE 1992, according to experimental results from Pettersson and Saito (1965)).

have an influence on it, as well as available constitutive models for explicit consideration of transient creep is given by Torelli et al. (2016). In short, this complex phenomenon is considered to be essentially caused by the thermal incompatibility of aggregate and cement paste that causes chemical and physical reactions in the cement paste, due to their different dimensional variations. Main factors that influence transient creep are temperature, compressive strength of concrete, moisture content, loading and mix proportions.

Among the available constitutive models for concrete, the term for transient creep is considered either in implicit or explicit manner. The widely used EN 1992-1-2 constitutive law is based on standard fire curve and considers the transient creep only implicitly, lumping this strain component together with the instantaneous stress-related strain. The stress then becomes a function of mechanical strain, which is simply obtained by subtracting the thermal strain from the total strain. The main drawback of implicit models is that they cannot capture

the difference between steady-state and transient heating regimes: as a consequence, they are suitable only for loaded-then-heated conditions, but even here they present problems when it comes to mechanical unloading of the material, as they treat transient strain in the same way as the other strain components.

$$\varepsilon_{tot} = \varepsilon_m + \varepsilon_{th} \tag{2.2}$$

On the other hand, in the explicit models, the mechanical strain is the sum of instantaneous stress-related strain and transient creep strain; therefore, the term for transient creep is integrated explicitly and the stress is directly related to the instantaneous stress-related strain only. Explicit models aim to overcome what are considered to be the major issues of implicit models. The first issue of implicit models, as already pointed out, is that the mechanical strain is the same, whether the concrete is being loaded and then heated under constant stress (transient conditions) or heated and then loaded at constant temperature (steady-state conditions). In such a situation of (approximately) constant stress and increasing temperature, implicit and explicit models lead to the same results, i.e. the same values of the mechanical strain. On the other hand, in a situation that corresponds to steady-state tests, no transient creep develops, as there is no increase in temperature. Nevertheless, this behaviour is not properly described by implicit models, where the transient creep is implicitly included, leading to significant underestimation of the stiffness. Second issue of implicit models is the unloading stiffness. The transient creep decreases when the structural member undergoes unloading, which is fundamentally wrong. Explicit models allow for the increase in the transient creep, whether the stress is increasing or decreasing, as long as the temperature is increasing and the stress in the material remains compressive.

$$\varepsilon_{tot} = \varepsilon_\sigma + \varepsilon_{tr} + \varepsilon_{th} \tag{2.3}$$

Several uniaxial explicit models are available, such as the model

by Anderberg and Thelandersson (1976), Nielsen et al. (2002), Terro (1998), Schneider et al. (2008), to name a few. However, neither one of these models established itself as a far superior compared to the others. Generally, in most of these models transient creep strain is a linear function of the applied stress and increases with the temperature but in a nonlinear fashion. Lack of experimental data is evident, partly because it is difficult to directly quantify transient strain. Therefore, in most of the models proposed by Schneider et al. (2008), Anderberg and Thelandersson (1976), Gernay and Franssen (2012), transient strain is lumped together with creep strain- transient creep strain and is explicitly included in the stress-strain model. Recently, an explicit constitutive model (ETC model) was developed by Gernay and Franssen (2012). In fact, this is a modified Eurocode implicit model, in such a way that the transient creep strain is explicitly computed and the stress-strain constitutive relationship is expressed as a function of instantaneous stress-related strain only. The advantage of such model is the fact that it accounts for all the possible load-temperature combinations, hence accounting for the behaviour also in the cooling phase of a fire, where unloading may take place. Having the same generic form as the EC2 model, the formulation of ETC model is rather simple. In the following Chapter, this explicit model will be used in the calculations. Gernay and Franssen (2012) developed the new formulation, calibrated to yield the same results as Eurocode model in the case of transient tests

$$\begin{aligned}\varepsilon_{tr}(T,\sigma) &= \frac{\sigma}{E_{EC2}} - \frac{\sigma}{E_{ENV}} = \\ &= \frac{2}{3}\frac{(\varepsilon_{c1,EC2} - \varepsilon_{c1,min})}{\frac{f_c}{f_{ck}}}\frac{\sigma}{f_{ck}} = \phi(T)\frac{\sigma}{f_{ck}}\end{aligned} \tag{2.4}$$

where the function $\phi(T)$ is a nonlinear function of temperature, irreversible during cooling, and f_{ck} is the concrete compressive strength at ambient temperature.
The mathematical expression to model the instantaneous stress-strain

relationship is approximated by a direct relationship $\sigma = f(\varepsilon_{\sigma}^{explicit})$

$$\frac{\sigma}{f_c(T)} = \frac{n\varepsilon_{\sigma}^{explicit}}{\varepsilon_{c1,ETC}(T)[(n-1) + (\frac{\varepsilon_{\sigma}^{explicit}}{\varepsilon_{c1,ETC}(T)})^n]} \tag{2.5}$$

$$\varepsilon_{\sigma,i+1}^{explicit} = \varepsilon_{m,i+1}^{implicit} - \phi(T_{i+1})\frac{\sigma_{i+1}}{f_{ck}} \tag{2.6}$$

where $\varepsilon_{c1,ETC}(T)$ is the peak strain for the ETC relationship and $n = 2$ is the parameter used for all the temperatures.
Transient creep strain is computed at the beginning of the time step as a function of the stress at the previous time step. This was done to avoid any iterative process for the transient creep strain calculation and any additional complexity. Written in incremental form:

$$\Delta\varepsilon_{tr} = [\phi(T)^{(s)} - \phi(T)^{(s-1)}]\frac{\sigma^{(s-1)}}{f_{ck}} \tag{2.7}$$

$$\Delta\varepsilon_{tr}^{(s)} = \Delta\varepsilon_{tr}^{(s-1)} + \Delta\varepsilon_{tr} \tag{2.8}$$

Transient strain can only increase. The increment of transient strain is equal to zero if the temperature between the time step $s-1$ and s has decreased or remained constant or if the material is in the descending branch of the stress strain curve. Moreover, the transient creep strain is the same for loading and unloading, under the condition that the stress is in compression. In tension, transient creep is equal to zero. At elevated temperature, the transient strain is much larger than the instantaneous stress-related strain, and as such, can have a large influence on the deformation of reinforced concrete members in fire and particularly columns that have large compressive area and thus significant normal stresses. Results from various studies (e.g. Huang and Burgess, 2012, Gernay and Dimia, 2012, Wu et al., 2010) suggest that transient strain in the constitutive relationship generally causes increase in the deflections and has a significant influence on the fire behaviour of columns, and especially if the cooling phase is taken into account. By contrast, the research on the influence that

the explicit consideration of transient creep has on the fire behaviour of beams is still limited. Lu et al. (2015) performed a set of simulations on RC beams in fire, where they compared the most widely used EN1992-1-2 implicit model against some of the available explicit models. They studied parameters such as heating curve, reinforcement and cross section size. The results from the parametric study showed that the EN 1992-1-2 model gives slightly conservative displacement prediction. The difference between the deflections of simply supported RC beams calculated with implicit and explicit model increases with heating time and then decrease to be negligible after cooling. Cross section size proved to have no considerable effect, while increasing the quantity of reinforcing steel reduces the influence of the transient creep on fire behaviour of RC beams. Finally, it was concluded that the influence that transient creep has on midspan deflection of fire exposed RC simply supported beams is minor and can be neglected.

2.1.4 Residual properties

Residual properties are the ones evaluated after the member went through the full heating-cooling cycle. Experience from tests shows that residual properties can be sizably different than those measured in the ”hot” state. During cooling, thermal gradients induce thermal stresses which can cause severe cracks after first heating, accompanied by a crack development and breakage of the bond between aggregate and cement paste (Bingol and Gul, 2009). Decrease of the temperature inside the member does not really start as soon as gas temperature starts to decrease. Due to the thermal inertia of concrete, increase in the temperature can continue for three or four hours after the onset of cooling (Abramowicz and Kowalski, 2007). Superficial layers of the member will start cooling sooner than the inner layers, which may be exposed to increasing temperatures for a significant duration during cooling stage, depending on section geometry. Rate of cooling also plays a role. Cooling in air is slow and grad-

ual; therefore, sharp thermal gradients are usually avoided. Still, the problem of continued increase in temperature in the inner zones of the section arises, which prolongs the development of thermal damage. On the other hand, cooling in water is rapid and steep thermal gradients develop in the section. This is causing the so called *thermal shock*, where cracking is accelerated and thermal damage is inevitable. For the aforementioned reasons, it is clear that substantial loss of load-bearing capacity of reinforced and prestressed concrete members takes place during cooling, when the failure of the structure/member may happen as well. Deeper investigation on this topic can be of practical significance. Moreover, knowledge on the residual and post-fire properties of concrete/steel can help the engineers to decide whether the structure can be repaired after being exposed to fire or demolition is inevitable.
A number of experiments have been carried out to measure residual properties of both concrete and steel. However, residual properties are influenced by a few factors which have to be kept in mind when analysing different experimental results.
Main parameters influencing residual properties of concrete are aggregate type, heat treatment (heating and cooling conditions), mix proportions and age of concrete (RILEM, 1985). Before relating to the original experimental source, however, it is necessary to recognize the influence of factors such as the test conditions (especially the cooling conditions), recovery conditions and rest time at high temperature, as any variation on these factors has a significant effect on the test results (RILEM, 1985). General conclusions can be drawn from all the available experimental results: residual strength is indeed lower than the ”hot” strength, i.e. strength measured at high temperatures. Following a full heating-cooling cycle, concrete compressive strength will not recover to their initial values (European Committee for Standardization, 2005a). As summed up in (RILEM, 1985) and regarding various experiments, following conclusions can be drawn:

- Type of cement does not have significant influence

- Type of aggregate proved to play a major role- carbonate aggregate concretes exhibit the highest reduction in strength
- Age of concrete may play a role at low-medium temperatures (up to 400°C)
- Heat treatment (especially cooling conditions) is of great importance
- Increase in the pre-load level proved to increase residual strength

Residual properties were the object of few more or less recent experimental investigations, most of them focused on the residual compressive strength and few on the Elastic modulus. Different variables and their influence on residual properties were tested: aggregate and cement type, age of concrete and fire scenario (heating and cooling phase duration and cooling regime). Results are, generally, in good agreement with theoretical principles. Even though the test specimens, parameters and test methods greatly varied, some common conclusions can be drawn. Conducted experimental works and the obtained results and conclusions will be briefly described below.
In the experiments conducted by Bamonte et al. (2008), residual properties of concrete with varying aggregate and cement type were investigated. Specimens were heated at a heating rate of 60°C/h, held at maximum temperature for 2h and then cooled down to ambient temperature, at a cooling rate of 30°C/h. In terms of residual compressive strength, concretes with siliceous, carbonate and basalt aggregates performed differently: basalt and carbonate aggregate concretes performed better than the siliceous, as they even exhibited a small increase in residual compressive strength at temperatures between 20 and 350°C, and, more generally, proved to be little affected at temperatures below 400°C. Influence of concrete grade was also examined, and HSC exhibited a more pronounced decay of the residual compressive strength than NSC, for all the three aggregate types. Residual elastic modulus was also inspected. The residual compressive strength as a property is significantly less affected by the tem-

perature than the elastic modulus, which lost around 50-75% of its initial value at temperatures around 400°C. Abramowicz and Kowalski (2007) tested cubic concrete specimens of variable dimensions, to measure their residual strength, heating them up to 800°C and keeping them in the oven chamber until temperature of 500°C was reached at middle point. Afterwards, they were allowed to cool down slowly in air. They observed that the maximum temperature in the middle point was reached long after the heating had stopped, even in smaller specimens (maximum was $40 \times 40 \times 40 cm^3$). Considering that in actual structural members thermal inertia can be much greater, the temperature in the inner zones of the element may increase even several hours after the onset of cooling. Due to continued increase in temperature, the damaged zone of concrete becomes wider and wider. Structural members whose load-bearing capacity primarily depends on concrete compressive strength may suffer a significant reduction of safety even after exposure to fire. Abrams (1971), Klingsch et al. (2009) and Malhotra (1956) tested cylindrical specimens containing siliceous aggregate, by exposing them to slow heating and slow free cooling in air afterwards. In the test performed by Abrams (1971), the difference between "hot" and residual compressive strength is significant in the temperature range from 200 to 500°C. In the whole temperature range residual strength is lower than the "hot" strength. In the tests performed by Malhotra (1956), the difference is significant in the whole temperature range. Klingsch et al. (2009) obtained similar results: values from residual testing proved that the residual strength is lower than the hot strength, and the difference becomes more evident as the maximum temperature reached during the heating phase increases. For instance, for a maximum temperature of 300°C, residual strength after cooling down to ambient temperature was 91% of the hot strength; at 500°C average residual strength was 72% and after cooling down from 700°C it was only 69% of the hot strength.

In their experimental campaign, Chan et al. (1999) adopted a slow cooling and found that the reduction in compressive strength depends

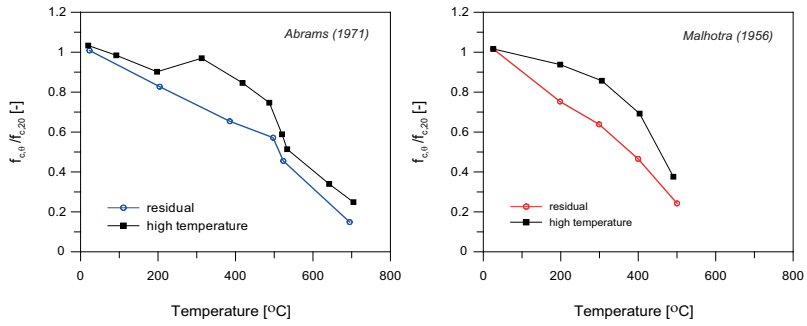

(a) (b)

FIGURE 2.5: Degradation of concrete compressive strength ("hot" and residual conditions) in tests by: (a) Abrams (1971) and (b) Malhotra (1956).

on the maximum experienced temperature. Therefore, the specimens that suffered temperatures as high as 800°C lost a great part of their original strength. Sarshar and Khoury (1993) showed that the loss in strength greatly varies depending on the duration of the exposure to high temperatures, so for the shorter exposure to the low temperatures (up to around 300°C) the strength decreases, while for the longer exposure, the strength can eventually be regained. This is in agreement with the results obtained by Annerel (2010), who concluded that exposure to low temperatures leads to a strength loss of up to 20%, while after exposure to temperatures up to 300°C the strength can be even fully recovered. This is not valid though for higher temperatures (from 300 to 800°C), in which case a significant share of the strength is permanently lost. Compressive stress-strain curves at elevated temperature and after cooling were measured by Fischer in 1970 and the results are reported in (Anderberg and Thelandersson, 1973). Cylindrical concrete specimens were loaded during the heat treatment, then unloaded and stabilized for 3h before the compression test has been conducted. When the specimens were tested in hot con-

ditions, the stress-strain response is unaffected by temperatures up to 450C, which was explained by the fact that specimens were loaded during heating. In the case of unloaded specimens, deformability and strength would be largely affected by high temperatures. However, tests on the cooled specimens showed large influence of the temperature on the residual strength. Residual strength was measured as 10% (on average) lower than hot strength, which is somewhat consistent with the provisions of European Committee for Standardization (2005a). Toric et al. (2014) tested cylindrical specimens made of light-weight concrete. Mechanical properties were determined by heating the specimens up to 200°C, 400°C and 600°C, followed by conditioning at the maximum temperatures for 2.5h and then cooling the specimens down to ambient temperature. Some of the specimens were tested immediately after cooling (residual properties) and the rest were tested 48 and 96h after the initial cooling (post-fire properties), respectively. Results from experiments showed further increase in compressive strength upon cooling. Though the magnitude of strength decrease was dependent on the mix properties, the general trend was the same. Residual values are higher than post-fire values of compressive strength. For instance, after exposing specimens to a temperature of 400°C, residual strength varied in the range of 58 to 74% of initial strength value, while further decrease was observed when tested after 48h- values were in range from 46 to 67% of initial strength and finally, when tested after 96h, degradation of strength is most pronounced- post-fire values range from 41 to 59% of their initial values. Various studies performed on different properties of concrete so far focused mainly on the residual properties of concrete after being exposed to a heating and cooling (with a fixed cooling regime) On the other hand, influence of cooling rate (fast or slow cooling) was the object of far less studies. As regards the cooling method, the available studies suggest that fast cooling is disadvantageous when it comes to strength recovery. This is probably due to the thermal shock, characterized by a strong temperature decrease in a short time, that results in an additional strength loss when compared to natural or

slow cooling. However, it is important to highlight that for high temperature exposure (>600°C), the effect of temperature on the additional strength loss is more important than the cooling method itself. Botte and Caspeele (2017) performed an experimental campaign to investigate the effect of two cooling methods on different properties of concrete. Test specimens were produced with NSC, containing siliceous aggregates. Cubic specimens of $150mm$ side length were used to test the strength (immediately after cooling), while cylinders of height $330mm$ and diameter $106mm$ were tested to determine the stress-strain diagram (after a post-cooling period of 56 days). Specimens were heated at a constant heating rate of 1°C/min to either 175, 350 or 600°C, while the heating lasted 90 min. Two cooling regimes were employed: quenching in water or 5 minutes spraying, followed by natural cooling, until the specimens cooled down to room temperature. Quenching the specimens in water after heating results in the most severe strength loss, with an additional reduction of around 38% compared to slowly-cooled specimens (even for low temperatures). Spraying results in intermediate strength loss, with values comprised between those corresponding to natural cooling and quenching. The difference among different cooling methods, however, seems to be less pronounced at high temperatures.

Influence of the cooling regime and the maximum temperature on the residual compressive strength of NSC was investigated by Bingol and Gul (2009) that tested specimens cooled either slowly in air or rapidly in water. Concrete with compressive strength of 20 and 35 MPa were tested. Residual strength of C20 specimens showed a small increase when heated to 50°C, for both cooling regimes. On the other hand, at 100°C only air-cooled specimens exhibited higher strength than the initial value. For maximum temperatures higher than 100°C, residual strength is gradually decreasing for both cooling regimes. The influence of the cooling regime is evident - residual strength is lower for water cooled specimens, at every temperature.

The most significant loss of strength is observed for the highest temperature (700 °C), with concrete residual strength loss is 60 and

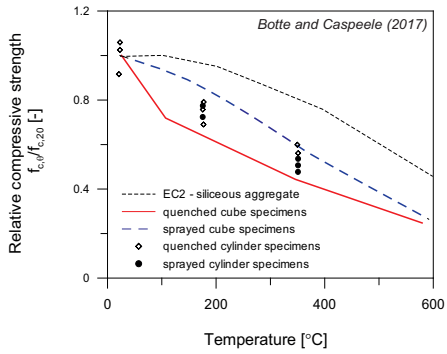

FIGURE 2.6: Relative compressive stregth of cube and cylinder specimens as a function of the exposure temperature for different cooling methods (from Botte and Caspeele (2017)).

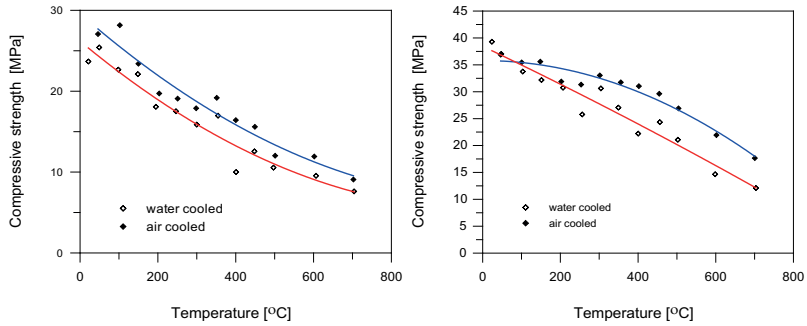

(a) (b)

FIGURE 2.7: Residual compressive strength for the concrete: (a) C20 and (b) C35 (Bingol and Gul, 2009).

70% of its initial value, for air cooled and water cooled specimens, respectively. Specimens C35 performed in a similar manner - except that the increase in residual compressive strength compared to the corresponding initial value did not occur. Decrease in residual strength is gradual, with increasing maximum temperature. As in the

case of C20 specimens, no significant strength loss occurred for maximum temperatures below 300°C, which is the upper bound of the temperature range where most of the aggregates are stable. However, at 700Â°°C, significant loss of strength occurred. Cooling regime influenced the overall decay in residual strength also for C35 specimens - water cooled specimens performed worse than the air cooled specimens in terms of strength loss.

Residual thermal strain

After cooling, concrete does not completely recover its thermal strain (RILEM, 1985, Franssen, 1993). As thermal dilation is, at least in part, due to irreversible phenomena (micro- and macro-cracking) that take place upon heating because of the thermal incompatibility between aggregates and cement paste, a certain amount of residual deformation is to be expected after cooling (Khoury et al., 1986). As reported in (Franssen, 1993), a significant increase of the thermal expansion can be observed between 500 and 600°C. This increase is probably due to macro-cracking caused by thermal stresses between aggregates and cement paste. Those macro-cracks were observed on the specimens after the tests. Clearly, at the macroscopic level it is difficult to separate the thermal expansion of the concrete from the deformation due to cracking. Whatever the real cause, a certain amount of residual elongation ensuing from heating will remain also after the cooling phase. The main factors governing the amount of residual thermal deformation are the maximum temperature experienced, and the aggregate type used in the concrete mix. The rather limited number of experimental results (RILEM, 1985) on residual thermal deformation suggests that concrete thermal deformation can be considered as fully recoverable if the maximum temperature experienced is lower than 100°C. On the other hand, if the maximum temperature is in the range between 200 to 400°C, little residual shrinkage is to be expected. For higher maximum temperature values, residual elongation is to be expected. As for the influence of the aggregate,

concretes with siliceous aggregates exhibit larger residual deformations than limestone or expanded clay concretes. Results from the experiments performed by Franssen (1993) suggest that the maximum temperature governs the amount of residual elongation, and that for maximum temperatures lower than 500°C, no significant residual elongation is to be expected. For maximum temperatures beyond 500°C, residual deformation varies between 55 and 65% of the elongation corresponding to the maximum temperature. As shown by Guo and Shi (2011), there is a certain amount of irrecoverable (residual) strain, which is strictly dependent on the maximum temperature attained during heating phase. When the maximum temperature during heating is below 300°C, the residual strain is negligible. Nevertheless, residual thermal strain increases quickly for maximum heating temperatures greater than 500°C, while for 700°C it becomes significant, reaching values as high as 40% of the thermal strain corresponding to the maximum temperature. In RILEM (1985), influence of aggregate size/type, water content as well as type of cement on the residual thermal strain are studied. Mortars made with siliceous sand exhibited mostly residual shortening. Limestone and siliceous aggregates showed residual expansion. Normal-weight concretes exhibited residual expansion in the temperature range between 300-900°C, while light-weight concretes exhibited residual shortening in the same temperature range. Influence of water content is visible only at relatively low temperatures (below 300°C), in the sense that the higher the initial water content, the higher the residual shrinkage.

2.2 Material properties of steel at elevated temperatures

2.2.1 Mechanical properties

The stress-strain curve of steel is usually described on the basis of three independent parameters: elastic modulus, yield and ultimate strength, all of which are temperature dependent. A unique stress-strain curve can be defined for each value of temperature experienced by the steel rebar. EN 1992-1-2 proposes an idealized stress-strain curve. The stress-strain response of both prestressed steel and ordinary reinforcing steel is characterized by an initial linear part, with the slope defined by the elastic modulus $E_{s,\theta}$, until the proportional limit stress $f_{p,\theta}$ or the corresponding strain $\varepsilon_{p,\theta}$ is reached. Guidance in EC2 adopts a terminology through which the stress corresponding to the deviation from linearity is referred to as proportional strength, $f_{sp,\theta}$. On the other hand, the yield strength $f_{sy,\theta}$ corresponds to the maximum level of stress in the bar at temperature θ, neglecting the strain hardening beyond a specific level of strain $\varepsilon_{sy,\theta}$.
Further straining results in a nonlinear parabolic branch that corresponds to the onset of plastic behaviour. Limit of parabolic branch is given by the yield strength/strain. For strains exceeding the yield strain, strength is defined as constant (any hardening effect is neglected), thereby simulating an elastic-perfectly plastic behaviour. This means that the yield stress is equivalent to the maximum (ultimate) stress that steel can experience. The strain limits (except the proportional strain limit) are considered constant with temperature, with their values depending on the class of reinforcement (A, B or C). Therefore, the code assumes that the ductility is not affected by the elevated temperature, something that has been questioned by some researchers (Elghazouli et al., 2009).

Mechanical properties of reinforcing steel at elevated temperature

Yield Strength

While yield strength at room temperature is relatively easy to establish, this is not the case at elevated temperatures. As stress-strain is characterized by increasing nonlinearity, there is the need to establish a criterion to define the yield point- typically 0.1 or 0.2% at ambient temperature and 1-2% at elevated temperatures (Elghazouli et al., 2009). Yield strength is therefore evaluated as the point on the stress-strain curve which results from the intersection with a line parallel to the linear elastic branch of the curve and passing through a conventional *proof* strain. Yield strength (or 0.2% proof strength where applicable) decreases with temperature, to an extent that depends on the steel type. Cold-worked and prestressing steel exhibit a more pronounced decay in comparison to hot-rolled steel. Hot rolled reinforcing steel maintains its yield strength until a temperature of about 400°C is reached, while cold-worked steel starts to lose its strength alredy at 100 °C.
In the tests performed by Gardner et al. (2016), it can be seen that at very high temperatures (800°C and above), the beneficial effect of cold-working is lost. At those temperatures, the elevated 0.2% proof strength should be based on recommended reduction factors, but multiplied by the room temperature 0.2% proof strength of the annealed material. The reduction is compared with the reduction factors given in EN 1992-1-2 for carbon steel rebars (cold-worked) and the agreement is relatively good, especially at temperatures below 400°C, while at higher temperatures, the coefficients proposed in EN 1992-1-2 are somewhat conservative.
Similar conclusions can be drawn from (Elghazouli et al., 2009). The trend observed in the experiments for both hot-rolled and cold-worked steel is in agreement with the strength decay proposed in EC2, which is, in most of the cases, conservative.
Test results from Dotreppe (1997) have been compared with the rec-

ommendations given in Eurocode 2 - Part 1-2. The experimental results concerning the 0.2% proof strength of quenched and tempered (QST) bars are compared with the values recommended in EC2 for hot-rolled steel (the metallurgical properties of QST bars are closer to those of hot-rolled rather than cold-worked steel). Despite the fact that EC2 strength decay is conservative, the general agreement is rather good.

Ultimate strength

Reduction factors for ultimate strength obtained experimentally by Gardner et al. (2016) are in slight disagreement with the reduction factors for carbon steel rebars proposed in Eurocode, but in good agreement with the reduction factors for stainless steel, established by the same authors in their previous work. At lower temperatures (less than 500°C), it seems that stainless steel loses ultimate strength to a larger extent than what is suggested in European Committee for Standardization (2005b), while the opposite is true at higher temperatures. Given this experimental evidence, the decay of the mechanical properties of stainless steel with temperature should be investigated in more detail.

The experimentally obtained reduction coefficients in (Elghazouli et al., 2009) are compared against those proposed in EC2, for the maximum stress level (denoted as $f_{sy,\theta}$). EC2 assumes strain hardening as negligible at all temperatures, while from the experimentally obtained stress-strain curves it can be seen that this assumption may be true only for the temperatures above 400°C. Thus, depending on the attained temperature, steel bars can exhibit strain hardening, which would then result in an ultimate or maximum stress level $f_{su,\theta}$ higher than $f_{sy,\theta}$. Reduction of the ultimate strength was notable at temperatures higher than 250°C or 400°C, depending on the bar configuration. At 700°C, steel kept only 10 or 20% of the strength value at ambient temperature. Moreover, manufacturing process seemed not to play a significant role. Though there is general consensus

about the fact that cold-worked steel exhibits more pronounced decay of the strength at elevated temperatures (after losing the effects of cold-working at about 400°C), both steel types exhibited similar trends of ultimate strength.

Modulus of elasticity

As should be expected, the initial stiffness of both prestressing and reinforcing steel decreases with temperature, making the material more deformable. It should be mentioned that the creep strain, which becomes significant when very high sustained temperatures occur, is included implicitly and in approximate way in EN 1992-1-2 constitutive model, which is generally adequate approach for structures with relatively low percentage of steel reinforcement (Anderberg, 1988).
As per EN 1992-1-2, reduction factors for stiffness for hot-rolled and cold-worked steel are similar, until temperature of 700°C is reached. Above that temperature, cold-worked steel exhibits a somewhat greater decay. Still, it will maintain considerable portion of its stiffness at temperatures below 400°C, whereas hot-rolled steel deformability starts rapidly increasing once the temperature of 100°C is exceeded. Moreover, hot rolled steel will completely lose its stiffness at 1200°C, while for cold-worked this happens at 1000°C. Reduction factors for the modulus of elasticity derived from steady-state tests (Gardner et al., 2016) are compared against the reduction factors for carbon steel given in EN 1992-1-2 and stainless steel in Annex C of EN 1993-1-2. The test results show a good agreement with the values given in Eurocode for temperatures up to 600°C, while at higher temperatures, the experimental values are generally lower than the values from Annex C and higher than the values for carbon steel.
In addition, the reduction factors for initial stiffness obtained from the tests in (Elghazouli et al., 2009) are in good agreement with the values proposed in EN 1992-1-2, especially for cold-worked specimens.

Ductility

Regarding ductility, ultimate strain values at elevated temperatures are measured for both hot-rolled and cold-worked steel bars in (Elghazouli et al., 2009). Results are in good agreement with the EN 1992-1-2 values for temperatures below 300°C. As the temperature increases, discrepancy between EN 1992-1-2 values and experimental values starts to widen. Furthermore, at 700°C, measured ultimate strains are several times higher than the values proposed in EN 1992-1-2. Hot-rolled bars proved to be less affected than cold-worked bars: at 700°C ultimate strain for cold-worked steel reached 7-9 times higher values than at ambient temperature, while hot-rolled steel bars reached 2-3 times higher values. This difference in ductility between cold-worked and hot-rolled steel bars diminishes at high temperatures. This might be explained considering the different manufacturing process: cold-worked steel is losing the cold-working effect at temperatures above 400°C; as a consequence, ductility significantly increases, in comparison to the very low values found at low temperatures. These results question the assumption in EN 1992-1-2 that ductility is not affected by the elevated temperatures. In (Gardner et al., 2016), the reduction factors for the ultimate strain are compared to the values given in Annex C of EN 1993-1-2 for stainless steel. Test values are consistently well below the values predicted by EN 1993-1-2.

Mechanical properties of prestressing steel at elevated temperature

Yield Strength

As reported by Im et al. (2010), the reduction of the yield strength is moderate for temperatures up to 300°C (corresponding to a reduction of 20% of the initial yield strength), but for temperatures between 300 and 600°C, the decay becomes significant. At 500°C, only about 30% of the initial yield strength is left, while at 700°C, the steel is

practically useless from the structural point of view.Reduction factors for yield strength of two types of steel wires showed less scatter in the results presented in Zhang et al. (2015). The reduction factors proposed in EN 1992-1-2 are conservative at temperatures of 200-500°C, but from 500-800°C they are adequate. In (Hertz, Hertz), an idealized curve for strength reduction coefficients is proposed. The strength reduction for 0.2% proof strength starts already at temperatures of around 100°C, while at 200°C steel loses about 20% of its initial strength. At 400°C, steel has only about 40% of its original 0.2% proof strength left, and at 600-800°C, there is almost no strength left. Reduction of ultimate strength (maximum stress) follows a similar trend.

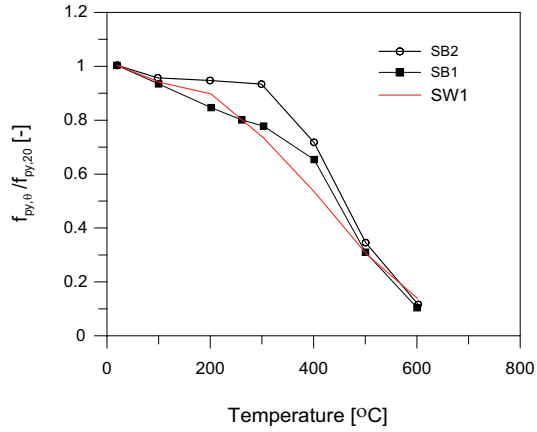

FIGURE 2.8: Reduction factors for steel bars and prestressing wire, test by (Im et al., 2010).

Ultimate strength

As for the ultimate strength, it decreases for temperatures beyond 200°C, as reported in [Im et al. (2010)]. At 500°C, the ultimate strength is around 35 to 40% of the initial value, depending on the geometry (bar or strand). The decay of the tensile strength is more

pronounced in the case of strands than bars. Ultimate strength reduction showed even less scattering than yield strength Zhang et al. (2015), with reduction factors from EN 1992-1-2 being again on the safe side for temperatures in the range 200-500°C, while agreeing well for higher temperatures.

Modulus of elasticity

In the study by Galvez et al. (2011), it was concluded that the influence of the temperature on the initial modulus of elasticity is not significant. However, Im et al. (2010) reported that the reduction becomes significant for temperatures that exceed 300°C, and at 600°C, the modulus of elasticity is only 20% of its initial value. In (Zhang et al., 2015), Young's Moduli of prestressing steel wires conforming to two standards showed comparable level of degradation for temperatures below 500°C. At higher temperatures steel wires conforming to BS 5896 exhibited less decay. The values specified in BS EN 1992-1-2 are conservative at temperatures of 500-800°C compared with those for BS 5896.

2.2.2 Residual properties

While numerous experimental studies were performed in order to investigate mechanical properties of reinforcing and prestressing steel at elevated temperatures, only few have been conducted to investigate the residual properties. One of the most significant research works on this topic was conducted by Neves et al. (1996). An extensive experimental campaign on 425 steel bar specimens was performed, by exposing them to the full heating-cooling cycle. Three distinct cooling regimes were tested: cooling in air, cooling in water and complete immersion in water. The specimens were exposed to temperatures in the range from 200°C to 900°C. Slow heating regime was employed, then samples were kept for 1h at the maximum temperature and then cooled down to ambient temperature. Different bar diameters were

investigated for reinforcing steel (6, 12 and 20 mm), while for prestressing steel a 7-wire strand was tested. After the thermal cycles, the residual tensile strength and ultimate strain were measured. From the results obtained on reinforcing steel, the following conclusions can be drawn on the residual tensile strength:

- the results depend on bar diameter and cooling regime
- the residual strength does not depend on temperature below 600°C; above this temperature, a reduction and/or increase in residual tensile strength takes place
- cooling method significantly influences the reduction of the residual tensile strength, with the faster cooling (i.e. immersion in water) leading to the least reduction (as a matter of fact, it lead to increase) of the residual strength, and this increase is greater for small bar diameters, de to more rapid cooling
- the bars with larger diameter exhibit more pronounced residual tensile strength reduction

Results from tests on prestressing steel showed somewhat different behaviour in comparison to reinforcing steel. Following conclusions can be drawn:

- residual tensile strength is approximately constant for maximum temperatures up to 400°C, followed by a decrease for temperatures up to 700°C
- specimens cooled in air exhibited increase in residual tensile strength for maximum temperatures between 700°C and 900°C
- specimens cooled in water showed a slightly greater increase in residual tensile strength in the temperature range between 700-800°C than specimens cooled in air. However, a sharp decline was noted at 800-900°C so that at 900°C, there was no residual tensile strength left.

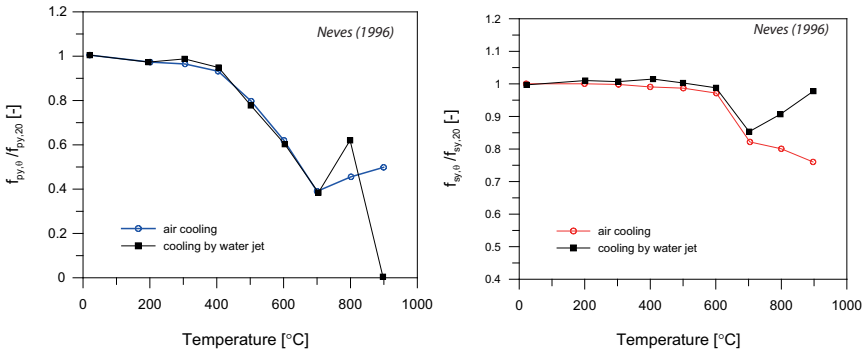

(a) (b)

FIGURE 2.9: Decay of the yield strength for: (a) reinforcing steel and (b) prestressing steel (Neves et al., 1996).

Another property tested was residual ultimate strain. Specimens exhibited no significant variations for maximum temperatures below 600°C. Moreover, specimens cooled in air exhibited a more ductile behavior at maximum temperatures above 600°C, as the greater increase in residual ultimate strain is not accompanied by an equivalent increase in strength. For maximum temperatures below 600°C, brittle behaviour was observed. Specimens cooled by water jet exhibited ductile behavior for maximum temperature of 600°C to 700°C, while at maximum temperatures above 700°C, brittle response was found, as residual ultimate strain decreased while residual tensile strength increased, as a consequence of rapid cooling. This transformation was more apparent for smaller bar diameters

More recent study has been conducted by Felicetti et al. (2009). Obtained results suggest that yield strength is affected by the temperature, to a different extent for a different material. Hot-rolled QST (Tempcore) bars are not influenced by the heating up to 550°C, but at higher temperatures exhibit marked decay. Looking at the stress-strain curves obtained, an increase in ductility when bars are heated

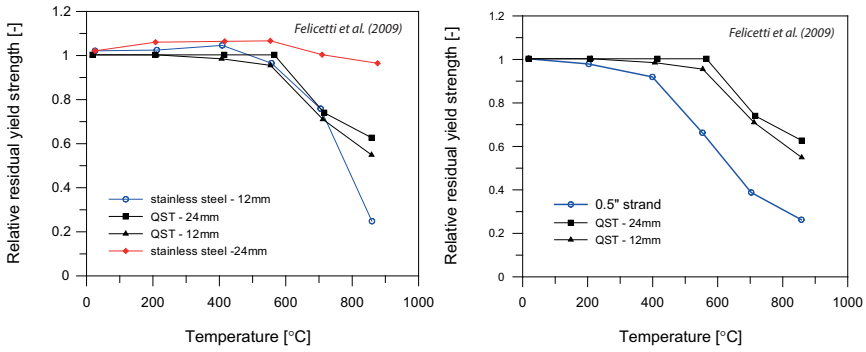

FIGURE 2.10: Decay of the yield strength for: (a) stainless steel bars and (b) prestressing strand and QST bars (Felicetti et al., 2009).

to a temperature of 850°C can be noticed. The residual strength at 850°C is close to 60% of the value at room temperature. The behavior of QST bars is rather size-independent. On the other hand, tested prestressing 7-wire 0.5" strand suffers a sizable loss of strength when heated to temperatures above 200°C and at 800°C it has only around 30% of the initial strength left (Figure 2.10).

Behavior of stainless-steel bars is influenced by the manufacturing process: hot-rolled bars exhibited a very good behavior while cold-worked bars suffered sizable strength loss. Residual Elastic modulus proved not to be influenced by the thermal treatment, while other properties, such as yield strength, the ultimate strength and the ultimate strain were strongly influenced by the thermal cycle. Residual strength of hot-rolled stainless-steel bars is just slightly lower than the initial value, while cold-worked stainless-steel bars lost around 80% of their initial strength. Large-diameter (ϕ29 mm) carbon-steel bars have an edge over QST bars, while small-diameter (ϕ9 mm) carbon-steel bars showed a behavior typical for cold-worked bars. Above

550°C, the yield strength decreases while the ultimate strength remains rather constant. As for the residual values, carbon-steel bars suffer reduction of their initial strength for about 20%. Remarkable differences in the residual behavior of various tested steel bars can be explained by their different metallurgical structure, which makes it difficult to draw a unified formulation to the residual stress-strain curves and their main parameters. Similar conclusions can be drawn from the study by Zhang et al. (2015). The residual behaviour of prestressing strands after exposure to the temperatures from 100 to 600°C and subsequent cooling to ambient temperature has been investigated. The amount of strength recovery is strongly dependent on the maximum temperature experienced. For the peak temperatures up to 400°C, the strength is hardly affected. For peak temperatures above 400°C, the residual strength starts to decay. At 500°C, the residual strength is around 80% of the initial value, while at temperatures as high as 800°C, the residual yield strength is only around 30% of the value in virgin conditions. As concerns the modulus of elasticity, it is largely recovered after cooling. In the work performed by Elghazouli et al. (2009), the residual properties of both cold-worked and hot-rolled bars are examined. Test specimens were heated to a specified temperature level, and then maintained at the maximum temperature for at least 30 minutes before cooling them down slowly. The results indicate the differences in the behaviour between the two types of steel. Hot-rolled bars tend to recover their original stiffness and strength upon cooling, in the investigated temperature range(20-600°C). Regarding the residual ductility, the ultimate strain retains its ambient value for peak temperatures up to 400°C; beyond this temperature value, it starts to increase, reaching around 1.5 times its ambient value at 600°C. Cold-worked steel bars showed no significant variations in strength, stiffness and ductility for peak temperatures up to 400°C; beyond this temperature, they exhibited a reduction of around 10-15% of their initial strength, and most Importantly, the residual ductility proved to be signficantly affected for temperatures above 400°C, and at 600°C reached a value

that is 2.5 times larger than the ambient value. Commercial cold-drawn and stress relived prestressing wires with 5mm diameter were tested by Galvez et al. (2011). The tests were performed at different designated maximum temperatures (20, 100, 200, 300, 400, 500 and 600°C) with duration of 4 hours and loaded at 70% of their initial tensile strength. After cooling, two tensile tests were performed for each designated maximum temperature. At Figure 2.11, residual tensile strength and residual yield stress, normalized with respect to initial values (at room temperature) after heating at different temperatures (for 4 hours) are shown (Galvez et al., 2011). If prestressing steel is heated up to 300°C, residual strength and elastic limit are not affected, however, for maximum temperatures acquired during heating, steel suffers damage which is not recovered upon cooling-manifested by a steep decrease in residual strength and residual yield stress. However, as Galvez et al. (2011) are suggesting, this plot should be seen as a simple and conservative estimation, given that fire scenario duration was very conservative; more in-depth analysis would require several more variable to be included.

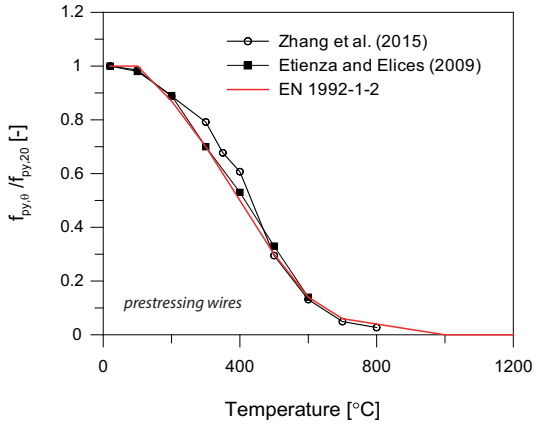

FIGURE 2.11: Cross-sections tested in (Wu et al., 2010).

2.3 Structural behaviour - experimental evidence and numerical studies

2.3.1 Prestressed Concrete Structures

As reported in (Bamonte et al., 2018), the first systematic researches on the fire resistance of prestressed concrete members were reported by Troxell (1962), who compared fire resistance tests conducted in Europe and in the United States. A basic finding was that prestressed members could resist fires lasting up to 4 hours, by providing a suitable concrete cover. Moreover, the beneficial effects of the continuity over intermediate supports and of axial restraints were pointed out. Finally, no major differences were found between pre- and post-tensioned members (with bonded tendons). Another systematic research on the behaviour of prestressed concrete members exposed to fire was carried out by Gustaferro (1973), who studied the behaviour of prestressed concrete members exposed to standard fires. Once again, the key role played by cover and restraint conditions was pointed out. Moreover, for continuous (and thus redundant) structures, the importance of providing negative reinforcement over the supports to allow moment redistributions was highlighted. A summary of the fundamentals concerning precast prestressed members can be found in (Gustaferro and Martin, 1989): as regards simply-supported members without end restraints, a simple and straightforward method to determine the structural end point (and thus the fire resistance) is devised, which consists in comparing the applied moment with the moment capacity in the most stressed section (midspan). In recent years, post-tensioned flat slabs with unbonded tendons and prestressed hollow core slabs stand out as the most investigated prestressed members among those available on the market nowadays. The reason for this is to be found in the high sensitivity to fire of the former (especially if there no ordinary reinforcement is provided for additional flexural capacity), and in the shear-deficient behaviour of the latter (since no transverse reinforcement is present). One of

the most significant studies on bonded and unbonded post-tensioned concrete slabs was carried out by Ellobody and Bailey (2008), who investigated the influence on the structural behaviour of several parameters, such as aggregate type, duct material and restraint conditions. The results showed that the presence of boundary restraints and the use of aggregates without silica are beneficial. As for the duct material, slabs with metallic ducts exhibited larger deflections than those with plastic ducts. Regarding hollow-core slabs, they have been the object of several studies in recent years (Aguado et al., 2012, Kodur and Shakya, 2014, Venanzi et al., 2014). The results show that the thermal and structural response can be adequately simulated by means of numerical models (despite some peculiarities, such as the presence of voids with the ensuing problems related to heat transfer by cavity radiation), and that factors such as load level, concrete cover and hole size considerably affect fire resistance. Moreover, the failure of hollow-core slabs is primarily governed by the fire scenario, or, in fact, by strength and stiffness loss in the strands, which results in a decrease of the load-bearing capacity and an increase of deflections. Finally, as previously mentioned, another critical issue in hollow-core slabs is the shear strength (Fellinger, 2005), in consideration of the fact that these elements do not have transverse reinforcement. More recently, extensive fire resistance experiments on nine bonded prestressed continuous concrete beams were performed by Hou et al. (2014), investigating the influence of several variables, including concrete cover, load level and prestressing level. The test results proved that the influence of load level and concrete cover is very significant. Moreover, as should be expected, continuous beams are characterized by a higher fire resistance than simply supported beams. All the aforementioned research works are focused on the standard fire (that is in the reference scenario for laboratory testing), i.e. a post-flashover fire without cooling phase. When focusing on buildings consisting of prestressed concrete members, however, natural fires are undoubtedly more significant, mainly because of the large room and variable amount of fire load that characterizes this

type of structures (Stern-Gottfried et al., 2010). Within this context, in the design phase it may be advantageous from the economic point of view (and also more realistic) to resort to natural fires, based on the actual geometry of the compartment and on the available fire load. As a matter of fact, the most recent version of EN 1991-1-2 (European Committee for Standardization, 2005b) allows resorting to performance-based design through the use of natural fires, taking as many significant parameters as possible into consideration, so as to eventually yield a more accurate representation of the real behaviour. Within this framework, it is clear that the structural behaviour of pre-stressed concrete members exposed to natural fires is definitely of interest for the designer. Research works dealing with natural fires are rather few to this day. The experimental research carried out by Gales et al. (2016), who investigated the response of continuous and restrained post-tensioned concrete slabs, with unbonded tendons, exposed to natural fires, should be mentioned. Despite the relatively simple structural system, the deflection seems to be governed by several parameters, and is not yet fully understood.

2.3.2 Reinforced Concrete Beams

Available studies on the fire resistance of beams mainly come from standard fire testing and those few studies investigate the influence of a limited number of parameters. On the other hand, as Kodur and Agrawal (2016) pointed out, the number of experimental and numerical studies that investigated the residual behaviour of RC beams is rather limited. Numerical studies utilized two approaches. The first approach is simplified sectional analysis (Kodur et al., 2013, Kodur and Dwaikat, 2008, Kodur et al., 2003), which is based mainly on empirical equations to predict the residual and post-fire load capacity of RC beams. The maximum temperature in the rebar is identified as the key parameter. In most of the studies, the temperature induced decay of materials' mechanical properties is based on the heating phase alone, not accounting for the irrecoverable material damage that takes

place upon cooling. Through the current simplified approaches, it is not possible to predict post-fire residual deformations. The second approach is a detailed FEM analysis (Kodur and Agrawal, 2016, Ozbolt et al., 2014), where the latter model does not use distinct material properties for the heating, cooling and residual phases.

Experimental studies

Elingwood and Lin (1988) conducted six full-scale fire tests to study the behaviour of RC beams exposed to severe fires. The beams were continuous over one support, and were fabricated from normal weight concrete. Four out of six beams were exposed to the standard ASTM E119 fire for long fire durations (3.5 hours or more), while the remaining two beams were exposed to a SDHI fire (short duration - high intensity) for an overall duration of heating and cooling phase around 4 hours. During the fire test, all six beams developed significant shear cracks near the continuous support and rather in the early stages of fire. However, the beams failed from excessive flexural cracking and deformation. Flexural cracks formed in the positive moment region of the span and continued to widen during fire exposure to a maximum width of approximately 6 mm through 3.5 hours of fire exposure. The maximum deflection at the end of each test was about 150 mm. It was concluded that the most important factor affecting the behaviour of a properly designed reinforced concrete flexural member is the temperature history in the reinforcement. The direct computation of these temperatures from a two-dimensional thermal analysis tends to be conservative because the capacity of the reinforcement to conduct heat along the longitudinal axis of the member is not taken into account. On the other hand, properties such as the compressive strength and stiffness of concrete are less sensitive to the variations in temperatures typically developed during a fire, and therefore the accuracy in predicting concrete temperatures is of lesser importance. Kumar and Kumar (2003) tested five RC beams, exposed to ISO834

fires with cooling phase. The aim was to measure the residual load capacity of the fire exposed beams. Unfortunately, the temperature and displacement measurements during the cooling phase have not been reported. Four beams were exposed to standard ISO834 fire for 1, 1.5, 2 and 2.5 hours, without any load applied. Thereafter, five beams were loaded, while the sixth beam (the one exposed to the longest fire duration) failed to meet a serviceability criterion for its residual deflection after fire, before even performing the load test. It was concluded that the residual deflections increase with fire exposure time regardless of load level. Ultimate load at failure reduces with the time of fire exposure. After being exposed to fire for one hour, the beam retained 83% of its reference bearing capacity at ambient temperature. This reduction, however, was shown to increase with the fire exposure: after 2.5 hours, the beam did not have any strength left.

Kodur et al. (2003) tested a set of three reinforced concrete beams by subjecting them to fire curves with heating and cooling phase. Following, the beams were tested for measuring their residual bearing capacity. Two beams, B1 and B3, were tested with axial restraints at the extremities, while B2 was simply supported. Beams B2 and B3 were made of high-strength concrete while the beam B1 consisted of normal-strength concrete. The results of the tests indicate that the beams tested retained most of their room-temperature flexural capacity after exposure to fire. Data from fire tests and numerical studies are utilised to develop a simplified approach for evaluating the post-fire residual strength of RC beams. The approach has been validated against the measured values of the residual strength obtained from the tests and showed sufficient accuracy for practical applications.

Dwaikat and Kodur (2009) performed fire experiments on six RC beams, comparing performance capabilities of NSC and HSC. The test variables included concrete strength, boundary conditions, fire scenario and load ratio. Four of the tested beams were made of HSC, while two were made of NSC. The specimens were either simply supported or axially restrained. Three fire scenarios were investi-

gated: standard ASTM E119 fire and two design fires with cooling phase (short severe fire and long severe fire). HSC beams suffered moderate to severe spalling. The beams were loaded with two-point loads, corresponding to 55% of their flexural capacity. The load was kept constant throughout the test and the beams were considered at failure when the hydraulic jack could no longer maintain the load. When exposed to a design fire scenario, RC beams did not experience failure (except one simply supported beam made of HSC, that suffered severe spalling), while under standard fire scenarios, the beams failed after at 160 and 180 min. It was concluded that the strength of the concrete has a significant influence on the fire resistance of RC beams: HSC beams have lower fire resistance than NSC beams. This can be attributed to the spalling sensitivity of HSC and also to its higher sensitivity to temperature in comparison to NSC. Beams loaded with lower loads exhibited higher fire resistance. Restraint conditions also played a role: axially restrained beams proved to have better fire resistance than simply supported beams.

Moetaz et al. (1996) tested four groups of RC beams. The beams were exposed to fire at 650°C for time durations of 0, 30, 60 and 120 min and then cooled by water. Non-destructive testing (NDT) methods were applied to determine the compressive strength of concrete. Strains and deflections were measured at each load increment and cracking loads, crack propagation and ultimate loads were recorded for each beam. A reduction of ultimate loads, increase in deflection, increase in tensile strains and reduction in concrete compressive strength due to fire exposure were observed. One beam was not exposed to fire and was kept as reference (Beam B), while three beams (B1, B2 and B3) were exposed to fire for durations of 30, 60 and 120 min, respectively. The results indicate that a considerable reduction in the ultimate loads of fire-exposed beams, in comparison with the reference beam, took place. These reductions varied from 12 to 39% approximately. The results also indicate that the deflections of the fire-exposed beams increase as the fire duration increases. Relationship between loads and maximum deflections is almost linear. The effect

that fire has on concrete is larger than its effect on reinforcing bars. Moreover, conducting NDT after exposure to fire (Schmidthammer) in order to measure the residual compressive strength showed that the beams suffered a considerable reduction of the compressive strength, with values between 42% and 73% of the compressive strength in virgin conditions.

A recent study has been performed at Michigan State University. Agrawal and Kodur (2018) performed a three-stage experimental approach to evaluate the residual capacity of fire-damaged concrete members. The behaviour of two fire-exposed concrete beams is monitored during three stages: pre-fire exposure conditions, during the fire exposure (full heating-cooling cycle) and finally during post-fire exposure conditions, when the residual load-bearing capacity is determined. The residual response of fire-damaged concrete members is strongly influenced by the conditions present prior to the fire, as well as during the complete heating-cooling down to ambient temperature-cycle. In the pre-fire stage, the concrete members are loaded in small increments until service conditions are reached and until deflections stabilize. In the second stage, the loaded beams were exposed to a realistic fire scenario, with heating phase duration of 90 to 120 minutes and a distinct cooling phase. If the members did not fail during the second stage, they were incrementally loaded to failure, in order to assess their residual load capacity. Deflections, temperatures, cracking propagation patterns, spalling and post-fire residual deformations have been monitored. The importance of assessing if the residual capacity left after fire is sufficient for re-occupancy has been recognized.
Beam B1 was made of HSC, having a test day compressive strength of 106 MPa, while beam B2 was made of NSC, with compressive strength of 62 MPa. Yield strength of the reinforcing bars was 420 MPa. Neither of the two beams failed during fire. Beam B1 suffered spalling equal to 1.5% of the volume ratio. Beams were two-point loaded, with the loads equal to 50-55% of their capacity, calculated

according to ACI 318. It was concluded that the extent of recovery observed in fire-damaged members is strongly influenced by a cooling rate as well as load level present on the member during fire. Irrecoverable residual deformations will be present after the complete cooldown of the member. These deformations are significant as they can give an indication of the stiffness degradation in fire damaged members. Moreover, it was shown that much of the beams' flexural capacity has been recovered, provided that the temperatures reached in the rebars are not extremely high (not exceeding 600°C) and that significant spalling did not occur during heating and cooling of the member.

Numerical studies

Available numerical studies utilized two approaches so far. First approach is simplified cross-sectional analysis (Kodur et al., 2003, Kodur et al., 2013, Kodur and Dwaikat, 2008). Simplified cross-sectional approaches are based mainly on empirical equations to predict the residual and post-fire load capacity of RC beams and columns. Maximum temperature in the rebar is identified as a key parameter. The behaviour of a fire-exposed RC beam depends on the internal temperatures in the beam, the load level during the fire event, the cooling method and rate, as well as the strength recovery time following the cooling period. In most of the studies, temperature-induced degradation of materials' mechanical properties is based on the heating phase alone, not accounting for the irrecoverable material damage that takes place during cooling. Through the current simplified approaches, it is not possible to accurately predict post-fire residual deformations. Second used approach is detailed FEM analysis (Ozbolt et al., 2014, Kodur and Agrawal, 2016, Gao et al., 2013), where the latter model does not use distinct material properties during heating, cooling and residual phases.
Gao et al. (2017) presented a design approach for predicting the fire resistance of reinforced concrete beams. The method is based on the

energy-based time equivalence method in combination with a correction factor, formulated as a function of concrete cover and characteristics of the compartment. In short, the proposed approach suggests the fire resistance of a reinforced concrete beam exposed to a design fire to be deduced from the fire resistance of the same reinforced concrete beam exposed to the standard fire. Fire resistance data of reinforced concrete beams under design fire exposure, which were used to formulate and validate the proposed approach, were generated using a reliable finite-element approach. The results showed that the use of the energy-based time equivalence method in combination with a correction factor is reasonably accurate in predicting the fire response of reinforced concrete beams under parametric design fires.

Kodur and Dwaikat (2008) developed a numerical model, in the form of a computer program, for tracing the response of reinforced concrete beams exposed to fire. Model is based on macroscopic FE approach and uses a series of moment- curvature relationships for tracing the response of the beam in the entire range of behaviour (from linear-elastic to collapse stage, under any given fire and loading conditions). Model is developed specifically for simply supported beams, i.e. with bending moment as a dominant action and it incorporates spalling in a simplified way. The beam is divided into a number of segments along its length and the mid-section of the segment is assumed to represent the behaviour of the whole segment. Moment-curvature relationship is generated for each longitudinal segment at various time steps. The secant stiffness of each segment is determined from M-χ relationships, based on the moment reached at that particular segment. The deflection of the beam is then evaluated through the stiffness approach, by working out the average stiffness of the beam. Transient and creep strain are explicitly accounted for, by using Anderberg and Thelandersson (1976) and Harmathy (1993) model. The ultimate curvature (curvature at collapse) increases with the fire duration, and this is due to the degradation of material strength and stiffness as well as to the transient and creep strain which becomes significant prior to failure. Four sets of failure criteria have been used:

thermal, by limiting the temperature inside the steel bars to 593C, strength, deflection and rate of deflection criterion. Limiting criterion used for determining failure of a reinforced concrete beam has a significant influence, and finally it was suggested to use the failure criteria that concerns deflection and rate of deflection. Wu and Lu (2009) developed a beam-element model for reinforced concrete beams at elevated temperature by using the principle of virtual work, with the objective to study the influence of restraints. The investigated beams were axially and rotationally restrained. Imposed restraints can generate substantial unforeseen forces in the beams during fire bringing in another hazard that may cause uncalculated structural failure. The mathematical model for calculating the fire response of reinforced concrete members with rectangular cross section was developed and validated, and then used for a parametric study. Axial restraint may induce compressive forces and increase the midspan deflections when temperature is increasing: as a matter of fact, the higher the axial restraint stiffness, the larger the generated compressive force and also the larger the beam deflection due to P-δ effect. Increasing the rotational restraint (while keeping the value for axial restraint constant) decreases midspan deflections. The rotationally-restrained beam initially exhibits hogging moment at the ends upon rise in the temperature, but with the further rise in the temperature, hogging moments start to decrease.

Bratina et al. (2003) developed a FE program to study planar beams that included 2D thermal model and 1D mechanical model. The model accounts for physical, material and geometrical nonlinearity as well as temperature-dependent material properties. Members were exposed to heating phase of the fire, no cooling was considered. Viscous creep in the rebars is explicitly accounted for, in order not to underestimate the displacements. The authors concluded that the non-uniform temperature distribution leads to considerable stress gradients, regardless of the fact that the structure is statically determinate or redundant.

Huang et al. (2009) developed a robust nonlinear finite-element pro-

cedure for three-dimensional modelling of concrete beam-column structures in fire conditions. In their formulation, both material and geometrical nonlinearity are taken into account. Spalling is also modelled, through the use of void segments. Model has been validated against a series of experimental results where it proved able to predict the behaviour of reinforced concrete members in the heating phase of fire with sufficient accuracy. It was concluded that surface spalling has a significant effect on both thermal and structural behaviour of reinforced concrete members. Transient state strains also proved to have a sizeable effect on the deflections, but little effect on the failure time of simple structural members.
Capua and Mari (2007) presented a methodology for a sectional analysis of reinforced concrete members exposed to fire. A nonlinear finite element procedure is proposed to predict the temperature distribution. Subsequent mechanical nonlinear analysis is performed for each temperature distribution and for the applied external load, using an algorithm based on arc-length control. Thermal and mechanical properties have been assumed as suggested in European Committee for Standardization (2005b). Numerical model is validated against experimental data with satisfying accuracy. Kodur et al. (2003) developed an approach for evaluating the residual strength of fire-exposed reinforced concrete beams was proposed. Two of the beams were made of HSC and one was made of NSC concrete. The beams had different restraint conditions: two of them were axially restrained and one was simply supported. Results from experimental post-fire residual strength tests on the three beams indicate that most of their room-temperature flexural capacity was retained after exposure to fire. Data from fire tests and numerical studies are then utilised to develop a simplified approach for evaluating the post-fire residual strength of reinforced concrete beams. The behaviour of a fire-exposed RC beam depends on several factors, such as the internal temperatures in the beam, the load level during the fire event, the cooling method, the rate of cooling. Focus was put on the residual strength of reinforcing steel (which depends on the maximum temperature experienced

by the rebars) rather than on the residual strength of concrete. The temperature of 500°C in the steel bars was taken as a limit value to determine if steel recovers (or not) its original mechanical properties upon cooling. Their approach consists of the following steps: (a) estimation of the maximum fire temperature and fire duration; (b) estimation of maximum temperature in the rebars through a simplified empirical equation; (c) estimation of the residual strength of reinforcing steel using typical decay curves for reinforcing steel; (d) computation of the residual capacity of the beam by applying ACI 318 (ACI, 2008) strength equation at ambient temperature and with reduction factors to account for reduced strength of steel reinforcement and damaged concrete section (through the use of effective depth and effective width of the concrete section). It was concluded that the rebar temperature is the main factor governing the flexural capacity of RC beams after fire exposure. Such a simple approach can serve to provide an estimate of the residual flexural capacity of a reinforced concrete beam after fire exposure. It is a rapid evaluation and it does not evaluate exact residual flexural capacity. The proposed approach also has some limitations in terms of axis distance value (i.e. concrete cover thickness) and spalling is not considered.

Gao et al. (2013) developed a 3D FE model to study the behaviour of simply supported reinforced concrete beams exposed to fire. Particular attention is paid at modelling the bond-slip behaviour of the interface between reinforcing steel and concrete, something that is seldom found in the previous studies. In this way, the prediction of the displacements at elevated temperature is more accurate. At ambient temperature, the maximum slip always occurs close to the midspan, due to the midspan crack which is widest among all the cracks. At elevated temperatures, however, the maximum slip occurs, unexpectedly, in the transition zones between heated and unheated areas within the anchorage zone. Slips at high temperature are mainly caused by different thermal deformations between concrete and steel bars, and are much larger than the slips that are induced by the loads at ambient temperature. An improved FE model that included a temperature-

dependent bond-slip model for reinforcing steel is proposed, but still more work is needed for a more accurate definition of the bond-slip relationship. The authors concluded that the explicit inclusion of the bond-slip behaviour does lead to a more accurate prediction of displacements and enables in-depth examination of the local behaviour of reinforced concrete beams, but can be neglected if the focus is only on studying the global response of RC beam.

2.3.3 Reinforced Concrete Columns

In the next Section, the results from the experimental tests that served as a basis for the numerical model validation will be recalled. More details however will be given in the following chapters.
Among the most significant experimental studies on concentrically loaded columns exposed to standard fire are the ones by (Lie and Irwin, 1990, Lie and Irwin, 1988), who completed an extensive test program on 40 full-scale reinforced concrete columns and the results for four columns have been discussed. The tests were carried out by exposing the columns fire inside a test furnace. Average temperature in the furnace followed closely the ASTM E119 time-temperature curve, except for Column 3, which followed a specific time-temperature curve. Failure of the columns took place when the load, applied by hydraulic jack, could no longer be maintained. Axial deformation of the columns was obtained by measuring the displacement of the jack supporting the column. Column 1 failed during the test, after 208 minutes into fire exposure. Column 3 failed in the later stage of fire, after 396 minutes.
Hass (1986) performed a series of full-scale tests on heated reinforced concrete columns subjected to eccentric axial loads and under standard fire exposure. Several columns were chosen for the numerical model validation, and more details on the geometry and material properties of the selected columns will be given in the next chapters. Selected columns were loaded with an eccentricity varying from 30 to 90 mm. Column 1 failed during the test, after 86 minutes, Col-

umn 2 failed after 75 minutes and Column 3 failed after 125 minutes. Second-order effects proved to have a significant influence on the structural behaviour of these columns.
As concerns the tests in residual conditions, an extensive experimental campaign has been performed at South China University of Technology (Wu et al., 2010), where 12 axially restrained columns (four for each type of cross-section, i.e. cross-shaped, T-shaped and L-shaped sections) were tested. The columns were not insulated, but they were part of a frame; thus, they exhibit different behaviour in fire due to considerable restraint and continuity provided by the surrounding structure.
The main objective was to investigate the effect of axial restraint during both heating and cooling (i.e. expanding and contracting) phase. The columns were initially concentrically loaded and subjected to the ISO834 fire on all four sides. Axial restraints were imposed at the top of the columns, to simulate the restraining effect of the rest of the frame. Axial restraint stiffness varied from 34.5 to 51.9 MN/m. Temperature acquisition was obtained through K-type thermocouples located at the mid-height cross-section for each test specimen. Axial deformations were measured using four LVDTs, located at the top end plate of the column. Each column was heated and then cooled down. Temperature and displacement measurements were taken throughout the whole fire exposure. For both the L-shaped and T-shaped columns, the sectional thermal field is not double-symmetrical; therefore the concentrically loaded columns changed to be eccentrically loaded during the tests (effect of restraint bending moment caused by the fire). During the tests, none of the columns failed and only minor spalling was observed in some columns. The beneficial effect of axial restraints can be observed looking at the displacements, where the higher restraint led to smaller displacements.
The results from the tests performed at the Testing Centre of Michigan State University on six reinforced concrete columns were presented in Raut and Kodur (2011). The test variables included con-

crete strength, fire scenario, load ratio and the role of polypropylene fibers in the concrete mix. Experimental data served to validate a numerical model developed for tracing the fire response of reinforced concrete columns. All columns were 3350 mm long, with a square cross section (203 x 203 mm2). Four ⌀20 rebars acted as a longitudinal reinforcement ($f_y = 420MPa$), as well as 10 mm stirrups, with a spacing of 200 mm, as transverse reinforcement. The bottom end of the column was bolted to a steel plate fixed to the floor, thus it can be assumed as fully restrained against rotation.

Columns were exposed to three different fire scenarios: either a standard, ASTM E119 fire, or the design fires, denoted as SF and LF, which follow similar temperature profile in the heating phase of fire, but have a well-defined decay - cooling phase. Axial deformations were measured at the top of each column. The columns responded in a similar way: expanding in the early stages of fire exposure and contracting later. Raut and Kodur (2011) explained that early expansion can be mainly attributed to the thermal expansion of concrete and steel. Contraction in the later stages is a result of loss of strength in steel reinforcement and concrete, due to the increasing temperatures within the cross-section and also due to load redistribution from concrete to reinforcement.

Kodur et al. (2017) presented the results from residual capacity tests performed on two columns. Columns were first loaded then heated and finally, after complete cooldown, tested to failure to determine the residual load capacity. Results indicate that the two columns do retain significant residual capacity after fire. The columns, designated as C1 and C2 were exposed to the design fires DF-1 an DF-2. The heating phase for DF-2 was 30 minutes longer than for DF-1, with the same cooling rate. Temperatures reached in the rebars are rather high, with peak values of 550 °C for C1 and around 600 °C for C2. Columns had a length of 3350 mm but only the central portion of 1700 mm was exposed to fire. Both columns were made of NSC with carbonate aggregate, with compressive strengths at the test day being 50 MPa and 62 MPa for C1 and C2, respectively. Column C1 was loaded with

a compressive force corresponding to 50 % of its factored ACI design capacity, while the load level of Column C2 was 55%. The load was maintained during both phases of the fire. Structural behaviour is traced through the evolution of axial displacements, measured at the top of each column by LVDTs. The behaviour of the two columns is rather similar. Initially, the displacements increase due to thermal expansion, due to increasing temperatures. Then, it the second stage, a rapid decrease in axial deformations is observed and the columns start to contract due to degradation of strength and stiffness in concrete and rebars. Once the temperatures in the member start to decrease, a recovery in the deflections is observed. Rate of recovery in the deflections is significantly lower than the rate of increase, due to the nonlinear nature of the cooling phase and also irrecoverable damage that took place during heating and cooling. Residual deformation of Column C1 is about 50% greater than what was observed in Column C2, which makes the residual deformation very sensitive to the duration of the heating phase.

Recently, an extensive experimental campaign was carried out at the University of Edinburgh, as part of the PhD thesis of (MacLean, 2018), with the aim to determine the effect that various parameters have on the behaviour of reinforced concrete members when exposed to severe and localized heating and subsequent cooling. The obtained results can serve to question the validity of the specific design methods and calculations currently used in the analysis of reinforced concrete columns for evaluating the structural response to fire and also for post-fire analysis. A total of 46 geometrically identical reinforced concrete columns have been tested. Conditions at the boundaries of the member are pin-pin.

All the columns were eccentrically loaded, with varying values of the eccentricity (5-25 mm) and the load was kept constant during the fire exposure. Differently from conventional heating methods usually applied in laboratory testing (i.e. heating in the furnace following a predefined time-temperature curve), the columns were exposed to a constant incident radiant heat flux, for a total duration of 90 min-

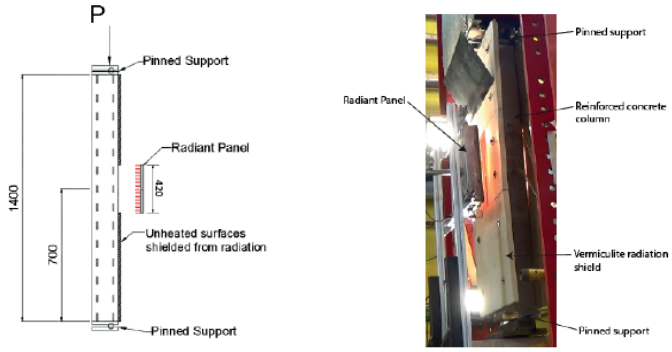

FIGURE 2.12: Schematic and image of the test setup from (MacLean, 2018).

utes. Radiant panels of dimensions 320 mm x 420 mm were fixed at an offset distance from the target surface to achieve a predefined level of heat flux ($50kW/m^2$ or $70kW/m^2$). Only the central part of the column was heated: therefore the heating was localized and non-uniform. The rise in the temperature away from the heated surface was dominated by conduction within the concrete member, rather than by the radiation from the panels. Following the heating phase, each member was then allowed to cool down in the laboratory for 24 hours. For all the columns that did not fail during the full heating-cooling cycle, an assessment of damage through the use of NDTs and finally a destructive load test to determine the residual capacity have been performed. Temperatures within a section were measured at a sufficient number of locations. Schematic representation of thermo-couples locations can be found in the Figure 2.13.
Vertical deflections at the base of the column and lateral deflections at different heights of the column were measured by using both linear potentiometers and Digital Image Correlation, in all the phases of the testing programme. Vertical displacement is measured at the base of the column, while lateral deflection was measured at 350 mm, 700 mm and 1050 mm height from the base.

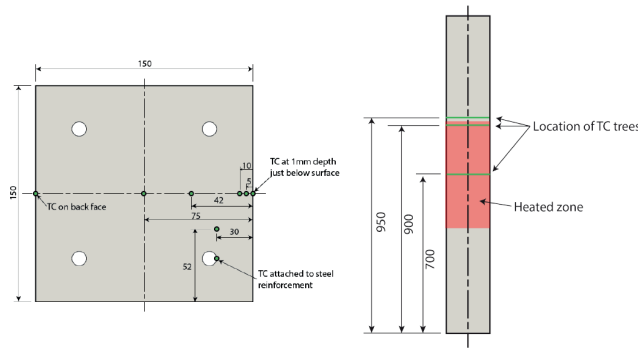

FIGURE 2.13: Location of thermocouples in plan and elevation from (MacLean, 2018).

Influence of the various parameters on the columns performance during heating, cooling and residual phase has been investigated. Parameters varied were load magnitude, eccentricity of the applied load, concrete compressive strength, applied initial incident radiant heat flux and the sides exposed to fire. In the following Chapters, more words will be dedicated to this extensive experimental study, as some of the results were used for numerical model validation.

Chapter 3

Sectional analysis at elevated temperature

Sectional analysis is a very efficient tool for analysing many structural members that are modeled and designed as simply supported, or, more generally, statically determined. In these cases, the distribution of internal forces is not affected by the stiffness of the member and is determined solely by equilibrium equations. Structural behaviour of columns, simply supported beams and the vast majority of prestressed concrete members can be analysed by considering only the most-stressed section. In addition, sectional analysis forms the basis for most code provisions, and is still nowadays the only tool available for everyday structural fire design. This chapter will address the principles of sectional analysis in fire conditions with the related computational problems, in order to lay the fundaments for more general considerations on the structural behaviour, which will be the subject of the following chapters. After recalling the basic principles of sectional analysis, the general procedure to perform sequentially coupled thermo-mechanical analysis through an ad-hoc developed code will be outlined. Finally, some examples on the application of sectional analysis on fire exposed structural members will be shown and the results from some preliminary analyses will be discussed. The method

was applied on two typical prestressed concrete sections, as well as on several reinforced concrete beams tested at Michigan State University and exposed to natural fires. Parametric analyses have been conducted, to study the influence of the parameters that were deemed significant. Finally, some considerations on the sectional analysis of columns will be given, through the application of the method based on nominal curvature (Annex B3 method from EN 1992-1-2).

3.1 General approach

The basic kinematic assumptions of sectional analysis at room temperature are retained also at elevated temperatures:

- the Bernoulli-Navier hypothesis, namely that plane sections remain plane
- perfect bond between the steel bars (ordinary and prestressed) and the surrounding concrete

While the first assumption is widely accepted for performing the structural analysis of members such as beams and columns, the second assumption is reasonable in zones where large bending moments are expected and the shear forces are low. Both assumptions are reasonable when failure is governed by normal stresses, this being typically the case for slender elements, as widely documented in the literature, with very few (and peculiar) cases of shear failures in fire. For instance, the shear failure of the column in the underground parking Montreaux in Switzerland was caused by the fire: not by the high temperatures in the collapsed member but by the indirect actions induced by redundancy (Burnier, 2016).
Relying on the Bernoulli-Navier hypothesis, at any point the total concrete strain can be calculated using only two variables, deformation at the reference point and curvature ε_o and χ, respectively:

$$\varepsilon(y)=\varepsilon_o+\chi y$$

where y is the distance of the point of interest from the reference point of the cross-section and should be taken with negative sign if the point of interest is above the reference point.

As per strain compatibility hypothesis, total strains for reinforcing and prestressing steel bars can be written in a similar manner:

$$\varepsilon_s{=}\varepsilon(y) {=}\varepsilon_o{+}\chi y$$

$$\varepsilon_{ps} = \varepsilon(y) + \Delta\varepsilon_{p0} = \varepsilon_o + \chi y + \Delta\varepsilon_{p0}$$

Even though the basic assumptions of sectional analysis are still valid at elevated temperature, the procedure for sectional analysis at room temperature has to be properly modified for the application in fire conditions. The effects of fire, namely the thermal deformations and the decay of the materials' properties, have to be properly accounted for. The heating process induces thermal strains on the section. To comply with Bernoulli's hypothesis, total strain profile on the section must be linear, which means that the thermal strains are not free to occur. The effects of the thermal strains can be presented as the sum of three components: the first component of strain is responsible for the contraction or elongation of the member, while the second component implies a curvature of the element. These two components are not causing additional internal forces in statically determinate members, whereas they do in statically indeterminate members whose axial elongations and/or deflections are restrained at the boundaries. The third component, by contrast, generates self-equilibrating stresses, both in statically determinate and indeterminate members. Nevertheless, it results only in an additional material effort, as its contribution to the deformations of the element as a whole (Kowalski, 2010) are included in the first and second component. If a statically determinate structural member is exposed to a linear temperature profile causing uniform or linear thermal strains, hypothesis of plane sections can be fulfilled without self-stresses. Nonetheless, in a statically determinate member exposed to fire, nonlinear thermal strain profile over the depth of the cross section oc-

curs, due to nonlinear temperature profile and to the dependence of the coefficient of thermal dilation on temperature. The fact that fibers are not free to expand, as they are connected to adjacent fibers, together with the assumption that the section has to remain plane leads to the creation of additional strains due to self-equilibrating (Ghali and Favre, 1994).

3.1.1 Free thermal strain contribution

For an RC section exposed to fire, the free thermal strain due to the temperature variation (that would occur in each fiber if it was free to expand) can be evaluated at each point $P(x, y)$ of the section, if the variation of the coefficient of the thermal dilation $\alpha = \alpha(T)$ with temperature is known:

$$\varepsilon_{th} = \int_{T_0}^{T} \alpha dT$$

where $T(x, y)$ is the temperature at any point of the cross-section, and α is the coefficient of thermal dilation, that is function of the temperature only.

If the free thermal strain is artificially restrained, the restraining stress would be:

$$\sigma_{th} = -E\varepsilon_{th}$$

where E is the modulus of elasticity.

The resultant forces, N_{th} and M_{th} can be computed by integrating the restraining stresses over the area of the cross section:

$$N_{th} = \int \sigma_{th} dA = -\int E\varepsilon_{th} dA$$

$$M_{th} = \int \sigma_{th} y dA = -\int E\varepsilon_{th} y dA$$

The resulting deformation and curvature at the reference point are:

$$\left\{ \begin{array}{c} \Delta\varepsilon_0 \\ \Delta\chi \end{array} \right\} = \left[\begin{array}{cc} \overline{EA} & -\overline{ES} \\ -\overline{ES} & \overline{EI} \end{array} \right]^{-1} \left\{ \begin{array}{c} -N_{th} \\ -M_{th} \end{array} \right\}$$

$$\left\{ \begin{array}{c} \Delta\varepsilon_0 \\ \Delta\chi \end{array} \right\} = \frac{1}{\overline{E}(\overline{AI}-\overline{S}^2)} \left[\begin{array}{cc} \overline{EI} & \overline{ES} \\ \overline{ES} & \overline{EA} \end{array} \right] \left\{ \begin{array}{c} -N_{th} \\ -M_{th} \end{array} \right\}$$

3.1.2 Equilibrium equations

For any section, the resultant and moment of the stresses over the area must balance the applied loads (axial force and bending moment). In the case of a prestressed concrete section, the contribution of both prestressing and reinforcing steel must be taken into account.

The total concrete strain can be written as sum of the mechanical and thermal strain:

$$\varepsilon_{tot,c} = \varepsilon_{mech,c} + \varepsilon_{th,c}$$

and concrete mechanical strain is:

$$\varepsilon_{mech,c} = \varepsilon_{tot,c} - \varepsilon_{th,c} = \varepsilon_o + \chi y - \varepsilon_{th,c}$$

Total and mechanical strain in the prestressing and reinforcing steel are computed as follows:

$$\varepsilon_{tot,ps} = \varepsilon_{mech,ps} + \varepsilon_{th,ps}$$

$$\varepsilon_{mech,ps} = \varepsilon_{tot,ps} - \varepsilon_{th,ps} = \varepsilon_o + \chi y + \Delta\varepsilon_{p0} - \varepsilon_{th,ps}$$

$$\varepsilon_{tot,s} = \varepsilon_{mech,s} + \varepsilon_{th,s}$$

$$\varepsilon_{mech,s} = \varepsilon_{tot,s} - \varepsilon_{th,s} = \varepsilon_o + \chi y - \varepsilon_{th,s}$$

Finally, the integral of stress over the area must balance the applied axial load, therefore first equilibrium equation will be:

$$N = \int \sigma_c dA_c + \int \sigma_{ps} dA_{ps} + \int \sigma_s dA_s$$

$$\begin{aligned} N = \; &= \int \overline{E_c}(\varepsilon_o + \chi y - \varepsilon_{th}) dA_c + \\ &+ \int \overline{E_p s}(\varepsilon_o + \chi y + \Delta\varepsilon_{p0} - \varepsilon_{th,ps}) dA_{ps} + \\ &+ \int \overline{E_s}(\varepsilon_o + \chi y - \varepsilon_{th,s}) dA_s \end{aligned} \tag{3.1}$$

$$\begin{aligned} N = \varepsilon_o (&\sum_{i=1}^{n} \overline{E_c} A_{c,i} + \sum_{i=1}^{m} \overline{E_{ps}} A_{ps} + \sum_{i=1}^{s} \overline{E_s} A_s + \\ &+ \chi (\sum_{i=1}^{n} \overline{E_c} A_{c,i} y_{c,i} + \sum_{i=1}^{m} \overline{E_{ps}} A_{ps,i} y_{ps,i} + \sum_{i=1}^{s} \overline{E_s} A_{s,i} y_{s,i}) - \\ &- (\sum_{i=1}^{n} \overline{E_c} A_{c,i} \varepsilon_{thc,i} + \sum_{i=1}^{m} \overline{E_{ps}} A_{ps,i} \varepsilon_{thps,i} + \sum_{i=1}^{s} \overline{E_s} A_{s,i} \varepsilon_{ths,i}) + \\ &+ \sum_{i=1}^{m} \overline{E_p s} A_{ps,i} \Delta\varepsilon_{p0} \end{aligned} \tag{3.2}$$

The second equilibrium condition refers to the integral of stresses times the distance from the reference point axis which must balance the applied bending moment, calculated with reference to the same reference point:

$$\begin{aligned} M = \; &\int \sigma_c y_c dA_c + \int \sigma_{ps} y_{ps} dA_{ps} + \int \sigma_s y_s dA_s = \\ &= \int \overline{E_c}(\varepsilon_o + \chi y - \varepsilon_{th}) y dA_c + \\ &+ \int \overline{E_p s}(\varepsilon_o + \chi y + \Delta\varepsilon_{p0} - \varepsilon_{th,ps}) y dA_{ps} \\ &+ \int \overline{E_s}(\varepsilon_o + \chi y - \varepsilon_{th,s}) y dA_s \end{aligned} \tag{3.3}$$

$$
\begin{aligned}
M = \varepsilon_o(&\sum_{i=1}^{n} \overline{E_c} A_{c,i} y_{c,i} + \sum_{i=1}^{m} \overline{E_{ps}} A_{ps} y_{ps,i} + \sum_{i=1}^{s} \overline{E_s} A_s y_{s,i} + \\
&+ \chi(\sum_{i=1}^{n} \overline{E_c} A_{c,i} {y_{c,i}}^2 + \sum_{i=1}^{m} \overline{E_{ps}} A_{ps,i} {y_{ps,i}}^2 + \sum_{i=1}^{s} \overline{E_s} A_{s,i} {y_{s,i}}^2) - \\
&- (\sum_{i=1}^{n} \overline{E_c} A_{c,i} \varepsilon_{thc,i} y_{c,i} + \sum_{i=1}^{m} \overline{E_{ps}} A_{ps,i} \varepsilon_{thps,i} y_{ps,i} + \\
&\sum_{i=1}^{s} \overline{E_s} A_{s,i} \varepsilon_{ths,i} y_{s,i}) + \sum_{i=1}^{m} \overline{E_p s} A_{ps,i} \Delta\varepsilon_{p0} y_{ps,i}
\end{aligned}
\tag{3.4}
$$

Rewriting the equations in matrix form, we get:

$$
\left\{ \begin{array}{c} N_{eq} \\ M_{eq} \end{array} \right\} = \left[\begin{array}{cc} \overline{EA} & -\overline{ES} \\ -\overline{ES} & \overline{EI} \end{array} \right] \left\{ \begin{array}{c} \varepsilon_o \\ \chi \end{array} \right\}
$$

where:

$$
\overline{EA} = \sum_{i=0}^{n} E_{c,i} A_{c,i} + \sum_{i=0}^{m} E_{ps,i} A_{ps,i} + \sum_{i=0}^{s} E_{s,i} A_{s,i}
$$

$$
\overline{ES} = \sum_{i=0}^{n} E_{c,i} S_{c,i} + \sum_{i=0}^{m} E_{ps,i} S_{ps,i} + \sum_{i=0}^{s} E_{s,i} S_{s,i}
$$

$$
\overline{EI} = \sum_{i=0}^{n} E_{c,i} I_{c,i} + \sum_{i=0}^{m} E_{ps,i} I_{ps,i} + \sum_{i=0}^{s} E_{s,i} I_{s,i}
$$

$$
N_{eq} = N_{ext} + \sum_{i=0}^{n} N_{th,c,i} + \sum_{i=0}^{m} N_{th,ps,i} + \sum_{i=0}^{s} N_{th,s,i} - \sum_{i=1}^{m} \overline{Ep_s} A_{ps,i} \Delta\varepsilon_{p0}
$$

$$
M_{eq} = M_{ext} + \sum_{i=0}^{n} M_{th,c,i} + \sum_{i=0}^{m} M_{th,ps,i} + \sum_{i=0}^{s} M_{th,s,i} - \sum_{i=1}^{m} \overline{Ep_s} S_{ps,i} \Delta\varepsilon_{p0} y_{ps,i}
$$

$$\left\{ \begin{array}{c} \Delta\varepsilon_0 \\ \Delta\chi \end{array} \right\} = \left[\begin{array}{cc} \overline{EA} & -\overline{ES} \\ -\overline{ES} & \overline{EI} \end{array} \right]^{-1} \left\{ \begin{array}{c} N_{eq} \\ M_{eq} \end{array} \right\}$$

$$\left\{ \begin{array}{c} \Delta\varepsilon_0 \\ \Delta\chi \end{array} \right\} = \frac{1}{\overline{E}(\overline{AI} - \overline{S}^2)} \left[\begin{array}{cc} \overline{EI} & \overline{ES} \\ \overline{ES} & \overline{EA} \end{array} \right] \left\{ \begin{array}{c} N_{eq} \\ M_{eq} \end{array} \right\}$$

3.1.3 Approach for the application of the sectional analysis

The first step in performing a sequentially-coupled thermo-mechanical analysis is to perform a 2D thermal analysis of the section, given that the advanced methods for (sectional) mechanical analysis require the knowledge of the temperature at each point of the section, in order to explicitly evaluate the decay of the mechanical properties of concrete and steel. The heat transfer problem is uncoupled from the mechanical problem, which means that the temperature field inside the section can be determined without previous knowledge of the stress/strain field, i.e. the temperature distribution inside the section/member is not, in any way, influenced by the stress/strain state. On the other hand, the stress/strain field is obviously dependent on the temperature field. As a consequence, mechanical analysis cannot be performed without knowing the temperature at each point of the cross section, which makes the whole thermo-mechanical problem sequentially coupled. Thermal analyses were performed by means of the commercial software ABAQUS 6.16 (ABAQUS, 2016). The heat transfer within the element takes place through conduction, while at the boundaries heat is transferred through convection and radiation. The convection coefficient is set to 25 W/m^2K in the case of convection to hot environment and 9 W/m^2K in the case of convection to cold environment. Emissivity coefficient of the faces directly exposed to fire is set to 0.7, as prescribed in EN 1992-1-2, while at the faces in contact with cold air (20°C) the convection coefficient implicitly includes the radiation. In the case of reinforced concrete sections in fire, the heat transfer is a transient nonlinear problem, be-

cause of non-linearity and temperature-dependency of boundary conditions and materials' thermal properties. Iterative scheme is therefore used to obtain the solution. Sections are discretized into a number of finite elements. In the case of reinforced concrete sections, it is commonly accepted to model only the plain concrete section. This is because the high conductivity of steel (and therefore its high diffusivity) allows a quick attainment of the thermal equilibrium between the steel and the surrounding concrete and because the area of reinforcing steel is small compared to the area of the surrounding concrete. Hence, the temperature at the centroid of the steel bars is taken equal to the temperature of concrete at that position. In this work, linear triangular (DC2D3) and quadrilateral (DC2D4) heat transfer elements were used to discretize the concrete sections. In these elements, the only active degree of freedom is the nodal temperature. Clearly, the thermal field could be worked out equally well by means of other softwares, or taking advantage of other approaches, such as the approximated analytical expressions by Wickstrom (1986). The output of the thermal analysis, consisting of the temperature values, is used as input for the subsequent mechanical analysis, in order to work out the evolution of the mechanical properties of the materials as a function of temperature. The objective of the mechanical analysis is to obtain the deformations (axial strain and curvature) of the section as a function of time. The failure of the most stressed section is then indicated by a divergence of the deformation values. The sectional analysis requires an iterative procedure, where the final results for a given fire duration are obtained once the equilibrium equations are satisfied, within the prescribed tolerance on the total axial force N (in pure bending N = 0) acting on the section ($\Delta N < 10^{-5}$). The iterative procedure was implemented in a purposely developed code, and enabled the deformation history to be traced over the whole fire duration. Sectional failure is thus attained if equilibrium is not possible, with the aforementioned divergence of the deformations (structural end point). A schematic representation of the code structure is shown in Figure 3.1.

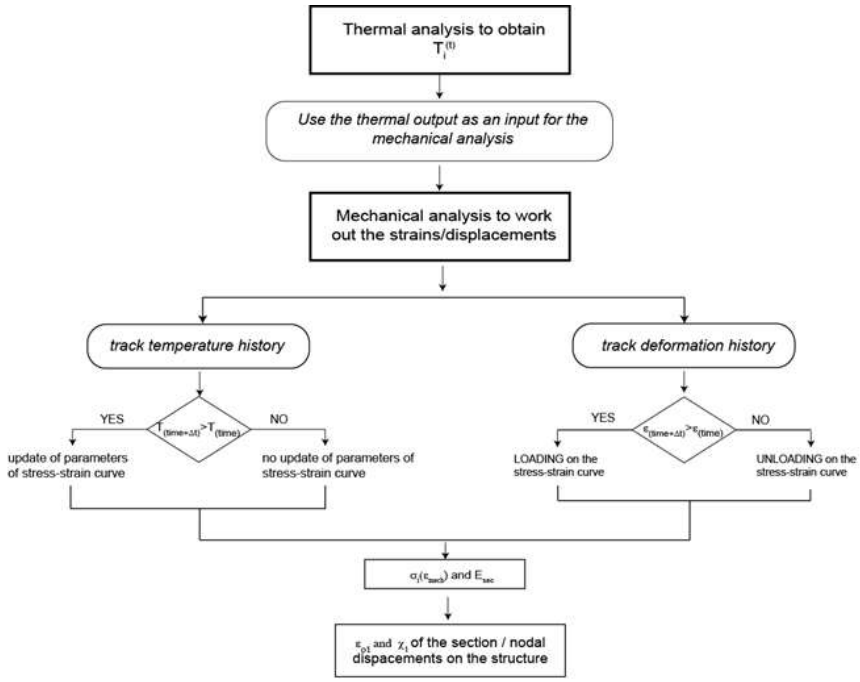

FIGURE 3.1: Flowchart of the code structure.

3.2 Mechanical properties of concrete

3.2.1 Thermal strain

The irreversibility of thermal dilation is one of the peculiar features of a full heating-cooling cycle. As thermal dilation is, at least in part, due to irreversible phenomena (micro- and macro-cracking) that take place upon heating because of the thermal incompatibility between aggregates and cement paste, a certain amount of residual deformation is to be expected after cooling (Khoury et al., 1986). Residual

thermal strain is discussed in more detail in Chapter 2.

Results from the experiments performed by Franssen (1993) suggest that the maximum temperature governs the amount of residual elongation, and that for maximum temperatures lower than 500°C, no significant residual elongation is to be expected (full reversibility of the thermal deformation). For maximum temperatures beyond 500°C, residual deformation varies between 55 and 65% of the elongation corresponding to the maximum temperature. Bearing in mind the aforementioned evidences, the following assumptions were adopted in the present work:

- the residual deformation for maximum temperatures below 500°C is negligible;
- above 500°C, the residual thermal deformation is equal to 50% of the maximum thermal dilation attained during the fire.

Clearly, these assumptions lead to a discontinuity of the residual thermal deformation at 500°C: whereas this may lead to in consistent numerical results in principle, it was not the case in all the analyses presented herein, also because the strain compatibility along the section tends to accommodate the strain discontinuities at different points. The adopted thermal strain evolution during heating and cooling is plotted as a function of temperature Figure 3.2: the evolution of the thermal dilation with temperature was computed according to the provisions by European Committee for Standardization (2005b) for concrete with siliceous aggregate.

3.2.2 Constitutive model

Accounting for the cooling phase in a constitutive model implies several peculiar issues to be addressed. If only the heating phase is considered, assuming monotonic loading at each point generally yields good results, though some unloading, due to thermal gradients, may occur in the core of the section. On the contrary, if the temperature-time curve includes a cooling phase, EN 1992-1-2 clearly points out

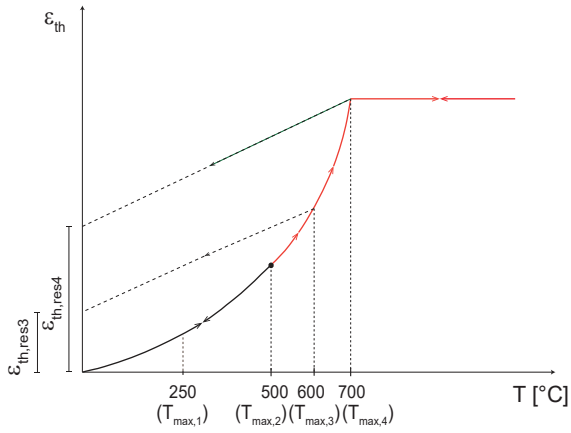

FIGURE 3.2: Free thermal strain of concrete at elevated temperatures and during subsequent cooling.

that the constitutive law for concrete in compression should be suitably modified; in more detail, the possibility of unloading should be explicitly included, as well as the additional strength decay in the cooling phase, and the constitutive law modified accordingly. In other words, concrete compressive behaviour cannot be considered elastic (though nonlinear, as done in previous research works - REF). In the following, the loading branch coincides with the stress-strain law provided by European Committee for Standardization (2005b), whereas unloading is assumed to take place along a linear branch, with the slope defined by the residual elastic modulus. This assumption complies with the fact that the transient and creep strains, that are responsible for the increased deformability of concrete upon first heating, are not recovered during unloading and are not present at all when the residual behaviour of concrete is considered (Khoury

et al., 1986, Torelli et al., 2016). As a consequence, the residual elastic modulus at any temperature is larger than the elastic modulus in hot conditions, the difference being the irreversible components of strain: $E_{res} = kE_{hot}$ where E_{hot} is the initial tangent modulus of elasticity in hot conditions, and k is a constant value (with $k > 1$, as commonly found in laboratory tests (Bamonte and Gambarova, 2014, Bamonte and Gambarova, 2016). As can be seen in Figure 3.4(a), once the stress corresponding to the peak strain is attained, only plastic loading (with increase in strain increment) or unloading along a linear branch (if strain increment is negative) can occur. It is worth noting that the stress can go to zero with a strain value (i.e. cracking strain) greater than zero. Below this strain value, as it is usually done in the numerical analysis of reinforced concrete members, the contribution of the tensile stresses is neglected. By keeping track of the strain corresponding to the peak stress, loading and unloading can occur as many times as required, with the cracking strain shifting and the stress-strain curve changing shape. Detailed representation of loading-unloading paths during heating phase (when the stress-strain curves are updated at each time increment) can be seen in the Figure 3.3). As for thermal damage, during the heating phase the stress-strain curves are adapted to allow for decreasing compressive strength and increasing deformability. During the cooling phase, since thermal damage is considered as a function of maximum temperature only, the parameters of the stress-strain curves are not updated. This last assumption implies that the extra-damage taking place during the cooling phase is neglected. As regards this last assumption, it is worth noting that the difference between "hot" and residual compressive strength is usually rather limited (10% according to the provisions contained in EN 1994-1-2).

3.3 Mechanical properties of steel bars

3.3.1 Thermal strain

The thermal strain for both prestressing and reinforcing steel is computed according to the provisions by European Committee for Standardization (2005b). Steel is considered to recover its thermal properties upon cooling; as a consequence, no residual thermal strain is assumed. This assumption is in agreement with the rather limited number of experimental results available to date (Elghazouli et al., 2009, Mohamed and Salah, 2012).

3.3.2 Constitutive model

For both prestressing and reinforcing steel, elastic-perfectly plastic stress-strain laws with linear unloading branch were assumed (Figure 3.4(b)). As a consequence, there is no difference between the proportional limit and the yield strength. Since for significant fire durations and/or at impending collapse steel is likely to be yielded, this assumption plays a minor role on the results. The constitutive model has the same shape for ordinary and prestressing steel, the only major difference being the thermal decay of the mechanical properties, that is higher in prestressing steel, as recalled in Chapter 2. The evolution of the stress-strain law at any given point is governed by the maximum experienced temperature and loading history. The accumulation of residual plastic deformation changes the position, but not the shape of the stress-strain diagram. The effects of creep (and the relaxation of prestressing steel) are implicitly taken into account by reducing the modulus of elasticity with increasing temperature.

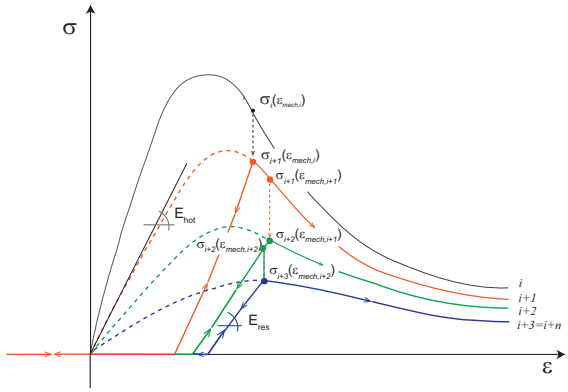

FIGURE 3.3: Qualitative sketch of the possible loading-unloading paths during heating phase - stress strain curve updated at each time increment i.

3.4 Sectional analysis of reinforced concrete beams

Sectional analysis is a very efficient tool for studying the behaviour of reinforced concrete beams that are simply supported at their ends. Behaviour of those beams can be well described by considering only the midspan section. In Chapter 2, some of the available experimental studies on reinforced concrete beams exposed to natural fires have been described. The residual tests performed on the RC beams at the Michigan State University (Agrawal and Kodur, 2018, Kodur et al., 2003) served as basis for the numerical analyses presented herein, given that the beams were simply supported and tested under natural fires. In Kodur et al. (2003), a set of three reinforced concrete beams were subjected to fire curves with heating and cooling phase, and then tested for measuring their residual bearing capacity. Two beams (B1 and B3) were tested with axial restraints at the extremities, while B2 was simply supported. For the purpose of validation, B2 was chosen, because of its structural layout. The reinforcement

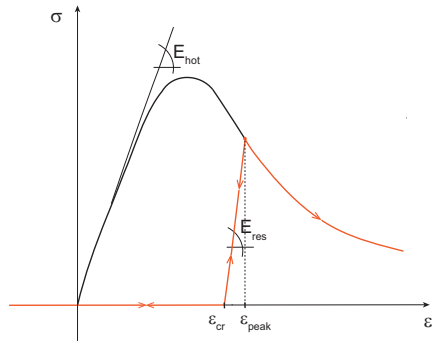

(a)

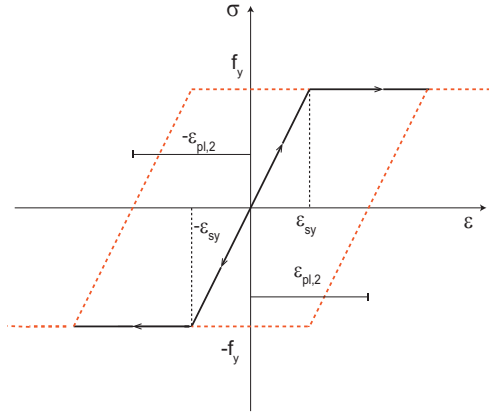

(b)

FIGURE 3.4: Material stress-strain model at a given temperature, in loading and unloading, for: (a) concrete in compression; (b) steel.

consisted of $\phi 19$ mm bars as bottom reinforcement, two $\phi 13$ mm bars as top reinforcement, while the shear reinforcement consisted of $\phi 6$ mm stirrups at a spacing of 150 mm (Figure 3.5). The steel of the flexural reinforcement had specified yield strength of 420 MPa.

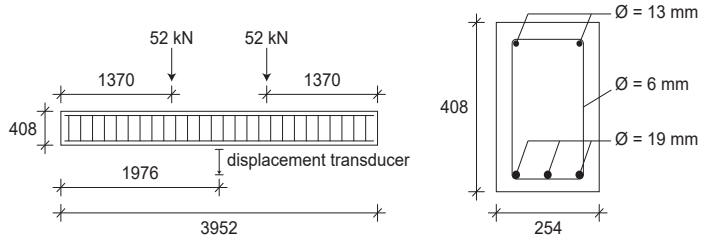

FIGURE 3.5: Geometry and transverse section of the beam tested in Kodur et al. (2003) and Agrawal and Kodur (2018).

Beam B2 was tested under a so called "short" design fire (SF), with the ambient temperature quickly peaking 1100°C, after what the temperature is kept constant for the next 45 minutes or so. This "rest" phase is followed by a descending branch with a cooling rate of approximately 5°C/min. The lower curve of thermal conductivity suggested in EN 1992-1-2 was used for the thermal analysis; moreover, the thermal behaviour was considered fully reversible. The comparison between numerical and experimental results is shown in Figure 3.6(a). On the whole, the agreement is good, both in the heating and in the cooling phase. There is a slight overestimation of the maximum temperature that could be due the heat dispersion along the length of the member, which is present in the tests but cannot be captured by means of 2D analyses.

Decay of the concrete strength, irrecoverable in the cooling phase, and thermal strain were assumed as per recommendations by European Committee for Standardization (2005b) for calcareous aggregate. The thermal strain was considered irreversible upon cooling if the maximum concrete temperature exceeds 500°C; the value of the residual thermal strain was taken equal to 50% of the value at the maximum temperature. The decay of the yield strength and elastic modulus of steel was assumed as per European Committee for Standardization (2005b) and the behaviour was considered irreversible,

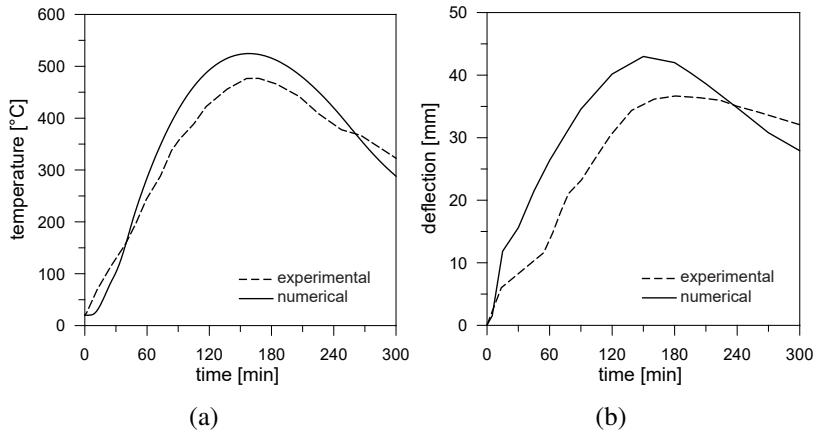

(a) (b)

FIGURE 3.6: Comparison between experimental results and numerical simulations: (a) temperature in the rebars; (b) deflection at midspan (Kodur et al., 2003).

while the thermal strain (also taken from EN 1992-1-2) was considered fully recoverable. The comparison between numerical and experimental results is shown in Figure 3.6(b). The agreement is satisfying, as regards the value of the maximum deflection and its time of occurrence: it is worth noting that no information were provided as regards the evolution of the thermal and mechanical properties with temperature. On the whole, the numerical approach appears to overestimate the deflections throughout the heating phase: this fact could be explained by bearing in mind that in the numerical analyses the contribution of concrete in tension was neglected. Moreover, the decay of the mechanical properties prescribed by European Committee for Standardization (2005b) is somewhat more severe than what was found in the literature (Abrams, 1971). Agrawal and Kodur (2018) tested two RC beams with rectangular cross section (Figure 3.5). Beam B1 was made of HSC and exposed to long-duration design fire (LF) , while B2, made of NSC, was exposed to short duration

design fire (SF) (Figure 3.7(a)). Both beams were made with calcareous aggregate concrete. The beams were simply supported, and subjected to two-point loading that produced bending moments corresponding to 58% (B1) and 54% (B2) of beam flexural capacity. In the case of beam B1, the applied loads were removed after approximately 300 minutes, once rebar temperatures dropped below 300°C and midspan deflections began to recover. Thermal and structural response of the beams was measured during both heating and extended cooling phase of fire, until the entire cross-section of the structural member cooled down to ambient temperature.

3.4.1 Parametric study and results

Results from the sectional analyses performed on the two beams is given in the following. Curvature is integrated along the length of the beam - more specifically, 10 sections along the half-span of the beam, subjected to different bending moments (from $M = 0$ to $M = M_{max}$), were considered for a midspan deflection calculation. The results are then compared against the deflections measured in the test, for both Beam B1 and B2 (Figure 3.10). Though the heating phase duration lasted 120 and 90 minutes for Beam B1 and B2 respectively, it can be seen that the rebar temperature increases well after the onset of cooling phase of fire. Temperature rise is observed until 180-200 minutes, and this prolonged heating inside the member is even more pronounced for Beam B2, due to the low cooling rate (Figure 3.7(b)). Beam B1 experienced higher temperatures than B2, due to the more severe fire scenario it was exposed to. Numerical prediction of the peak temperatures and temperatures during cooling is in agreement with the experimental values. Delayed heating is also correctly captured by the model. Thermal field inside the section is presented in Figure 3.8 and Figure 3.9, where it can be seen the non-uniform cooling of the concrete.
The displacement evolution can be described as a three-stage process. In the first stage, deflections increase due to thermal gradients

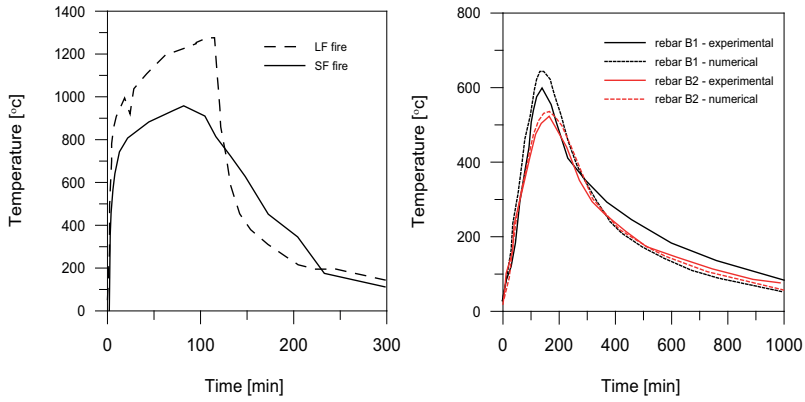

(a) (b)

FIGURE 3.7: (a) Time-temperature curve for the two design fires used in the test (from (Agrawal and Kodur, 2018)); (b) Measured and predicted rebar temperature as a function of time for B1 and B2 beams.

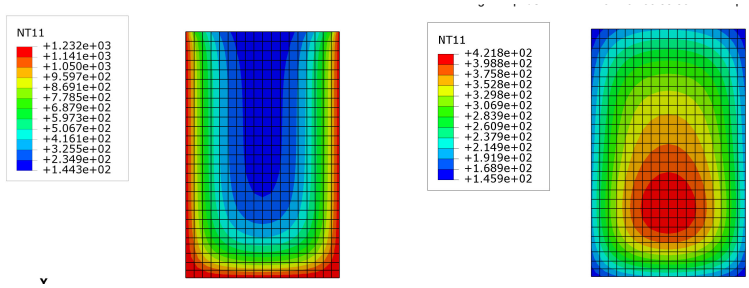

(a) (b)

FIGURE 3.8: Thermal field inside the section for the beam B1 (Agrawal and Kodur (2018)): (a) at the end of the heating phase (b) in the cooling phase, 3h into the fire exposure.

that develop within the section and also due to the quick increase of the deformability of concrete and steel. The second stage starts with

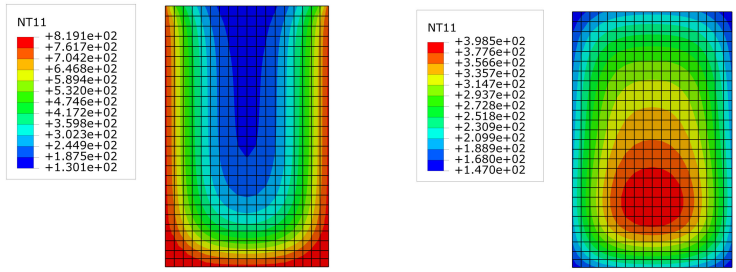

(a) (b)

FIGURE 3.9: Thermal field inside the section for the beam B2 (Agrawal and Kodur (2018)): (a) at the end of the heating phase of fire (b) in the cooling phase, 5h into the fire exposure.

the cooling down of the rebars, i.e. when the steel bars start to recover their strength and stiffness. This leads to deflection trend reversal and to a certain amount of recovery in the deflections. Eventually, deflection tends to stabilize in Stage III, once the rebar temperatures are below 150°C.

The test results proved that the rate of recovery in deflections during cooling mainly depends on the rate of cooling (slow or fast cooling) and also on the load acting on the beam. Beam B1 was cooled down faster than B2, which enhances the deflection recovery. Moreover, the load was removed from B1 at some point, finally leading to a relatively low residual deflection and recovery of around 80% with respect to the peak value. Though the peak deflection is somewhat underestimated by the numerical model, residual deflection is predicted well. Due to the load removal, numerical model produces a very steep deflection profile - with a sudden drop - at the moment of removal, while in the experiment, the load was probably removed more gradually. In the experiment, beam B2 recovered only 15% of their peak deflection during cooling, as a consequence of slower cooling rate and the continued presence of the load present during the test.

Slow cooling can be disadvantageous as it leads to prolonged temperature rise inside the member and delayed thermal damage. Numerical model for Beam B2 overestimates the deflections in Stage I, while the predicted deflections during cooling are consistently lower than the test values. Numerical model predicted around 40% of the deflections recovery with respect to the peak value, which is much more than what was observed during the test.

Influence of irrecoverable thermal damage in steel rebars

In the Figure 3.11 the influence of the recoverability of the strength and stiffness in the steel rebars on the deflections is presented. As it has been already pointed out, in simply supported beams under bending, it is the steel that governs the deflection response. Therefore, it is of practical interest to see how the loaded beam will respond to a thermal solicitation if the irrecoverable damage in the steel rebars that takes place during cooling is not accounted for. Maximum temperatures in the steel bars for Beam B1 is around 650°C while in Beam B2 is was around 540°C. note that these temperatures have been reached in the cooling phase of fire. For such high temperatures (especially in Beam B2), it is realistic to expect that significant creep will develop and the properties of the steel will not be recovered upon cooling. Looking at the deflection evolution in time, neglecting the thermal damage in the steel bars (recoverable properties) leads to a non-conservative displacement prediction. Residual deflections are significantly underestimated.

Influence of transient creep and residual thermal strain

Another interesting parameter to study is the transient creep consideration (Figure 3.12(a)). Two models have been compared - Eurocode model that considers the transient creep implicitly and the explicit model by Gernay and Franssen (2012). Slight difference in the deflection response for these two models can be seen in the cooling phase, with the explicit model yielding results that are slightly closer

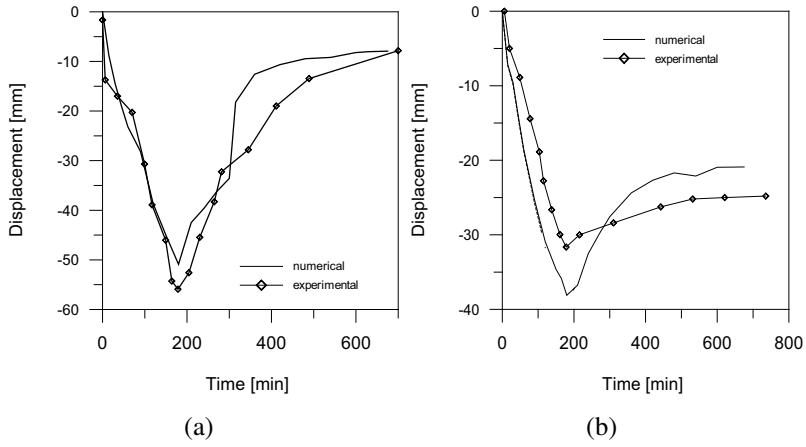

FIGURE 3.10: Displacement evolution for: (a) beam B1; and (b) beam B2; comparison between experimentally and numerically obtained values.

to the experimental ones, but on overall, the difference is not significant. Similar findings for the role of the transient creep strain in the structural response of RC beams were obtained in Lu et al. (2015). In addition, a set of analyses has been performed by considering the thermal strain of concrete as fully recovered upon cooling, so to check the influence of such parameter on the structural response of RC beams. As it can be seen in Figure 3.12(b), the two different assumptions regarding the reversibility of thermal strain lead to almost identical results. What has been demonstrated by the results in Figure 3.12 is rather expected, as these two parameters concern the concrete model; therefore, they would be more significant for structures whose behaviour is governed by concrete (for example, axially loaded RC columns) and not by steel, as it the case in beams, where the reinforcement ratio is kept low in order to ensure ductile failure.

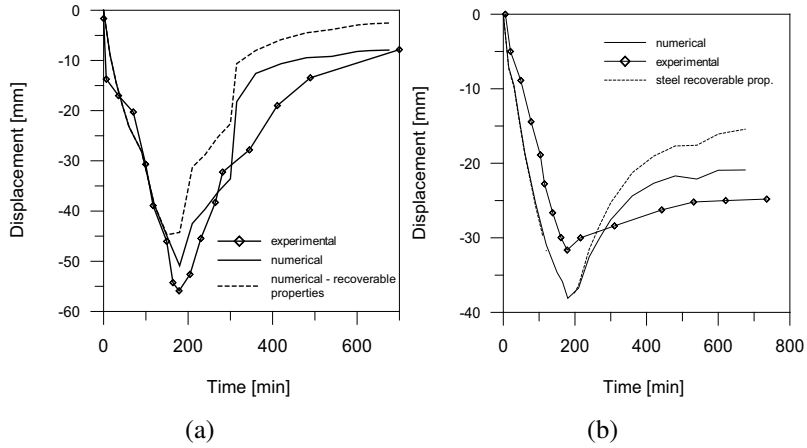

FIGURE 3.11: Displacement evolution for: (a) beam B1; and (b) beam B2; comparison between experimentally and numerically obtained values by considering steel mechanical properties as irrecoverable (label numerical) or recoverable upon cooling.

Influence of unloading modulus

Finally, influence of the unloading modulus on the response of Beam B2 has been studied. Constitutive model of concrete allows an unloading along a linear branch, defined by the residual elastic modulus. As a reference value, residual elastic modulus is considered 25% higher than the initial tangent modulus, as to account for the strain components that do not recover during cooling (Figure 3.4(a)). In addition, the unloading modulus equal to the initial tangent modulus (k=1) and a nonlinear elastic behaviour (loading and unloading along the same path - i.e. along the stress-strain curve) have been studied. As it can be seen in Figure 3.13, the obtained responses are very similar and the unloading effect proved not to play a big role. This is partly due to the fact that, as previously mentioned, the behaviour of beams is more sensitive to the changes in steel properties and also because the unloading mainly takes place during cooling, when the

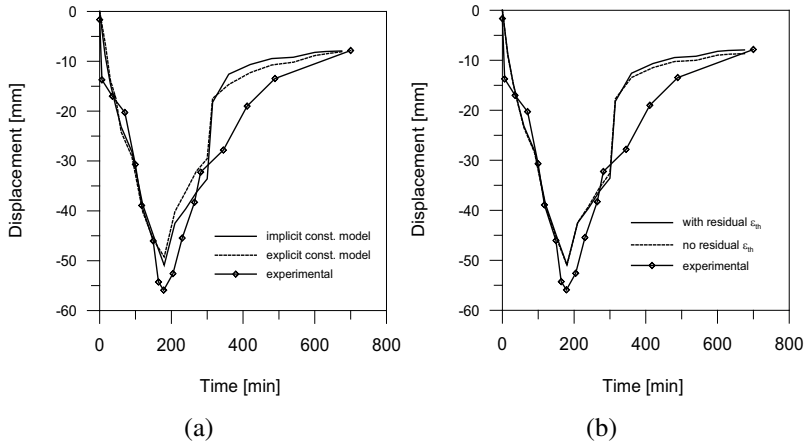

FIGURE 3.12: Displacement evolution for beam B1: (a) with explicit and implicit constitutive model; and (b) with and without residual thermal strain.

stresses on the section are quite low and any difference in stress calculation caused by allowed unloading is not significant.

3.5 Sectional analysis of prestressed concrete beams

Prestressed concrete members are widely used in a variety of structural applications. In comparison to ordinary reinforced concrete members, they offer several advantages, such as higher speed of construction and larger span-to-depth ratios (Collins and Mitchell, 1997). The use of prestressing allows improving the mechanical performance of reinforced concrete members, by limiting cracking phenomena, and thus increasing the stiffness. Optimization of structural behaviour, which is typical of the prefabrication industry where prestressing is widely used, makes it also possible to reduce the overall dimensions

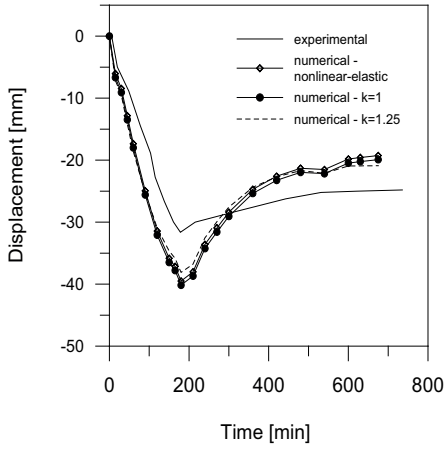

FIGURE 3.13: Influence of the unloading modulus on the deflection response of beam B2.

of the members: in fact, several types of prestressed members available on the market are characterized by thin concrete webs. In comparison to reinforced concrete members, prestressed concrete members are more sensitive to fire (Buchanan, 2001). In detail: (a) cold worked prestressing steel is more sensitive to high temperatures than ordinary hot rolled steel; (b) the reduced thickness that characterizes prestressed concrete members results in lower steel protection: this is particularly true in structures that were built before the publication of the current standards, where the typical prescriptions concerning concrete cover are not respected; and (c) the lack of connectivity between the structural members (which is directly related to construction time savings) results in statically-determinate structures, where the redistribution of the internal forces is not possible, to the detriment of the structure's global stability. Finally, prestressed concrete members in demanding structures (such as industrial facilities) are subjected to a higher risk of fire exposure, because of the higher availability of combustible materials. As previously mentioned, this is particularly dangerous for several existing structures, which do not com-

ply with current code provisions as regards concrete cover. Two of the abovementioned factors, namely the lack of connectivity between prestressed structural members in a variety of practical applications and the relevance (also from the economic point of view) of natural fires in demanding structures and facilities, point to importance of sectional analysis when prestressed members are at issue. The failure of simply supported prestressed members in fire can be identified by taking into consideration the most stressed section, i.e. midspan (Figure 3.14). This criterion is typically used for checking the safety under standard fires (Gustaferro, 1973, Gustaferro and Martin, 1989). The same basic concept is applied in the following to the case of natural fires to identify the structural end point, i.e. the situation when the moment capacity is overcome by the applied moment. For simply supported members under distributed loads (or similar) and uniformly exposed to fire, failure is still governed by the most stressed section. It is worth pointing out that this sectional approach is applicable to both pre-tensioned members and post-tensioned members with bonded tendons, thanks to the bond between the strands (in the former case) or the tendons (in the latter case, achieved by means of grouting) and the surrounding concrete. By contrast, in members post-tensioned with unbonded tendons, where the compliance between the tendons and the concrete takes place only at the extremities, the structural analysis requires the deformations along the whole member to be considered, and thus a complete structural analysis of the whole member.

3.5.1 Parametric study and results

Parametric analyses were performed on the sections of two typical prestressed concrete members, namely an I-girder and a double tee (Figure 3.15) (Bamonte et al., 2018). The two sections, representative of simply supported members commonly found in industrial buildings (Collins and Mitchell, 1997), are interesting for a variety of reasons: the I-girder has a thin web with a massive bottom flange

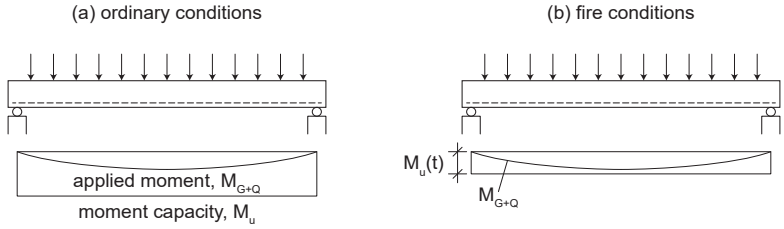

FIGURE 3.14: Moment capacity and applied moment in simply supported members: (a) at ambient temperature and (b) in fire conditions.

(where most of the prestressing steel is located), while the double tee has very thin webs and flange, and consequently a low cover to the prestressing steel located in the webs. The aforementioned characteristics are instrumental for highlighting the role played by the concrete cover in delaying the attainment of the maximum temperature in the prestressing steel. Moreover, more than 95% of the bending capacity in ordinary conditions of the double-tee section is provided by the prestressing steel, while in the I-girder section the prestressing steel provides 65% of the bending capacity, the remainder being provided by the ordinary reinforcing steel, that is present to ensure additional resources in the event of cracking.

As it was done in previous studies (Kodur and Agrawal, 2016, Gernay and Dimia, 2012, Gernay and Franssen, 2015), the time - temperature curve was derived from the parametric fire model devised in EN 1991-1-2 (European Committee for Standardization (2004a)), by setting the factor G (that accounts for parameters such as ventilation and thermal inertia of the enclosure) equal to 1. In this way, the heating phase coincides with the ISO-834 fire curve (Figure 3.16) (Gernay and Franssen (2012)). As for the cooling phase, a linear decrease of temperature with time was adopted (European Committee for Standardization, 2004a, Feasey and Buchanan, 2002). The thermal properties were assumed following the provisions of EN 1992-1-2. The mean value of conductivity was used. Moreover, the specific heat for

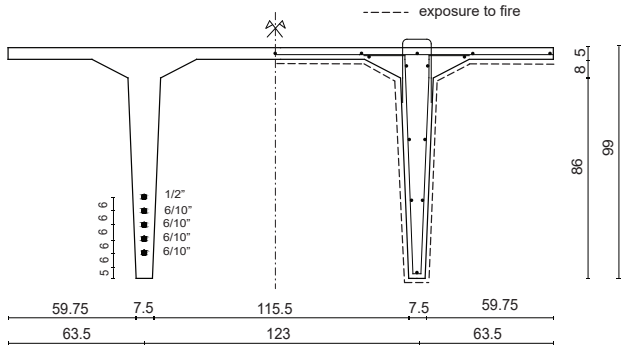

(a)

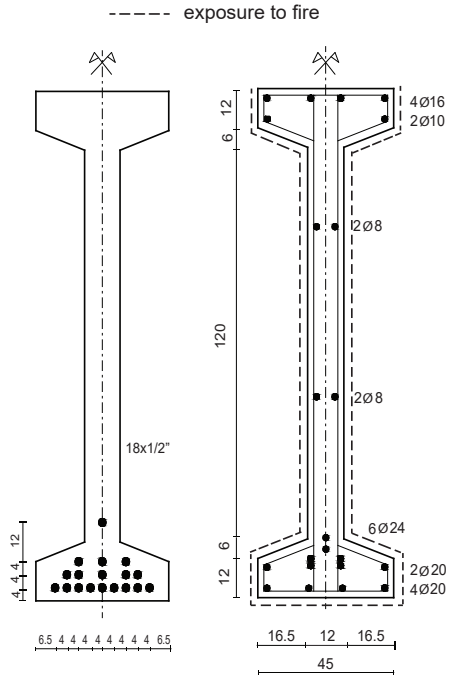

(b)

FIGURE 3.15: Prestressed sections considered in the numerical analyses (prestressing steel on the left, ordinary steel at the right): a) double-tee section; b) I-girder.

dry concrete was assumed. The thermal properties were considered reversible in cooling and are thus a function of temperature only. Finally, the presence of ordinary and prestressing steel was neglected in the thermal analysis. For both sections, the following reference mechanical properties at ambient temperature were assumed:

- concrete compressive strength: f_c= 40 MPa;
- modulus of elasticity and yield strength of mild steel: E_s = 210 GPa, f_{sy} = 500 MPa;
- modulus of elasticity and yield strength of prestressing steel: E_p = 195 GPa, f_{py} = 1860 MPa (note that since the constitutive law of prestressing steel is assumed to be elastic-perfectly plastic, Figure 3.4(b), there is no difference between yield and ultimate strength)
- prestressing level at the onset of fire: σ_0 = 1000 MPa.

The value of the prestressing level at the onset of fire was determined by considering the typical value of prestressing before long term losses (1200-1300 MPa), and accounting for 15-20% of decrease due to creep and shrinkage of concrete, and relaxation of the prestressing steel (Bamonte and Pisani, 2015, 209, 1992). As for the evolution of the mechanical properties with temperature, the values suggested in EN 1992-1-2 for siliceous concrete, ordinary and prestressing steel were assumed. Siliceous concrete was chosen, because it is known to be more sensitive to high temperatures than concretes containing other types of aggregate (e.g. calcareous or basalt). In prestressed concrete members, however, failure is expected to be governed by prestressing steel, and the thermal decay of concrete plays a minor role.

Several parameters were varied, in order to investigate their influence on the behaviour of the selected prestressed concrete beam sections, and thus to get sound conclusions about their influence on

the failure. A first set of preliminary analyses was devoted to investigate the role of the residual thermal deformation and level of prestressing, in order to check the validity of the assumptions made for the values of these two parameters. Moreover, the role of the irreversible strain components is studied through comparison of the proposed model with a recently formulated explicit model (Gernay and Franssen (2012)). Fire severity, determined by the duration of the heating phase and the cooling rate, is certainly among the most critical parameters governing the response. If the failure of the section, whether in the heating or in the cooling phase of a fire, is to be studied, then the maximum temperature in the section, and most importantly in the prestressing steel, can provide useful information. The duration of the heating phase was varied from 30 to 120 minutes for the I-girder and from 15 to 60 minutes for the double-tee (with the cooling rate fixed at 5°C/min). Different cooling rates were considered (3, 5 and 10°C/min), in accordance with European Committee for Standardization (2004a) (where cooling rates ranging from 250 to 625°C/h are devised), for a fixed heating phase duration of 60 minutes for the I-girder and 30 minutes for the double-tee.

Load level is a parameter of utmost importance. It is expressed as the ratio of the externally applied bending moment to the ultimate moment capacity at ambient temperature. Three values were considered in this work: $M/M_u = 0$, 0.15 and 0.30, where M is the bending moment acting at midspan at the onset of fire and M_u is the bearing capacity in bending at midspan assuming the characteristic values of the materials properties (partial safety factors γ_c= γ_s= γ_p = 1). While the largest value can be considered realistic for members with a significant share of variable loads (Q_{k1}/G_k = 1.5, $\psi_{1,1}$ = 0.2 (European Committee for Standardization (2005b)), the zero value is not possible in reality, as at the very least self-weight will be present. This value is interesting, however, in order to investigate the effects of prestressing alone, to better highlight its contribution to the in-time evolution of the curvature of the section.

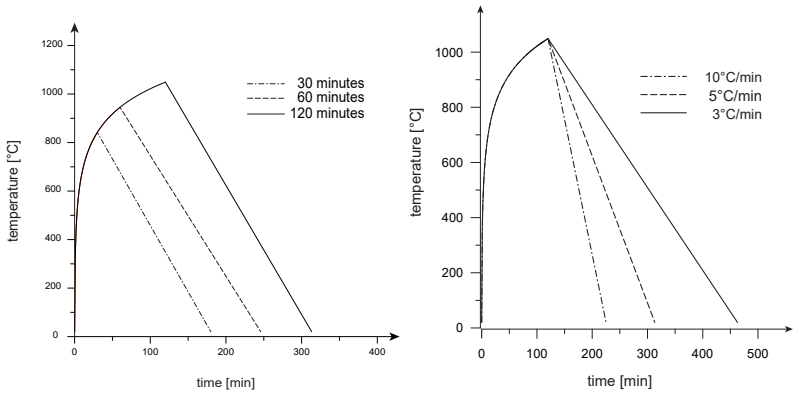

(a) (b)

FIGURE 3.16: Fire scenario: (a) variation of the duration of heating phase, at constant cooling rate (5°C/min); and (b) variation of the cooling rate, at constant duration of the heating phase (120 minutes).

Role of the thermal field

Given that almost the full moment capacity of the double-tee section is provided by the prestressing steel, it is more than clear that a sizable loss of stiffness and strength has to be prevented in order to avoid failure. However, since the concrete cover is rather thin (average of 3 cm, Figure 3.15), very high temperatures are likely to be attained in most cases. In Figure 3.17(a), the average temperature in the strands is plotted as a function of the duration of the heating phase, for the reference cooling rate of 5°C/min. It is worth noting that the temperature increase continues long after the onset of the cooling phase: as a matter of fact, the maximum temperature is reached at approximately 90 and 100 minutes for heating phase durations of 15 and 30 minutes respectively, and at 130 minutes for heating phase duration of 60 minutes. As previously mentioned, this can be attributed to the low conductivity and high thermal capacity of concrete, which delay the heat transfer towards the inner layers of the section. Note

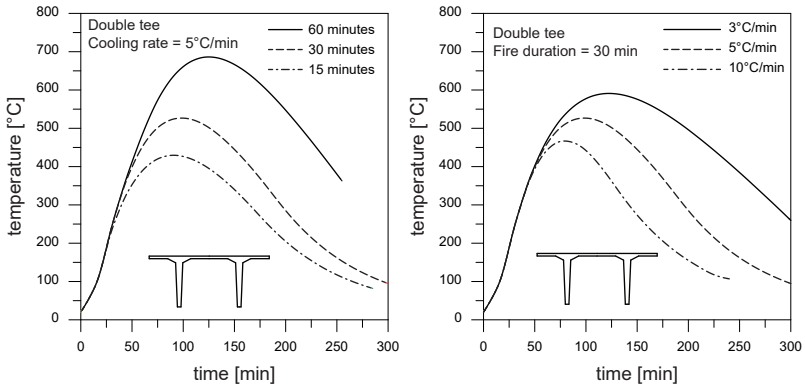

(a) (b)

FIGURE 3.17: Double-tee section: (a) average temperature in the strands as a function of the duration of the heating phase (cooling rate = 5°C/min); (b) average temperature in the strands as a function of the cooling rate (fire duration = 60 min).

that failing to account for the cooling phase leads to a significant underestimation of the maximum temperature (from -40 to -75%). In Figure 3.17(b), the average temperature in the strands is plotted as a function of the cooling rate, for the reference duration of the heating phase of 30 minutes. The maximum temperature in the prestressing steel is significantly lower for a cooling rate of 10°C/min than for 3°C/min (-25%), something that reduces the likelihood of delayed failure in the cooling phase. Similar considerations hold for the I girder (Figure 3.20): in this case the prestressing steel has better protection than in the double-tee section, since all prestressing strands are located in the massive bottom flange (Figure 3.15(b)). As a consequence, higher durations of the heating phase are needed to attain the same temperature levels attained in the double-tee section.

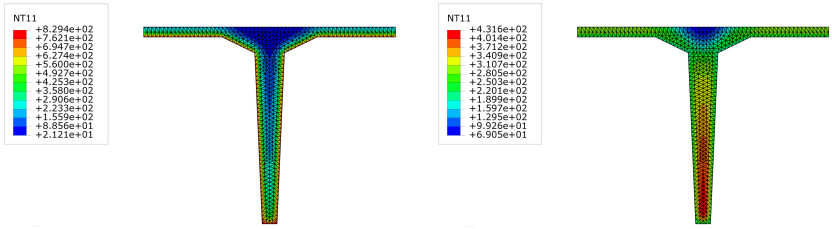

(a) (b)

FIGURE 3.18: Thermal field inside the double tee-beam: (a) at the end of the heating phase (b) in the cooling phase, 90 minutes into the fire exposure (fire duration of 30 minutes, cooling rate 5°C/min).

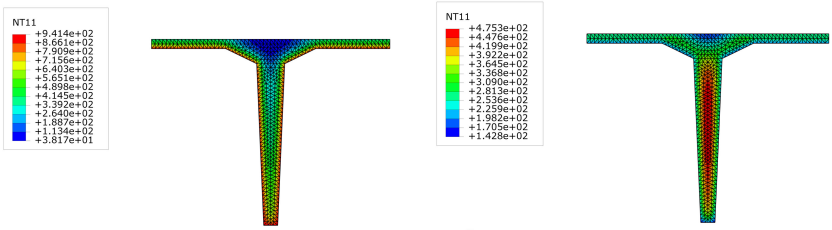

(a) (b)

FIGURE 3.19: Thermal field inside the double tee-beam: (a) at the end of the heating phase (b) in the cooling phase, 180 minutes into the fire exposure (fire duration of 60 minutes, cooling rate 5°C/min).

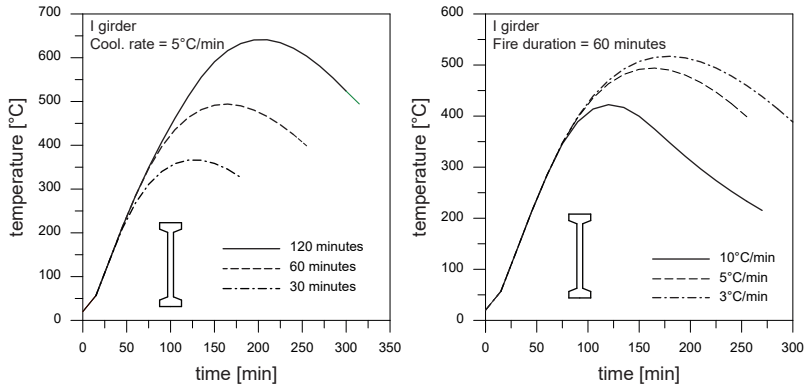

(a) (b)

FIGURE 3.20: I-girder section: (a) average temperature in the strands as a function of the duration of the heating phase (cooling rate = 5°C/min); (b) average temperature in the strands as a function of the cooling rate (fire duration = 60 min).

Role of residual thermal deformation and level of prestressing

Figure 3.22 shows typical curves of the mechanical response of the two sections, for a load ratio $M/M_u = 0.15$ and a cooling rate of 10°C/min, in order to highlight the role played by the residual thermal deformation and the level of prestressing. From Figure 3.22(a) (I-girder, duration of the heating phase = 60 minutes) it can be noted that the adopted value of the residual thermal deformation $\epsilon_{th,res}$ plays a marginal role on the maximum curvature, within a range of variation between 50 and 65% of the thermal deformation corresponding to the maximum temperature: this finding might explain why in some recent works (Kodur and Agrawal, 2016, Mohandes and Vecchio, 2016), where the residual behaviour was investigated, more simplified assumptions concerning the thermal and mechanical properties were adopted (no unloading considered). The role of the residual

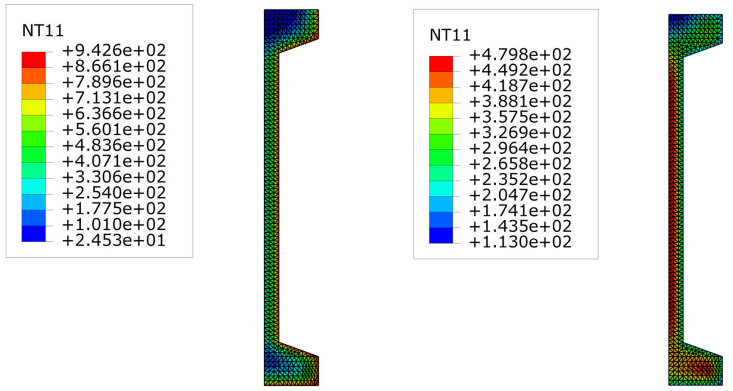

(a) (b)

FIGURE 3.21: Thermal field inside the I-girder section: (a) at the end of the heating phase (b) in the cooling phase, 180 minutes into the fire exposure (fire duration of 60 minutes, cooling rate 5°C/min).

thermal deformation increases when the strands are in the cooling phase: from Figure 3.22(a) it can be seen that the difference between the values of curvature for the two values of residual thermal deformation considered is increasing with time, reaching eventually 20%. As for the role of the prestressing level at the onset of fire σ_0, Figure 3.22(b) (double-tee, duration of the heating phase = 30 minutes) shows that within the typical range of 900-1100 MPa it is definitely of minor importance. It is worth noting that the initial decrease of curvature (corresponding to upward deflections) is due to the prevailing effect of prestressing (enhanced by the increased deformability of concrete at the beginning of the heating phase) over the thermal dilations (that would lead to downward deflections).

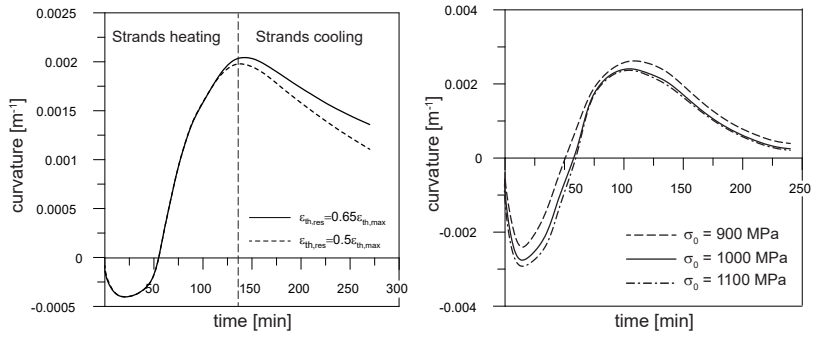

(a) (b)

FIGURE 3.22: Influence of the: (a) residual thermal strain; (b) prestressing level on the structural behaviour.

Role of different strain components - implicit vs explicit model

As previously mentioned, a key aspect concerning the behaviour of concrete in full heating-cooling cycles is the contribution of the different strain components, most of which are irreversible. Within the available constitutive models for concrete, the term accounting for transient creep is considered either implicitly or explicitly (Torelli et al., 2016), Bamonte and Monte, 2015). The widely used Eurocode model only considers transient strain implicitly, by summing this strain component to the instantaneous stress-related strain, to give the so-called mechanical strain ε_m. The total strain is then obtained as the sum of mechanical and thermal strain:

$$\varepsilon_{tot}=\varepsilon_{th}+\varepsilon_m$$

The stress can then be evaluated on the basis of the mechanical strain only. The same approach is adopted in this study, as regards the behaviour of concrete in the loading phase. Implicit models, such as the Eurocode model, are widely used because of their simplicity. In

explicit models, the mechanical strain is expressed as the sum of instantaneous stress-related strain and transient creep strain; therefore, the term for transient creep is explicitly introduced:

$$\varepsilon_{tot}=\varepsilon_{\sigma}+\varepsilon_{th}+\varepsilon_{tr}$$

Among the several explicit models available, the most recent is the one developed by (Gernay and Franssen, 2012), and validated against the results from tests on axially unrestrained concrete cylinders subjected to different stress-temperature regimes. The details about the model are presented in the Chapter 2. A limited number of analyses was performed (I girder exposed to fire with a heating phase duration of 60 minutes, cooling rate of 10°C/min and load level M/M_u =0.15), and the time evolution of the sectional curvature obtained with the two models was compared (Figure 3.23(a)). The agreement between the two models is definitely good: slight differences are visible only in the cooling phase, where unloading is likely to occur. As for the role played by the elastic modulus of concrete (taken as k$\times$ Ehot, where the reference value for k was chosen as 1.25), it proved to be marginal (Figure 3.23(b)).

Role of the duration of the heating phase

Figure 3.20 shows the response of the two sections as a function of the duration of the heating phase, for a load level $M/M_u = 0.15$ and a cooling rate = 5°C/min. The double-tee section is certainly more critical (Figure 3.24(a)): due to the extremely high temperatures attained in the strands (see also Figure 3.17(a)), it is only able to survive fires characterized by shorter durations of the heating phase (15 and 30 minutes), while it fails at the early stage of the cooling phase for a duration of the heating phase of 60 minutes. The I-girder section shows a more complex behaviour (Figure 3.24(b)). In the heating phase it does not exhibit failure for 30 and 60 minutes, while it fails for duration of the heating phase of 120 minutes. This was expected, since from Figure 3.20(a) it is evident that the average temperature

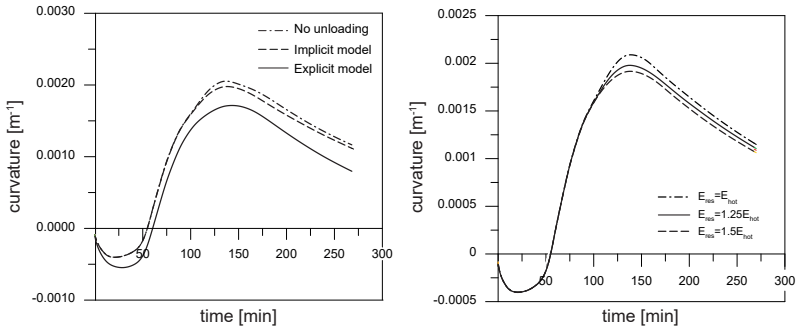

(a) (b)

FIGURE 3.23: (a) Comparison of the proposed stress-strain model (implicit model, Eres = 1.25Ehot) with the model by Gernay and Franssen (2012)) and with the EC2 constitutive model (without unloading); (b) Influence of residual elastic modulus adopted for the unloading phase.

of the strands starts decreasing long (almost 2 hours) after the onset of cooling. Even though the load level is rather low, upward bending only takes place in the very first phases of the fire, when the prestressing level and stiffness of the strands are to a great extent maintained. Later on, as the temperature in the prestressing steel further increases, the response is governed by downward bending. Note that for the fire duration of 60 minutes, the I-girder fails in the cooling phase, due to the delayed heating of the prestressing steel.

Influence of the cooling rate

Figure 3.25 shows the response of the two sections as a function of the cooling rate, for a load level $M/M_u = 0.15$ and fire durations = 30/60 minutes (double tee/I girder). Cooling rates are set to 3, 5, 10°C/min, to simulate different cooling regimes. Only in the case of the I girder, the additional value of 50°C/min is also considered. For

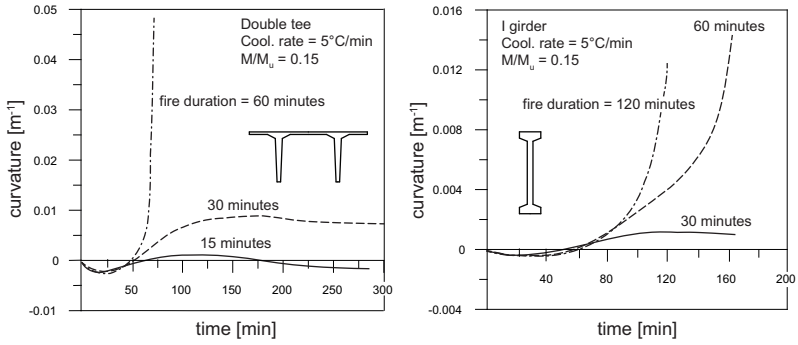

(a) (b)

FIGURE 3.24: Influence of fire duration on the sectional curvature (M/Mu = 0.15, 5°C/min): (a) double tee; and (b) I girder.

the reference load level, both sections fail during the cooling phase for the lowest cooling rate (3°C/min), while they are able to withstand the full heating-cooling cycle for higher cooling rates. In both cases, a variation of the cooling rate from 5 to 10°C/min brings in a sizable reduction of the residual displacements. For the I girder, the deflections caused by the largest value of cooling rate (50°C/min) are almost fully recovered in the cooling phase. In all cases, the structural behaviour (and the deformation reversal) is governed by the temperature decrease of the strands, that is indicated with a full dot in Figure 3.25. Clearly, fast cooling rates are beneficial, even more for shorter fire durations, as they prevent prestressing steel from reaching critically high temperatures; this considerations holds also in real cases, on the condition that spalling, caused by the large thermal gradients, does not occur.

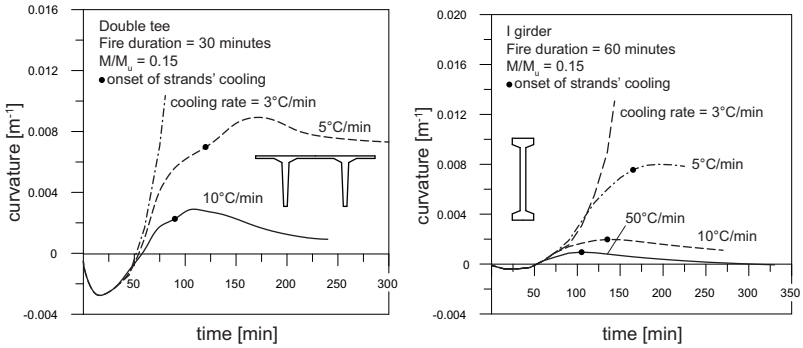

(a) (b)

FIGURE 3.25: Influence of the cooling rate: (a) double tee (fire duration = 30 minutes; M/Mu = 0.15); and (b) I girder (fire duration = 60 minutes; M/Mu = 0.15).

Influence of load level

The load level plays a very significant role in determining sectional response to fire (Figure 3.26). The bending moment due to external loads tends to induce downward bending (positive curvature), while prestressing alone tends to cause the opposite response of upward bending (negative curvature, (Figure 3.26(b), $M/M_u = 0$). In the double-tee section (Figure 3.26(a), duration of the heating phase = 15 minutes, cooling rate = 5°C/min), the load level $M/M_u = 0.15$ brings in a residual negative curvature (upward deflection) that is of the same order of magnitude of that at the beginning of the fire, while the load level $M/M_u = 0.30$, though not causing collapse, causes a residual downward deflection, that is several times larger than the initial one. In the case of the I girder (Figure 3.26(b), duration of the heating phase = 30 minutes, cooling rate = 5°C/min), varying the load level from $M/M_u = 0$ to 0.30 significantly changes the shape of the curves: as a matter of fact, without applied loads upward deflections prevail, while for the highest load level there is failure in the cooling

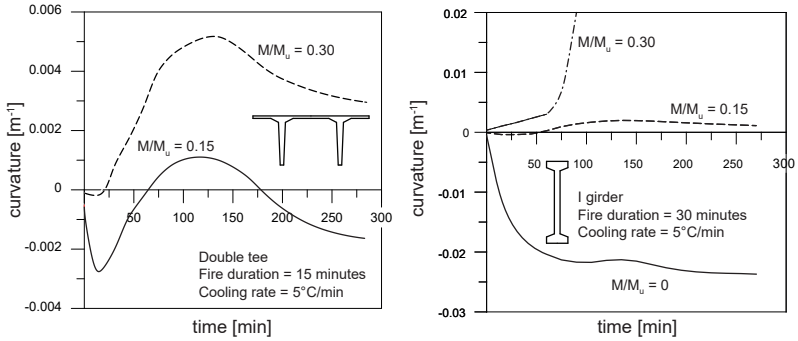

FIGURE 3.26: Influence of load level: (a) double tee (fire duration = 15 minutes; cooling rate = 5°C/min); and (b) I girder (fire duration = 30 minutes; cooling rate = 5°C/min).

phase (approximately 60 minutes after the onset of cooling).

3.6 Sectional analysis of columns - Annex B3 Method

The prediction of the behaviour of slender reinforced concrete structures is complicated by two types of nonlinearity. The first, *material nonlinearity*, results in nonlinear moment-curvature relationships which depend on the section shape, reinforcement ratio and layout and axial load. This nonlinearity is taken into account by using realistic material constitutive laws. The second type of nonlinearity, *geometrical nonlinearity*, results from the influence of the deflections on the total moments (Comite Euro-International du Beton, 1977). This effect, referred to as ”second-order effect”, is defined in EN 1992-1-1 (European Committee for Standardization, 2004b) as ”additional action effect caused by structural deformations”. It is taken into account by coupling the distribution of the bending moments with the deflec-

tions along the structural member. This coupling calls for the need of an iterative procedure, with the internal forces updated depending on the values attained by the deflections. For isolated structural members with constant axial force and a predefined effective length l_0, European Committee for Standardization (2004b) proposes the so-called "Method based on nominal curvature" for nonlinear analyses with second-order effects. This method gives a nominal second order moment based on a deflection, which in turn is based on the effective length and an estimated maximum curvature. In fire conditions, in Annex B3 of European Committee for Standardization (2005b), the same method based on estimation of curvature is proposed for the assessment of slender reinforced concrete members. This section of the Eurocode deals with columns in which the structural behavior is significantly influenced by second order effects under fire conditions. In view of the high temperatures in the outer layers of the member under fire conditions, a significant decrease of the stiffness is to be expected. Because of this, second order effects can become significant in fire conditions, even if they are negligible at ambient temperature.

3.6.1 General assumptions

In order to perform numerical analysis of slender reinforced concrete columns using a method based on nominal curvature, several assumptions are valid (Comite Euro-International du Beton (1977), European Committee for Standardization (2004b)):

- cross-section of the column is constant along the length
- The column is exposed to a normal force N that is constant and uni-axial bending moment M, that can be expressed as a sum of first order moment M_I and second-order moment $M_I I$
- The first order moment is constant along the column axis and it is determined on a basis of "accidental" eccentricity (imperfectly applied axial laod) equal to $e = L/1000$

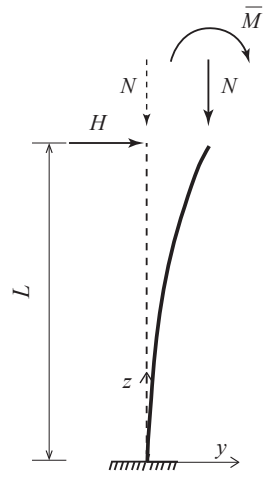

FIGURE 3.27: A typical column according to the Annex B3 Method from EC2.

- The second order moment is expressed as a function of curvature
- Column's effective length l_o can be determined from the column length L and support conditions
- Column is heated uniformly along the length and heating is symmetrical along the axis of symmetry of the cross-section

An example of a column fixed at the base and with the top end free is given in (Ferretti et al., 2002). Column is deformed because of external loads that may have an arbitrary distribution. Curvature and bending moment however have the same sign along the elements (Figure 3.27).
The deformed shape of the column is assumed a priori and in approximate way as:

$$y\left(z\right) = a(1 - cos\frac{\pi z}{L_0})$$

where L_0 is the column's effective length.

The value of the horizontal displacement a at the top of the column can be expressed as a function of the curvature at the critical - most stressed- section, which is the section at the bottom for a cantilever column:

$$y''(z) = a\frac{\pi^2}{{L_0}^2}\cos\frac{\pi z}{L_0} \;\rightarrow\; \chi \approx y''(0) = \frac{a\pi^2}{{L_0}^2}$$

Finally, the relationship between the top displacement and bottom curvature is linear:

$$a = \frac{{L_0}^2}{\pi^2}\chi$$

The second order bending moment, caused by the deformation of the column, is a function of the applied axial force and curvature at the bottom (most stressed) section:

$$M_{II} = Na = N\frac{{L_0}^2}{\pi^2}\chi$$

By considering the first order moment acting on the section (Figure 3.28) equal to

$$M_I = HL + \overline{M}$$

the total moment acting on the section, equal to the sum of first-order moment (due to the imposed external load on the column) and second-order moment (due to the structural deformations) is obtained:

$$M = M_I + M_{II} = HL + \overline{M} + N\frac{{L_0}^2}{\pi^2}\chi$$

For design purposes, the section at the base of the column can be checked by comparing the bearing capacity of the column (represented by the moment-curvature diagram corresponding to the applied axial load) and the applied moment, i.e. total bending moment. The properties of the materials, geometry of the section and the axial load applied should be known. This comparison leads to the identi-

fication of two possible situations: when the equilibrium is possible (stable configuration) and when it is not (unstable configuration). Stable equilibrium corresponds to Point A, when any further load increment corresponds to a situation where the bearing capacity (internal moment, i.e. the moment-curvature diagram) is higher than the externally applied moment (i.e. the straight line corresponding to Eq.XX). Unstable equilibrium corresponds to Point B, where the load increment produces a variation of external moment M greater than the bearing capacity of the section. On the other hand, missing intersection indicates the impossibility of attaining an equilibrium configuration, be it stable or unstable, for the given column, as in that case, the internal moment can never be higher than the external moment (Figure 3.28).

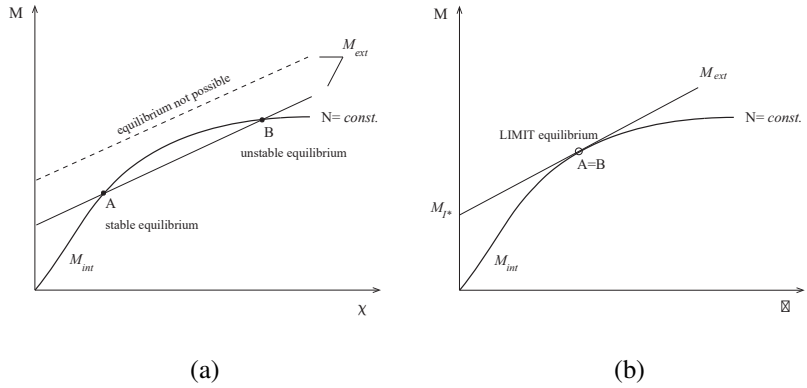

FIGURE 3.28: Comparison between internal resisting moment and externally applied moments - possible equilibrium states.

If we draw a straight line with slope equal to $NL_0{}^2/\pi^2$ and tangent to the moment-curvature diagram, we will get the limit equilibrium situation. The equilibrium can still be achieved, but the stable and unstable situation (point A and B in Figure 3.28(b)) are coincident. Intersection of this line with the moment axis ($\chi = 0$, no second-order

effects) is the first-order moment M_I^{cr} whose loads (N^{cr} and $\bar{M}^{cr}$) are the "critical loads", meaning that for a constant N^{cr} and any increase in moment larger than $\bar{M}^{cr}$) equilibrium is no longer stable.

In general, this procedure is relatively robust for studying the behaviour of slender RC columns at the sectional level, but it does simplify the behaviour of a member as a whole, reducing therefore the calculation effort (Stefan et al., 2019). The procedure was implemented in the ad-hoc Visual Basic code developed for the sectional analysis. The main purpose was to validate the model by simulating several experimentally available results on the slender RC columns exposed to a standard fire (Lie and Irwin, 1988, Hass, 1986) or tested in residual conditions (Raut and Kodur, 2011, Kodur et al., 2017) and to highlight the influence of the parameters such as recoverability of the mechanical properties, recoverability of the strain components and residual thermal strain.

3.6.2 Parametric study and results

In the following, results from the numerical analyses of some columns using Annex B3 method will be presented. Columns experimentally tested in the past (Hass, 1986, Lie and Irwin, 1988, Raut and Kodur, 2011 and Kodur et al., 2017) were analyzed by means of sectional analysis, and the axial displacements at the top of the column are compared against the experimental values. For the eccentrically loaded columns, simulations were performed both with and without second order effects. More details on the experimental tests that served as a basis for the analyses were given in Chapter 2.

Standard fire tests

Hass (1986) performed a series of full-scale tests on heated RC columns subjected to eccentrically applied axial loads. Three tested columns have been simulated numerically, all three of them having

the same cross-section geometry. Columns Hass1 and Hass16 were simply supported while Column Hass21 had a fixed bottom and a roller at the top. Details about the tested columns can be found in Table 3.1, where also experimental time to failure has been reported. Cross-section details and boundary conditions of the columns can be seen in the Figure 3.29.
The predicted lateral deflections at the midspan was plotted in Figure 3.30. The principal objective was not to compare the evolution of the lateral displacements but to understand if the sectional analysis can accurately predict the failure time of the columns that were tested under eccentric loading. Experimental time-to-failure is represented with a red dashed line on the plot. Two sets of simulations have been performed: first order analysis and second order analysis (including the second order moment caused by large deflections).

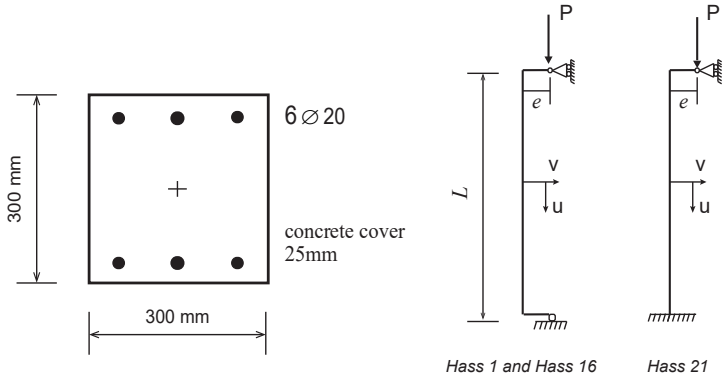

FIGURE 3.29: Geometry and boundary conditions of the column specimens (Hass, 1986).

The obtained failure times for the three columns are summarized in Table 4.1. It can be seen that first order analysis leads to unconservative failure time prediction for eccentrically loaded columns, which is not surprising. On the other hand, if the second order effects are included, even in the simplified way that forms the basis of the method

TABLE 3.1: Geometrical and mechanical properties of the columns tested by Hass (1986)

Column	Dimensions [mm x mm]	L [m]	fy[MPa]	fc[MPa]	Load [kN]	e [mm]	Failure time [min]
Hass 1	300 x 300	3.76	487	24.1	710	30	86
Hass 16	300 x 300	4.76	462	30.7	460	60	75
Hass 21	300 x 300	3.8	418	33.2	780	90	125

TABLE 3.2: Time to failure - experimental and numerical results (Hass, 1986)

Time to failure [min]	Hass 1	t/t_{exp}	Hass 16	t/t_{exp}	Hass 21	t/t_{exp}
sectional 1^{st} order	210	2.4	180	2.4	180	1.4
sectional 2^{nd} order	78	0.91	106	1.41	90	0.72
experimental	86	-	75	-	125	-

based on nominal curvature, a better prediction of the failure time is obtained (except for Column Hass16).

Sectional analysis has been performed on two concrete sections tested by **Lie and Irwin (1990)**, one square-shaped and the other rectangular-shaped (denoted as Column 1 and Column 3, respectively). Details about the tested columns can be found in Table 3.3 and the geometry of the cross-sections and structural layout can be seen in Figure 3.31. Columns were concentrically loaded in compression and exposed to the standard fire. The numerical axial displacement at the top of the columns is compared against the values from the tests. Two typical phases in the axial deformation evolution in time are visible in Figure 3.32. In the first stage, columns expand, due to increasing thermal gradients that occur, leading to thermal expansion of concrete and steel. This phase is followed by a contraction phase, due to the degradation of the material mechanical properties.

The general trend of the axial deformation in time is predicted well. Comparing the failure time prediction, it has to be mentioned that

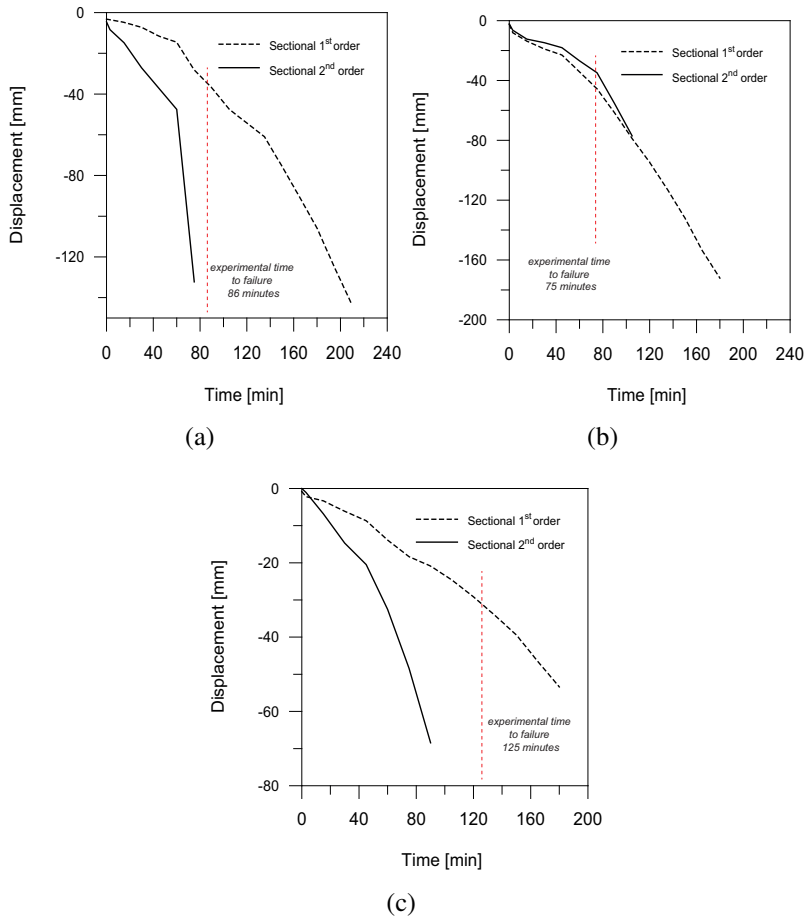

FIGURE 3.30: Evolution of the lateral displacements for the columns: (a) Hass 1; (b) Hass 16 and (c) Hass 21 from Hass (1986).

the failure in terms of divergence in the curvature of sectional deformation did not take place. Therefore, first order sectional analysis proved not to be able to capture time of failure; by contrast, the overall trend in the axial displacement was satisfying.

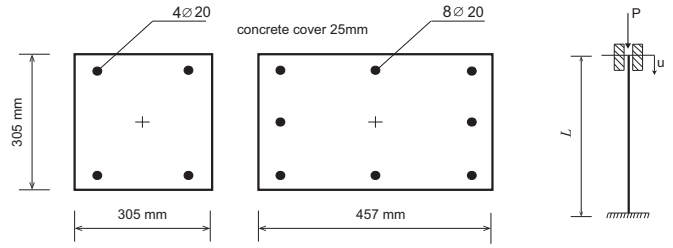

FIGURE 3.31: Geometry of the cross-sections (Lie and Irwin, 1990).

TABLE 3.3: Geometrical and mechanical properties of the columns tested by Lie and Irwin (1988)

Column	Dimensions [mm x mm]	L [m]	fy [MPa]	fc [MPa]	Load [kN]	e [mm]	Failure time [min]
1	305 x 305	3.8	444	36.1	1067	0	208
3	305 x 457	3.8	414	42.5	1413	0	398

Residual tests

Six reinforced concrete columns were tested at Michigan State University and the results were presented in **Raut and Kodur (2011)**. All columns were 3350 mm long, with a square-shaped cross section (203 $\times$ 203 mm). Four rebars $\phi 20$ acted as longitudinal reinforcement ($f_y = 420MPa$), as well as 10 mm stirrups, with a spacing of 200 mm, as transverse reinforcement. A summary of the main test parameters is reported in Table 3.4. Column exposed to standard fire failed after 183 minutes into the fire test. Other two columns were exposed to a long duration design fire, denoted as LF: the furnace temperature followed closely the ASTM E119 curve until 190 minutes; then, the cooling phase started at constant cooling rate, until the furnace temperature reached the ambient value (i.e. after around 270 minutes from the beginning of the test).

Axial deformations were measured at the top of each column. The

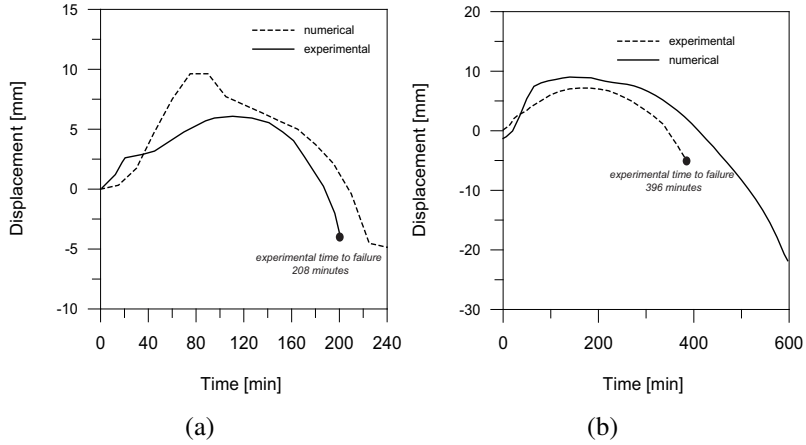

FIGURE 3.32: Evolution of the axial displacements for the columns: (a) C1; (b) C3 from Lie and Irwin (1990).

TABLE 3.4: Summary of test parameters and results from Raut and Kodur (2011)

Column	Fire Exposure	Concrete Type	Test day concrete strength (MPa)	Load ratio (%)	Fire resistance (min)	Spalling
NSC	ASTM E119	NSC	51	0.4	183	minor
HSCP1	LF	HSCP	93	0.4	NF	nil
HSCP2	LF	HSCP	93	0.6	221	nil

columns responded in a similar way: expanding in the early stages of fire exposure and contracting later. Early expansion can be mainly attributed to the thermal expansion of concrete and steel. Contraction in the later stages is a result of loss of strength in steel reinforcement and concrete, due to the increasing temperatures within a cross-section and also due to load redistribution from concrete to reinforcement. The time to reach failure is defined in Raut and Kodur (2011) as the fire resistance and failure is said to occur when the strength of the column decreases to a level at which the column cannot sustain the applied load. Axial displacement for the NSC col-

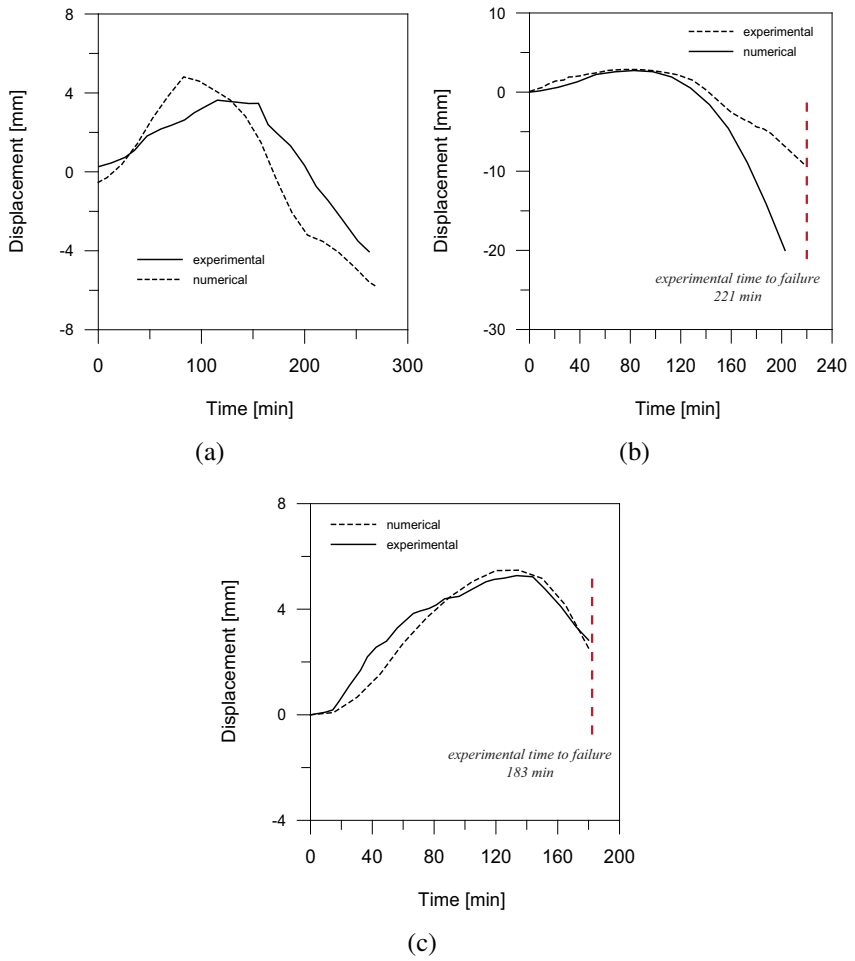

FIGURE 3.33: Evolution of the axial displacements for the columns: (a) HSCP1; (b) HSCP2 and (c) NSC from Raut and Kodur (2011).

umn is in a very good agreement with experimental values and the displacement at the time of failure is 2.5 mm against 2.7 mm from the experiment. HSCP2 column, failed just at the beginning of the cooling phase, and the failure time is anticipated with respect to the

experimental fire resistance. Due to the presence of a cooling phase, HSCP1 and HSCP2 did not attain such high temperatures and thus significant creep deformation might not have occurred in these columns. Column HSCP2 experienced higher deformations as compared to HSCP1 due to the higher stress ratios, caused by the higher load, and thus higher creep deformations. Sectional analysis gave somewhat conservative prediciton of the fire resistance with respect to the experiment.

Results from the residual capacity tests on two columns, designated as C1 and C2, are presented in **Kodur et al. (2017)**. Summary of the columns' properties can be seen in Table 3.5 while geometry of the column and cross-section details can be seen in Figure 3.34. Two columns were exposed to two design fires, DF-1 and DF-2. Heating duration was 90 minutes and 120 minutes for fire DF-1 and DF-2, respectively. Furnace temperature during the decay phase was controlled at a cooling rate of 5.5°C/min. Temperatures reached in the rebars are rather high, with peak values of 550 °C for C1 and around 600 °C for C2. Distribution of the temperature inside the C1 and C2 column section can be seen in Figure 3.35 and Figure 3.36. Structural behaviour is traced through the evolution of axial displacements, measured at the top of each column by means of LVDTs. The axial deformation of the two columns is given in Figure 3.37. Behaviour of the two columns is rather similar. Initially, the displacements increase due to thermal expansion caused by the increasing temperature. Then, it the second stage, axial deformation rapidly decreases and the columns start to contract, due to degradation of strength and stiffness in concrete and rebars. Once the temperatures in the member start to decrease, a recovery of the deflections takes place. Rate of recovery of the deflections is significantly slower than the rate of increase, due to nonlinear nature of the cooling phase and also irrecoverable damage that took place during heating and cooling. The residual deflection proved to be very sensitive to duration of the heating phase, as the residual deflection of Column C1 is about 50% greater than that of Column C2.

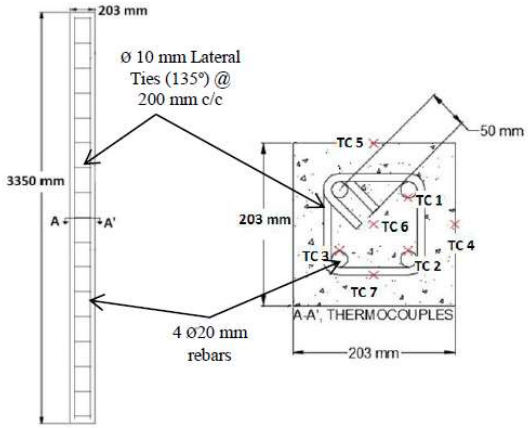

FIGURE 3.34: Geometry of the column and cross-sections from (Kodur et al., 2017).

TABLE 3.5: Summary of test parameters and results from Kodur et al. (2017)

Column	Fire Exposure	Column length (m)	Test day concrete strength (MPa)	ACI 318 design capacity (kN)	Load ratio (%)
C1	DF-1	3.35	49	732	0.5
C2	DF-2	3.35	62	732	0.55

With sectional analysis it was possible to obtain quite an accurate axial displacement prediction, both during heating and cooling phase of fire. Still, a sudden drop in the experimental displacement curve is notable, though it was not elaborated on the possible causes. For instance, such a sudden drop could be due to the load removal, though it was claimed that the load was present during both heating and cooling phase of fire. For Column C1, both peak and residual deflections are very close to the experimental values. For Column C2, the response is somewhat conservative (maybe even too conservative), but the general trend is correctly captured.

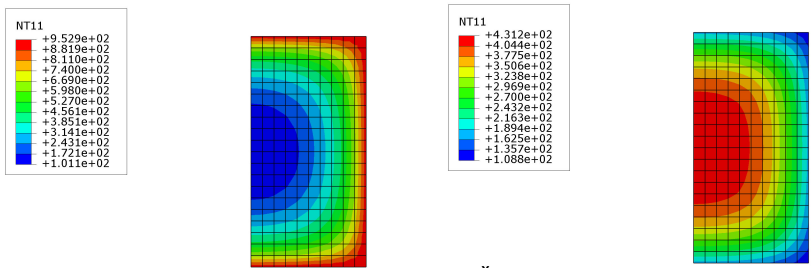

(a) (b)

FIGURE 3.35: Thermal field inside the C1 column section Kodur et al. (2017): (a) at the end of the heating phase (b) at the end of the cooling phase, 300 minutes into the fire exposure.

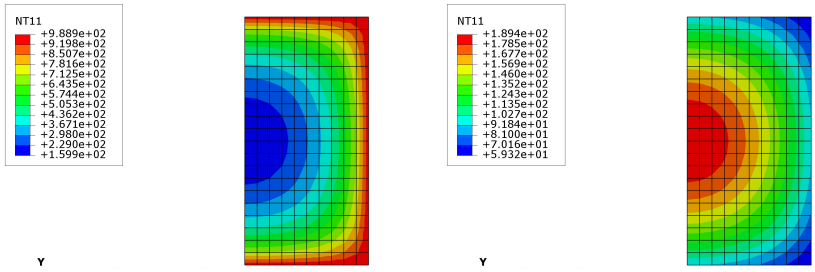

(a) (b)

FIGURE 3.36: Thermal field inside the C2 column section Kodur et al. (2017): (a) at the end of the heating phase (b) at the end of the cooling phase, 300 minutes into the fire exposure.

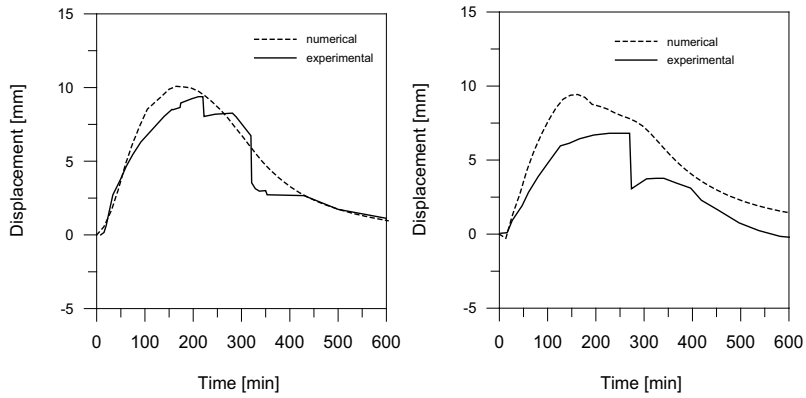

FIGURE 3.37: Evolution of the axial displacements for the columns: (a) C1; (b) C2 from Kodur et al. (2017).

Influence of irrecoverable thermal damage in concrete and steel rebars

In the Figure 3.38 the influence of the recoverability of the strength and stiffness in the concrete and steel rebars on the structural response is presented. Three analyses have been performed for each column: by considering only steel strength and stiffness recovered upon cooling, only concrete properties and finally; both concrete and steel mechanical properties recovered upon cooling. The response have been compared to the experimental curve but also numerically obtained curve, that considers all the properties as irrecoverable.

It can be seen that considering the mechanical properties as fully recovered upon cooling leads to the responsees that are quite different than what was observed in the experiments: rate of deformation in the cooling phase is mush slower and the amount of contraction is significantly underestimated. It can also be seen that for the influence of concrete is dominant in comparison to steel: considering only the steel properties as recovered leads to a very similar response

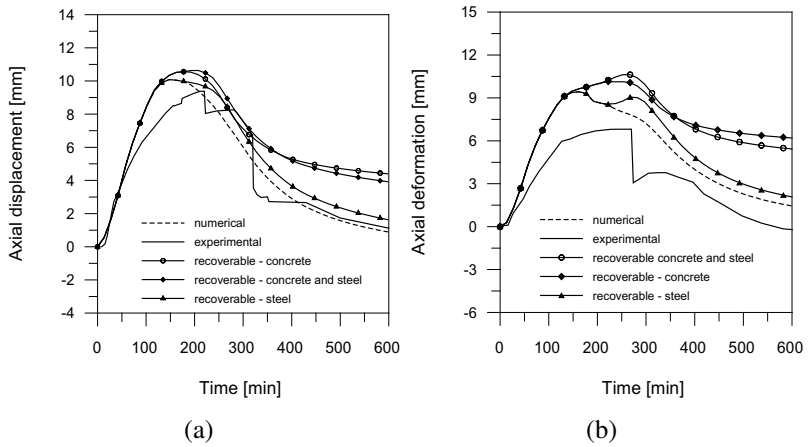

(a) (b)

FIGURE 3.38: Evolution of the axial displacements - the role of the material damage- for the columns : (a) C1; (b) C2 from Kodur et al. (2017).

to the curve where both steel and concrete properties are irrecoverable (”numerical” curve). On the other hand, consideration of concrete strength and stiffness as recovered changes the response during cooling phase sizably.

Influence of unloading modulus

Finally, influence of the unloading modulus on the response of the columns C1 and C2 (Kodur et al., 2017) has been studied. These columns were chosen because they were tested under full heating-cooling cycle and the axial deformation were measured and repoted throughout the whole test duration. Constitutive model of concrete allows an unloading along a linear branch, defined by the residual elastic modulus. As a reference value, residual elastic modulus is considered 25% higher than the initial tangent modulus, as to account for the strain components that do not recover during cooling (Figure 3.4(a)). In

addition, a nonlinear elastic behaviour (loading and unloading along the same path - i.e. along the stress-strain curve) has been studied, to check the influence of allowed unloading. As it can be seen in Figure 3.39, the obtained responses are very similar to each other and the unloading effect proved not to play a big role. Similarly as for the beams, unloading mainly takes place during cooling, when the stresses inside the section are quite low (compressive strength is "locked" at the value at maximum temperature) and any difference in calculated stress caused by allowed unloading is not significant.

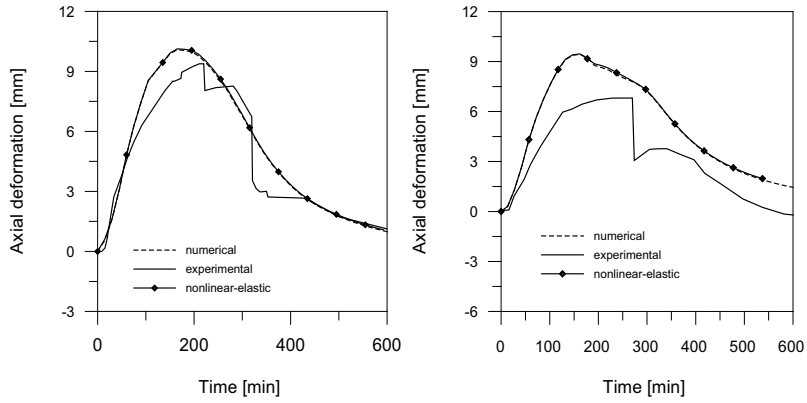

FIGURE 3.39: Evolution of the axial displacements - the role of the unloading modulus- for the columns : (a) C1; (b) C2 from Kodur et al. (2017).

Influence of residual thermal strain

A set of analyses has been performed on two columns, C1 and C2, by considering the thermal strain of concrete as fully recovered upon cooling, so to check the influence of such parameter on the structural response of RC columns. It is expected that residual thermal strain

will play bigger role in case of columns than beams, given that almost all of the columns' axial capacity is provided by concrete and. As it can be seen in Figure 3.40, two assumptions regarding the reversibility of thermal strain lead to somewhat different axial deformation prediction.

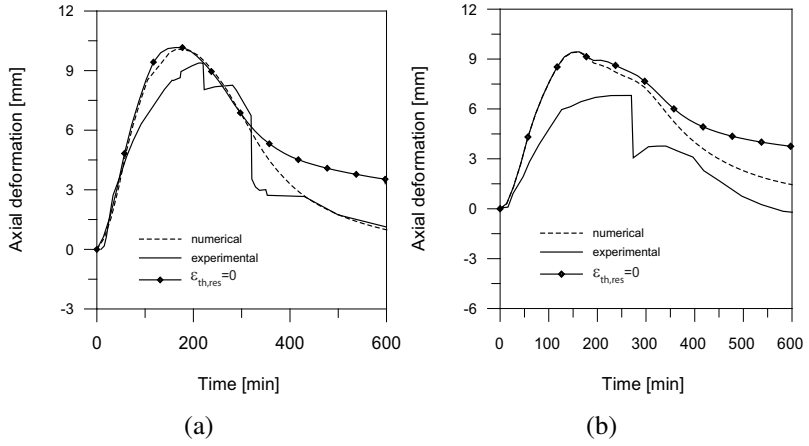

FIGURE 3.40: Evolution of the axial displacements - the role of the residual thermal strain - for: (a) column C1; (b) column C2 from Kodur et al. (2017).

It can be seen that residual thermal strain plays a role in the second and third stage of the displacement response, and especially in the later stages of cooling phase. Contraction in the later stages is underestimated if no residual strain is considered; it can be seen that deformation rate is slower in case of both columns for $\varepsilon_{th,res}$=0. The predicted response with consideration of residual thermal strain ("numerical" curve) is closer to the experimental results.

3.7 Unified view on the sectional failure

It is rather clear that the behaviour of statically determined members in flexure is governed by the steel rebars. In order to maintain the flexural load capacity during fire, the rebars should be prevented from reaching devastating temperatures. Decay of the strength in reinforcing steel is ruled by the maximum temperature attained in the rebars and prestressing strands, for PC sections. Furthermore, the maximum temperature is influenced by the fire exposure (i.e. duration of the heating phase, cooling regime) and the shape of the section and the reinforcement layout (i.e. massivity of the section, average cover to the prestressing steel). It is evident that a lot of factors play a role; however, a unified approach can be offered, lumping the several variables into one, with the aim to give a general overview on how the sectional failure is dependent on those factors. Fire exposure and section shape may be lumped into one indicator- average temperature in the rebars or prestressing strands. The second indicator is the load level, or more precisely the ratio between the externally applied load and the ultimate moment capacity of the section at the ambient temperature. For a given fire scenario and section shape, failure in the section will be attained when the critical temperature is reached, and this one depends on the imposed load level. The higher the load level, the lower the critical temperature and vice versa. Given that the maximum temperature in the steel rebars is reached typically in the cooling phase, it is clear that for the certain fire scenario, the section shape and reinforcement layout, the critical temperature (and as a consequence - the failure), is reached in the cooling phase of fire. Average rebar temperature acquired at failure is plotted against the load level acting on the section for the two sections: PC double-tee section and RC rectangular shaped section. The section will fail when the load level equals the normalized tensile yield strength of the prestressing steel at the maximum temperature reached in the strand. This greatly simplifies the approach: the only parameter needed to determine if the section will fail or not is to check if the maximum

temperature exceeds the critical temperature at which:

$$k = f_{yp}(T)/f_{yp,20C} \tag{3.5}$$

$$k = f_{ys}(T)/f_{ys,20C} \tag{3.6}$$

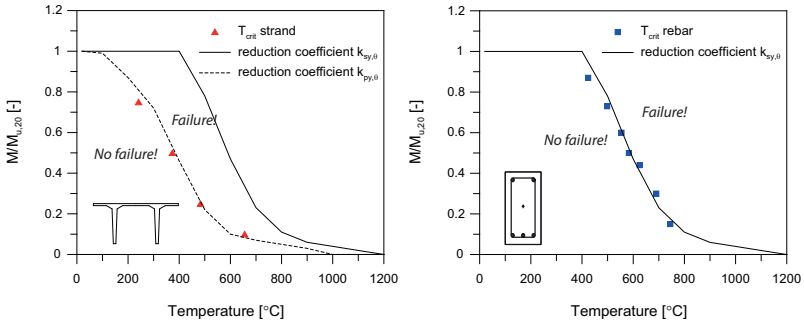

(a) (b)

FIGURE 3.41: Rebar/Strand temperature at failure - M/Mu curve for (a) double T-beam prestressed section; (b) reinforced concrete section.

Chapter 4

Nonlinear Structural Analysis via Beam Finite Elements

Sectional analysis provides a solid basis for the structural analysis of statically determined members in fire, and it is probably the most widely used method among engineers in practice. However, due to its simplified assumptions, its field of application is somewhat narrow and certainly has several limitations. Some of these limitations can be overcome by focusing on substructures or by modeling the whole structure. Structural analysis of RC frame structures is of interest for both researchers and design engineers. Using RC beam elements, both mechanical and geometrical nonlinearity of RC frames can be taken into account; the latter aspect, in detail, is of great importance if the structure is expected to suffer large deflections, as it is the case in fire exposure. Talking about the most investigated structural members in fire, beams and columns, a nonlinear structural analysis using beam elements is a good compromise between sectional analysis and complex 3D analysis (with linear members modelled using brick elements). Naturally, it has a wider field of application than sectional analysis. It can be used through an ad-hoc developed code, as it was the case in this work, or in readily available softwares for studying structural fire behaviour (e.g. SAFIR), and most importantly

it can be a great tool to analyze linear members, whatever the loading and restraint conditions. This is important, because not all the structural members' behaviour can be described just by considering the most stressed section. The results presented in the Chapter 3 suggest that while the sectional analysis is quite an efficient tool to predict the structural response of statically determinate flexural members, it is (too) conservative when it comes to slender structural members where second order effects play a role. In addition, studying the behaviour of redundant members, those where significant redistribution of forces takes place, axially restrained members or eccentrically loaded members through sectional analysis is either not feasible or not accurate enough. The need to resort to more complex methods should be recognized in these cases. For that purpose, a 1D Finite element code was developed for a structural analysis using beam finite element, aiming to overcome intrinsic limitations of the sectional analysis and to offer a more general approach to study simple structural members exposed to fire. Both material and geometric nonlinearity are taken into account, through the use of realistic stress-strain law, featuring also the softening branch, and by inclusion of the geometric stiffness matrix and second-order moment.

4.1 General methodology

An ad hoc nonlinear 1D FE code for the mechanical analysis of heated members has been developed by the author in Visual Basic (VB). A number of significant examples based on real-scale fire tests on columns were modeled, taking into account different heating, loading and boundary conditions. Using this ad-hoc developed code, the final objective is to calculate the evolution of the nodal displacements of the member during fire. At each time step, the code keeps track of the:

1. **Temperature history** - Nodal temperatures at the current time increment t is compared with the temperature from the previous

time increment $t-1$

2. **Deformation history** - Strain at the each node of the section at the current time increment t is compared with the strain from the previous time increment $t-1$ - in order to ascertain whether loading or unloading will take place, and thus use the appropriate stress-strain relationship

Many realistic parameters characterizing the full heating-cooling are taken into account, such as:

- realistic fire scenario, unheated boundaries, generic loading and restraint conditions
- thermal damage that takes place during cooling
- the second-order effects
- both explicit and implicit consideration of the transient creep strain

Several tests have been used as basis for the validation of the code, in view of subsequent parametric analyses. Predicted and experimentally measured temperatures as well as axial/lateral displacement are compared. The influence of second order effects on the results is discussed, where relevant. Both implicit and explicit constitutive model have been used and the results have been compared. Advanced methods for mechanical analysis require the knowledge of the temperature at each point of the section/structure, in order to explicitly evaluate the evolution with temperature of the mechanical properties of different materials. Thermal analyses on the sections are performed in ABAQUS 6.16 Software, following the procedure described in Chapter 3. Once the temperature at each point of the section is known, the mechanical analysis is performed.

4.2 General aspects relative to the nonlinear structural analysis

Basic assumptions concerning Euler-Bernoulli slender members are still valid, namely:

1. Bernoulli-Navier hypothesis: plane sections remain plane, allowing to assume linear strain distribution over the cross-section depth
2. Perfect bond between reinforcing bars and the surrounding concrete
3. Shear deformations of the sections are negligible (i.e. the rotation of the cross section coincides with the first derivative of the displacement of the geometric centroid of the section)

At any point, the total concrete strain can be calculated using only two variables. These two variables are generalized deformations - deformation at the centroid and curvature of the section, ε_o and χ, respectively:

$$\varepsilon(\mathrm{x},y)=\varepsilon_o+\chi y$$

where y is the distance of the point of interest from the reference point of the cross-section (centroid) and should be taken with negative sign if the point of interest is above the reference point.

As per strain compatibility hypothesis (perfect bond), total strains of the reinforcing steel bars can be written in a similar manner:

$$\varepsilon_s=\varepsilon(y)\ =\varepsilon_o+\chi y$$

Sign convention is such that negative deformations are contractions, while positive deformations are elongations of the fibers.

Generalized forces that are conjugated with the generalized deformations (in terms of energy), axial force N and moment M, are the resultant of the stresses acting on the section, that are worked out on the basis of the local values of deformations.

$$N = \int \sigma dA \text{ and } \quad M = \int \sigma y dA$$

General framework follows the sequence *section-beam element-node* (Figure 4.1). Firstly, sectional deformation is characterized through the values of deformation and curvature. For a detailed procedure on the sectional stiffness calculation, the assumed material properties and the corresponding constitutive models, reference to Chapter 3 is made, as the same principles are valid also here. Following the sectional calculation, the stiffness of the beam finite element(s) is then determined. Finally, the stiffness matrix of the global system is assembled, by taking into account all the contributions coming from the single beam finite elements. Equilibrium of the global system in terms of nodal forces, applied distributed loads and imposed displacements is then found. In the presence of both mechanical and geometrical nonlinearity, an iterative approach has to be employed in order to find the equilibrium, and this is done by using secant stiffness method. Equilibrium equations for the entire structure are obtained by assembling the stiffness contributions of all the RC beam finite elements into which the structure is discretized. For the iterative solution, it is necessary to define the process to obtain the nodal displacement vector $\underline{q}^i$ that corresponds to the i-th iteration, on the basis of predefined convergence criteria. In short, at the $i-th$ iteration the solution is considered converged if the following conditions are satisfied:

1. disequilibrium between the external and internal forces

$$e_F = \left\| r\left(\underline{q}^I\right) \right\| \leq \varepsilon_F$$

2. displacement between two consequtive iterations

$$e_q = \left\| \underline{q}^I - \underline{q}^{I-1} \right\| \leq \varepsilon_q$$

3. the norm on the work done by the forces

The tolerances are imposed as $\varepsilon_F = 0.001$ and $\varepsilon_q = 0.0001$. If the solution converged within a pre-defined tolerance, then the equilibrium state has been reached. Otherwise, the local collapse, due to reached limit deformation in one of the component materials, or a global collapse, due to missing convergence after a maximum defined number of iterations, can take place. Global collapse occurs when the acting load exceeds the load-bearing capacity of the structure.

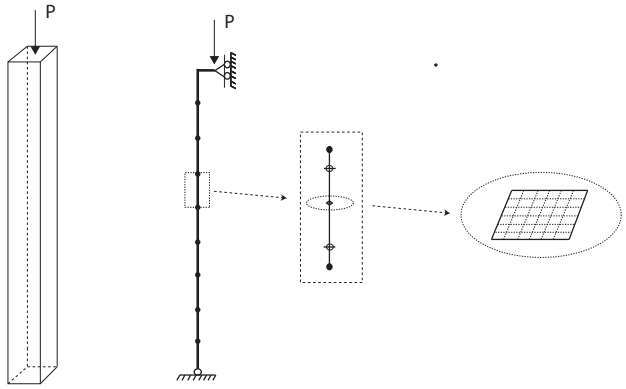

FIGURE 4.1: 1D FE code sequence - section-beam element - node.

4.3 Beam Finite Element Definition and the Code Structure

Thinking about the structure that is discretized into a number of finite elements and the acting loads on the structure that can be collected into a vector of equivalent nodal forces $\underline{P}$, primary unknowns of the structural problem are the displacements at the nodes that are used to subdivide the structure into finite elements. These displacements can be grouped into a vector $\underline{q}$. From this vector, we can go to (Malerba, 1998):

1. Displacement and deformation field at any point P of the structure: $\underline{u}\,(P) = \underline{\underline{N}}(P, \underline{q})\underline{q}$ and $\underline{\varepsilon}\,(P) = \underline{\underline{B}}(P, \underline{q})\underline{q}$
2. Stress field
3. Restraint reactions

Where $\underline{\underline{N}}$ is the matrix containing the shape functions relative to the $i - th$ degree of freedom $N_{i,x}$ (with i =1, 2, ..., 6) .

4.3.1 Formulation of the Beam element with ordinary reinforcement

Consider the beam element shown in Figure 4.2, with its local coordinate system and the conventional signs for the generalized displacements and internal actions . Being $u_0\,(x)$ and $v_0\,(x)$ the displacements in the direction parallel and orthogonal to the direction of the beam axis (coincident with the axis x), at the location of the centroid of the concrete section, the displacements corresponding to the generic fibre in the plane normal to the axes in the direction x and y will be, respectively:

$$\begin{gathered} u\,(x, y) = u_0\,(x) - y\frac{\partial v_0}{\partial x} \\ v\,(x) = v_0\,(x) \end{gathered}$$

Being $\varepsilon_0 = \frac{\partial u_0}{\partial x}$ and $\chi = \frac{\partial^2 v_0}{\partial x^2}$ the elongation of the centroidal fiber and curvature of the section, respectively, the only active component of deformation is:

$$\varepsilon = \varepsilon_x(x, y) = \varepsilon_o(x, y) - \chi(x)y \tag{4.1}$$

Deformed shape is a function of six nodal degrees of freedom, through the usual linear and cubic shape functions, grouped in the matrix $\underline{\underline{N}}(x)$. Reducing the problem to the algebraic form, we get:

$$\underline{u}\,(x) = \underline{\underline{N}}(x)\ \underline{q}$$

where $\underline{q}$ is the vector of generalized nodal displacements:

$$\underline{q}^T = \left[u_i \;\; u_j \vdots v_i \;\; v_j \;\; \varphi_i \;\; \varphi_j \right]$$

Corresponding generalized deformations $\varepsilon_o\,(\mathrm{x})$ and $\chi\,(x)$ are related to the vector of nodal displacements $\underline{q}$ through the compatibility matrix $\underline{\underline{B}}(x)$.

$$\underline{\varepsilon}\,(x) = \underline{\underline{B}}(x)\underline{q}$$

Deformation (strain) of the fiber at coordinate y of the section can be expressed as:

$$\varepsilon{=}\varepsilon_x{=}\varepsilon_o{-}\chi y = [1 \quad -y] \left[\begin{array}{c} \varepsilon_o \\ \chi \end{array} \right] = \underline{\underline{L}}\,(x)\,\underline{\varepsilon}\,(x) = \underline{\underline{L}}(x)\underline{\underline{B}}(x)\underline{q}$$

This strain includes both elastic and imposed strains, such as for example thermal dilation. If we want to express only the elastic strain component, any imposed strain should be subtracted.

$$\varepsilon(\mathrm{y},\mathrm{z}){=}\varepsilon_x{=}\varepsilon_o(\mathrm{x}){-}\chi(x)y - \varepsilon_{im}(y,z) = \underline{\underline{L}}\,(x)\,\underline{\underline{B}}\,(x)\,\underline{q} - \varepsilon_{im}(y,z)$$

Vector of equivalent nodal forces and the stiffness matrix are assembled according to the traditional Beam Finite Element Theory for linear elastic problems:

$$\left\{ \begin{array}{c} N \\ M \end{array} \right\} = \left[\begin{array}{cc} \overline{EI} & \overline{ES} \\ \overline{ES} & \overline{EA} \end{array} \right] \left\{ \begin{array}{c} \varepsilon_o \\ \chi \end{array} \right\} - \left\{ \begin{array}{c} N_{th} \\ M_{th} \end{array} \right\}$$

where the components of the stiffness matrix are calculated as:

$$\overline{EA} = \int E\,(y,z)\,dA$$

$$\overline{ES} = -\int E\,(y,z)\,y\;dA$$

$$\overline{EI} = \int E\,(y,z)\,y^{\,2} dA$$

$$N_{th} = \int \sigma_{th} dA = -\int E\,(y,z)\;\varepsilon_{th} dA$$

$$M_{th} = \int \sigma_{th} y dA = -\int E\,(y,z)\;\varepsilon_{th} y dA$$

Elastic modulus E is the *secant elastic modulus*, evaluated as the ratio between the applied stress and the load-induced strain, at each point of the cross-section. Given that it is a function of temperature and stress, thus of the solution itself, the structural problem is nonlinear and the solution procedure is iterative, as previously mentioned.

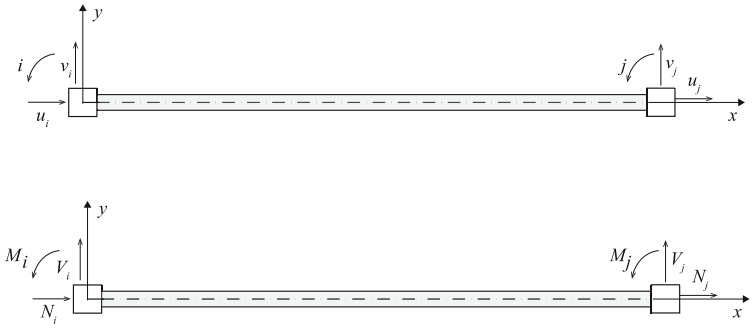

FIGURE 4.2: Sign convention for the generalized displacements and internal forces of the Beam Finite Element.

Finally, having assembled the stiffness matrix and the vector of equivalent nodal forces, equilibrium of the structure can be written:

$$\underline{\underline{K_E}}\;\underline{q} = \underline{F_{im}} + \underline{F_{ext}} = \underline{F_{th}} + \underline{F_{ext}} = \underline{f}$$

where $\underline{\underline{K_E}}$ is the structural stiffness matrix, $\underline{F_{im}}$ is the vector of the nodal forces equivalent to the restrained thermal strains, $\underline{F_{ext}}$ is the vector of external nodal forces.

In order to account for the coupling between axial loads and flex-

ural deformations/displacements (second-order effects), a geometric stiffness matrix needs to be added (Malerba (1998)):

$$(\underline{\underline{K_E}} - \underline{\underline{K_G}})\ \underline{q} = \underline{F_{im}} + \underline{F_{ext}} = \underline{F_{th}} + \underline{F_{ext}} = \underline{f}$$

The geometric stiffness matrix $\underline{\underline{K_G}}$ is obtained by derivation of the virtual work of the external loads - axial force P (positive if compression) for the corresponding displacement Δ, congruent with the deformed configuration of the element : $W = P \times \Delta$ (more details in Malerba, 1998).

This matrix is therefore indirectly dependent on the $\underline{q}$: axial force P present on the beam element and depends on the deformation along the entire structure. Finally, the system to be solved is:

$$(\underline{\underline{K_E}} - \underline{\underline{K_G}})\ \underline{q} = \underline{\underline{K}}\underline{q} = \ \underline{f}$$

Through the inclusion of the geometric stiffness matrix, equilibrium equations are written for the deformed structure, introducing the so-called $P - \delta$ effect.

4.3.2 Numerical integration of the stiffness matrix

Stiffness matrices are integrated along the whole substructure/structure, which is divided into a number of finite elements. Integration is performed at two Gauss points for each beam finite element. Integration of the stiffness matrix and vector of nodal equivalent forces is organized in the following steps:

- **external cycle**: integration of $\underline{\underline{\mathrm{K}}}$ and F along the beam axis x, at N_{pg} integration points, to which the weights W_i are associated
- **internal cycle**: integration on the section; to evaluate the sectional stiffness matrix - integrating the contribution of concrete and summing the contributions of steel bars

4.4 Structural behaviour and analysis of RC columns

Five sets of columns tested by several researchers in the past were used to validate the code for structural analysis (Lie and Irwin, 1990, Hass, 1986, Kodur et al., 2017, Wu et al., 2010, Raut and Kodur, 2011). Two sets of columns were tested under standard fire, and though the structural behaviour of members under standard fire was not the main study objective, these experimental studies are still very valuable, in order to validate the ability of the structural code to correctly predict the failure time under standard fire and also the large deflections of eccentrically loaded columns brought in by second-order effects. The rest of the columns that were chosen for the validation were tested in residual state, under different heating and restraint conditions. The ability of the model to predict the displacement evolution during both heating and cooling phase is tested.

4.4.1 Experimental tests with standard fire

Concentrically applied axial loads

Lie and Irwin (1990) completed an extensive test program on 40 reinforced concrete columns. Validation has been performed on two columns, one with a square-shaped cross section and the other with a rectangular-shaped cross-section, in the following denoted as Column 1 and Column 3, respectively. All columns were 3.81 m long, but only the central part of 3.0 m was exposed to fire. Details of the cross-sections are given in Figure 3.31.

The tests were carried out by exposing the columns to fire in a test furnace. Average temperature in the furnace followed closely the ASTM E119 time-temperature curve, while for Column 3 it followed a specific time-temperature curve, less severe than the ASTM E119 curve. Tile-temperature curve for the Column 3 followed the standard fire curve in the first 30 minutes or so, until it reached 850 °C, and

then it increased linearly until the end of fire, reaching the maximum temperature of 1000 °C after 600 minutes.
Failure of the columns took place when the load, applied by hydraulic jack, could no longer be maintained. Both columns failed during the test: Column 1 after 208 minutes into fire exposure, while Column 3 failed after 396 minutes.

Temperature distribution

Thermal properties are considered temperature - dependent, as per EN 1992-1-2. Specific heat is taken as for dry concrete, density is assumed equal to 2400 kg/m^3 and upper limit value prescribed by EC2 for conductivity is used. Agreement between experimentally and numerically obtained temperatures is satisfying for both columns. Calculated temperatures are compared against the temperature readings from the thermocouples positioned at 13 mm, 64 mm and 152 mm depth from the bottom heat-exposed concrete side (Figure 4.3).

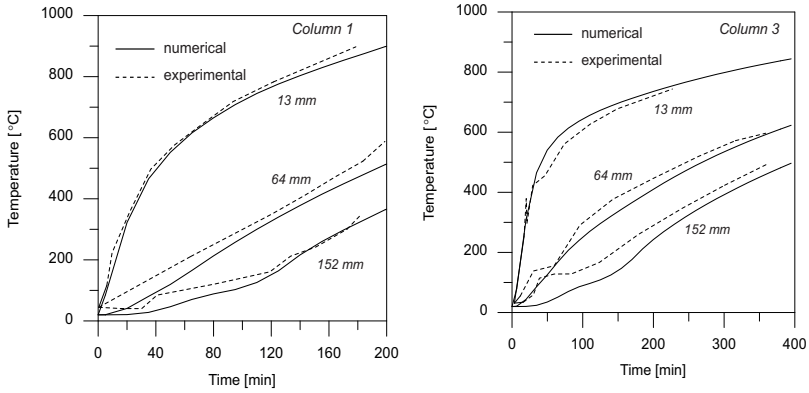

(a) (b)

FIGURE 4.3: Temperature distribution in : (a) Column 1 and (b) Column 3 (Lie and Irwin, 1990).

Structural behaviour

Evolution of the axial displacement at the top of the column has been compared against the values measured in the experimental test and the results are shown in Figure 4.4. Two constitutive models have been used: EN 1992-1-2 model (Figure 3.4(a)) and Eurocode Transient Creep (ETC) model by Gernay and Franssen (2012). No significant differences can be found in the responses obtained with these two models, as should be expected, given that explicit consideration of transient creep is expected to play a bigger role in the cooling than during the heating phase (Gernay and Franssen, 2012). The evolution of axial displacements in time is well predicted by both models and also the failure time of Column 3 is correctly captured (Figure 4.4). It is worth noting that performing a second-order analysis brings the numerically calculated values closer to the experimental ones. Failing to consider second-order effects leads to overly conservative results and failure time of 500 minutes, against 396 minutes from the experiment, is found.

Eccentrically loaded columns

Hass (1986) performed a series of full-scale tests on heated RC columns subjected to eccentrically applied axial loads. Three tested columns have been simulated numerically. Cross-section details and boundary conditions of the columns are shown in Figure 3.29.
Columns denoted as Hass 1 and Hass 16 are pin-ended, while Column Hass 21 was fixed at the bottom. In the Table below, dimensions of the section, length of the columns and properties of the materials are reported, together with the magnitude of the applied load and failure time. Columns were made of siliceous aggregate and were exposed to ISO834 fire on four sides.

In the following, the evolution of the axial and lateral displacements in time at mid-height are presented in Figure 4.5 for Column Hass 1, Figure 4.6 for Column Hass 16 and Figure 4.7 for Column Hass 21.

The failure is characterized by the typical steep increase of the dis-

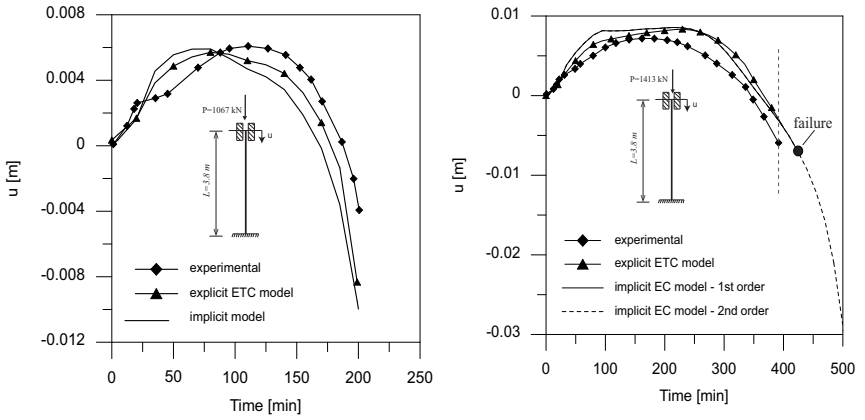

FIGURE 4.4: Axial deformation at the top of the column measured in: (a) Column 1 and (b) Column 3 (Lie and Irwin, 1990).

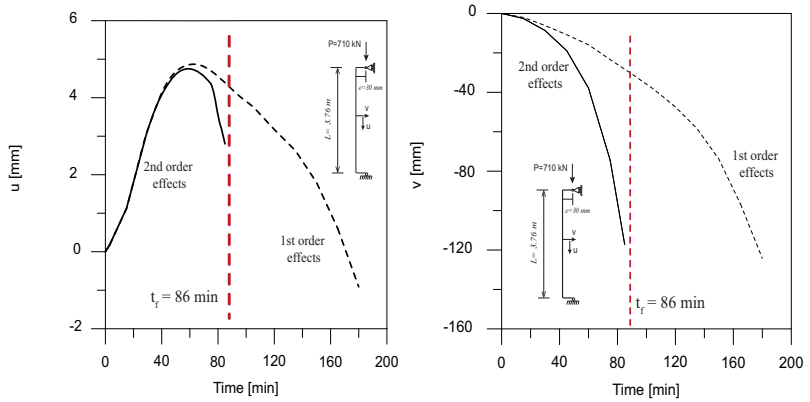

FIGURE 4.5: (a) Axial and (b) lateral displacement evolution in time for HASS 1 Column (Hass, 1986).

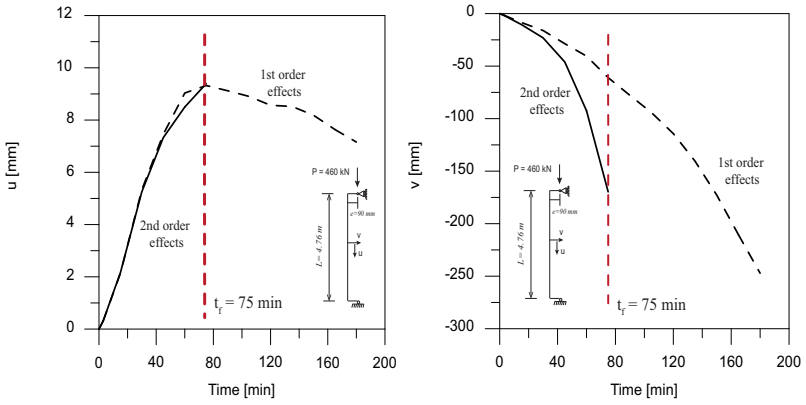

(a) (b)

FIGURE 4.6: (a) Axial and (b) lateral displacement evolution in time for HASS 16 Column (Hass, 1986).

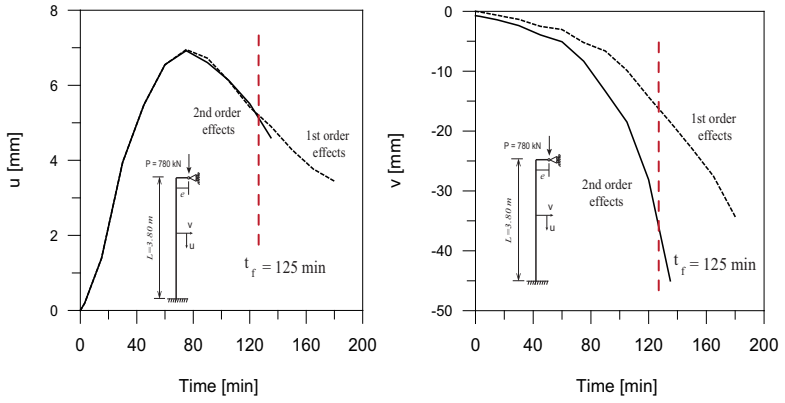

(a) (b)

FIGURE 4.7: (a) Axial and (b) lateral displacement evolution in time for Hass 21 Column (Hass, 1986).

placement rate (i.e. runaway failure), that is more pronounced when second-order effects are taken into account. In all cases, failure took place due to excessive lateral deflection. Initially, in the first 20 or 30 minutes of fire, the second order moments are still not developed to a significant extent: as a consequence, the two deflection curves are rather similar. With rise in temperature, the evolution of the mechanical properties (decrease of strength and increase of deformability) leads to the observed deflections' increase. Consequently, the second order moment contribution becomes significant, with the total acting moment on the structure being amplified, while in the first order analysis, the acting moment is constant. The introduction of second-order effects (continuous lines) causes, therefore, a very strong decrease of the fire resistance. Similarly to the sectional analysis, the first order analysis results in unsafe predictions of failure time. The failure for all three columns takes place at around 180 minutes.

TABLE 4.1: Time to failure - experimental and numerical results (Hass, 1986)

Time to failure [min]	Hass 1	t/t_{exp}	Hass 16	t/t_{exp}	Hass 21	t/t_{exp}
beam element - 1^{st} order	180	2.4	180	2.4	180	1.4
beam element - 2^{nd} order	85	0.91	75	1.41	135	0.72
experimental	86	-	75	-	125	-

4.4.2 Experimental tests in residual conditions

Experimental tests by Wu et al. (2010)

An extensive experimental campaign has been performed at South China University of Technology (Wu et al., 2010), where 12 elastically restrained columns (four for each type of cross-section, i.e. +-section, T-shaped and L-shaped cross section) were tested. Columns with +-shaped cross-sections were not simulated, because the results from the experiments were not available due to the erroneous mea-

surements. More details can be found in Chapter 2.

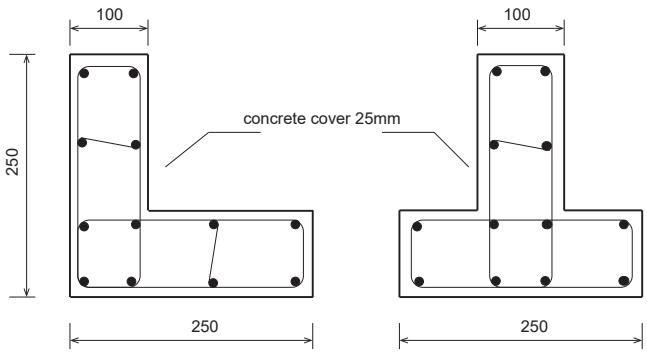

FIGURE 4.8: Cross-sections tested in (Wu et al., 2010).

Each column was reinforced with 12 HRB400 reinforcing bars with a diameter of 10 mm. The RC columns were initially concentrically loaded and subjected to ISO834 fire on all four sides. The stiffness of the axial restraint at the top of the column varied from 34.5 to 51.9 MN/m. All the columns had a length of 2340 mm, but only the central portion of the span (1650 mm) was heated. Recorded temperature inside the furnace followed closely the standard ISO834 fire for around 100 minutes, after which the cooling phase took place. The cooling phase lasted until approximately 180 minutes, when the fire temperature was around 300 °C. Location of the thermocouples is shown in Figure 4.9. Axial deformations were measured at the top end plate of the column, using four LVDTs.

During the tests, none of the columns failed and minor spalling was observed for some of the columns; therefore, it was not taken into account in the analyses.

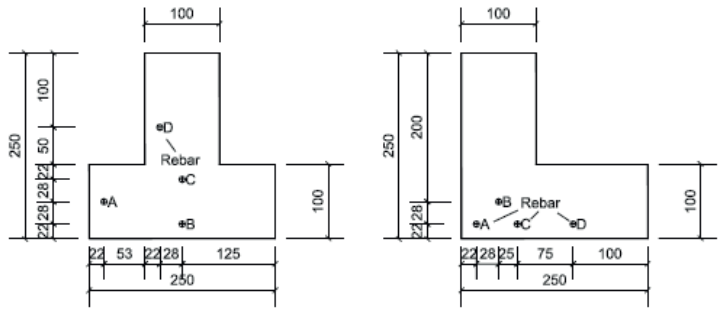

FIGURE 4.9: Locations of the thermocouples within a section in (from (Wu et al., 2010)).

Temperature distribution

Thermal analysis has been performed in ABAQUS 6.16 software and, as it was done before, only concrete has been modeled. Sections belonging to the unheated part of the column had a constant temperature of 20°C. The following thermal properties have been assigned to concrete: density equal to 2200 kg/m^2, upper limit value for conductivity (as per EN 1992-1-2) and the specific heat for dry concrete. All the column sections are exposed to fire on all four sides.

From Figure 4.10(a) and Figure 4.10(b) it is plain to see that the agreement between experimentally and numerically obtained results is satisfying, for both T-shaped and L-shaped columns.

Structural behaviour

Axial displacement at the top of each column was compared against the experimentally measured values. Structural model of the test assembly can be seen in Figure 4.11: only the movement in y-direction at the top of the column was allowed.

In Figure 4.13, time-displacement curves have been presented for all four columns with T-shaped section. The agreement in the ex-

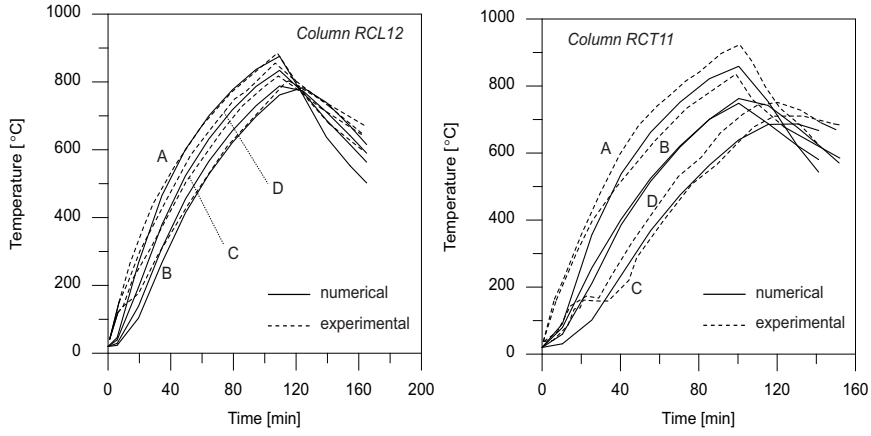

FIGURE 4.10: Temperature validation in (a) L-beam and (b) T-beam (Wu et al., 2010).

panding phase is rather good, while in the contracting phase there are some discrepancies, coming probably from the effect of axial restraint. The effect of axial restraint can be seen by looking at the displacements of Column RCT12 (k_l=51.9 MN/m), which deformed less than the column RCT11 (k_l=34.5 MN/m), both in expanding and contracting phase. The same is valid for RCT22, that deformed less than RCT21.

From the experimental results, it can be concluded that the maximum deformation during expansion phase depends mainly on the load level and less on the stiffness of the axial restraint. For a given load ratio, axial restraint plays a big role in the deformation evolution in the contracting phase (beyond zero deformation) and also the deformation went back to zero at almost the same time. The axial restraint reduces the residual deformation. Displacement trend is characterized by three stages - initial expansion due to thermal gradients, followed by contraction due to accelerated loss of strength

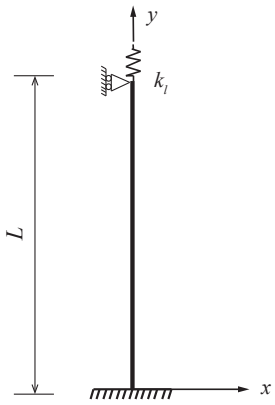

FIGURE 4.11: Structural scheme assumed for structural analysis (Wu et al., 2010).

and increase of deformability and finally, during the third and last stage, when the deflections tend to stabilize towards the end of the cooling phase. Numerical model was able to predict the axial deformation evolution in time quite well. The results are summarized in Table 4.2. It can be seen that explicit model gives closer prediction of the residual deformations with respect to the experimental values. In general, implicit model overestimates the deflection recovery, leading to lower residual deflections in comparison the measured ones. For the sake of comparison, RCL-12 column was also simulated as unrestrained(Figure 4.12(b)) and it can be seen that unrestrained column deforms much more than a restrained column, and failed due to excessive deformation at the end of the heating phase of fire.

Experimental tests by Raut and Kodur (2011)

Six reinforced concrete columns were tested at the Testing Laboratory of Michigan State University and the results were presented in

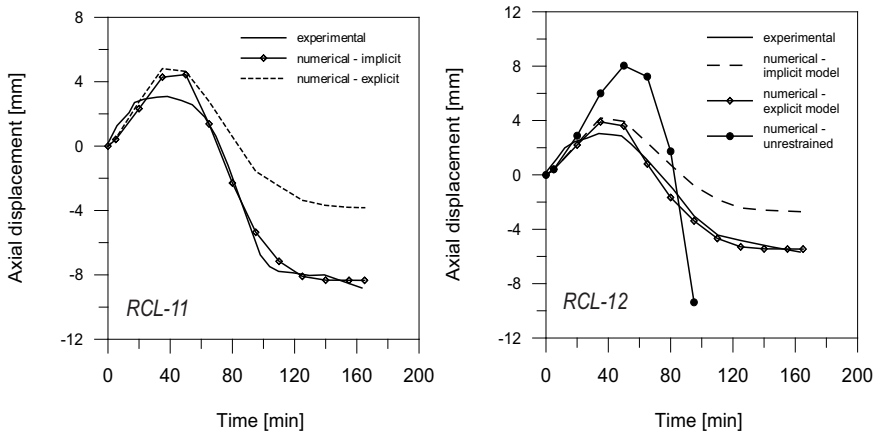

FIGURE 4.12: Displacement evolution in (a) RCL 11 and (b) RCL 12 column (Wu et al., 2010).

Raut and Kodur (2011). More details about the test are given in Chapter2. All columns were 3350 mm long, with a square-shaped cross section (203 x 203 mm). Geometry, cross-section and instrumentation location are shown in Figure 4.14. The details on the properties of the tested concrete columns can be seen in Table 3.4. Three columns were selected for the numerical analyses: NSC column exposed to standard fire and two high strength concrete columns with polypropilene fibers, exposed to a long duration design fire. These columns were chosen because they did not suffer spalling; therefore, the implementation of spalling phenomenon through the reduction of the concrete cross-section in the model could be avoided.

Axial deformations were measured at the top of each column. The columns responded in a similar way: expanding in the early stages of fire exposure and contracting later. Early expansion can be mainly attributed to the thermal expansion of concrete and steel. Contraction in the later stages is a result of loss of strength due to the increasing

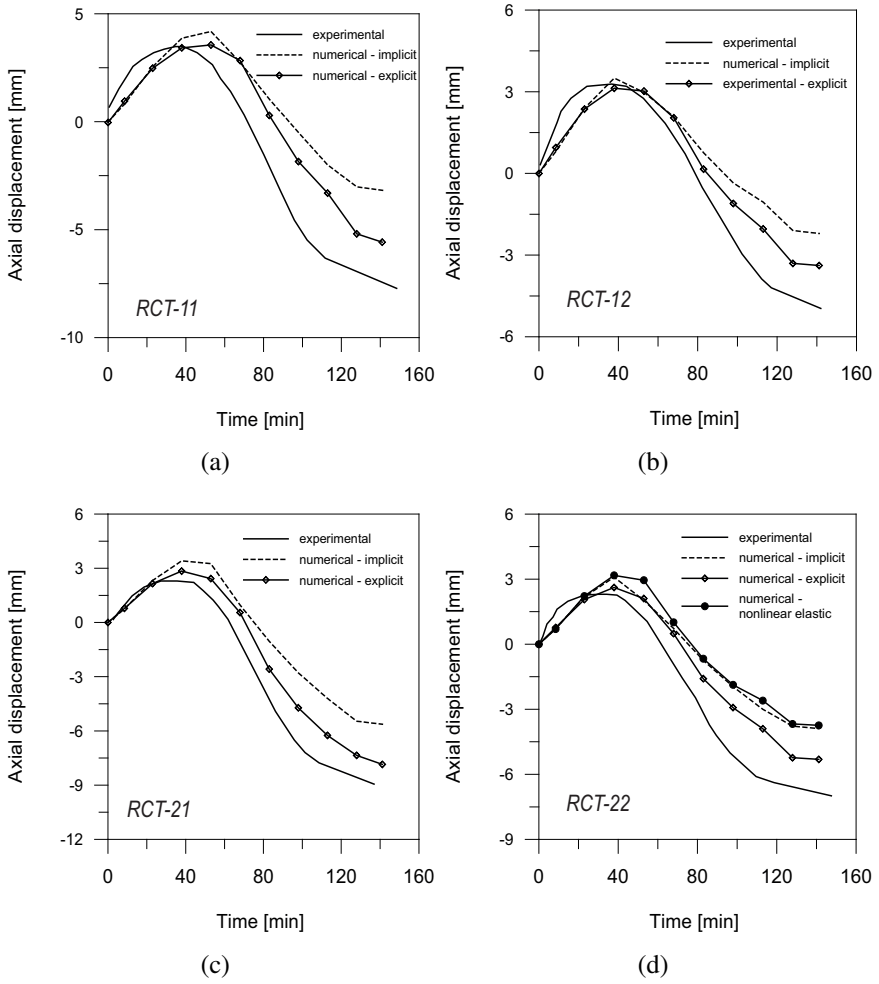

FIGURE 4.13: Displacement evolution in four T-shaped columns (Wu et al., 2010).

temperatures within the cross-section and also due to load redistribution from concrete to reinforcement.

The numerical model generally predicts well the displacement trend,

TABLE 4.2: Summary of test parameters and the results (Wu et al., 2010)

Column	Load ratio [%]	Axial restraint [MN/m]	Time at which displacement went back to zero [min]			Residual deformation [mm]		
			Implicit model	Explicit model	Experimental	Implicit model	Explicit model	Experimental
RCT11	0.24	34.5	95	85	71	-3.17	-5.57	-7.72
RCT12	0.24	51.9	90	85	76	-2.2	-3.38	-4.96
RCT21	0.34	34.5	75	70	64	-5.63	-7.85	-8.95
RCT22	0.34	51.9	75	72	62	-3.9	-5.31	-6.98
RCL11	0.24	34.5	80	75	72	-3.83	-8.4	-8.8
RCL12	0.24	51.9	85	70	73	-2.71	-5.45	-5.67

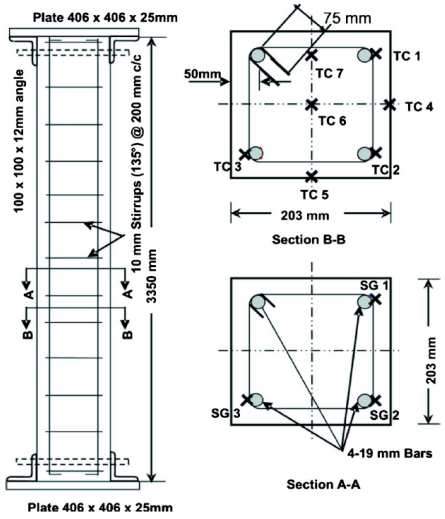

FIGURE 4.14: Columns dimensions and location of thermocouples and strain gauges (from Raut and Kodur (2011)).

and the axial deformation is overestimated with respect to the experimentally obtained values for the column HSCP2, while it is underestimated for the column HSCP1. The anticipated failure predicted by the model for column HSCP2 might have been caused by the delayed temperature rise inside the concrete (see Figure 4.16.

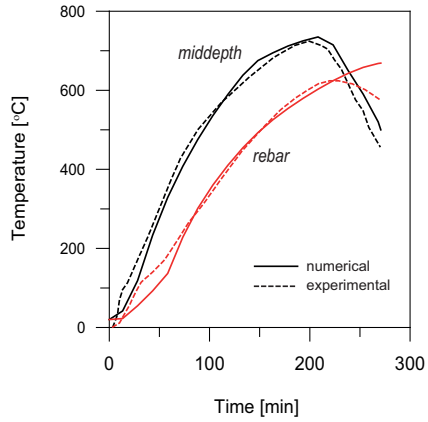

FIGURE 4.15: Temperature evolution in the concrete middepth and the rebar (Raut and Kodur, 2011).

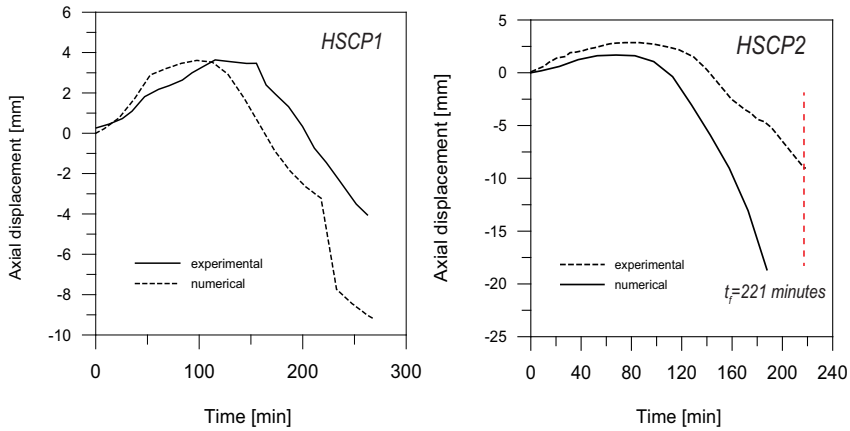

FIGURE 4.16: Axial deformation evolution in time for: (a) HSCP1 Column; (b) HSCP2 Columns Raut and Kodur (2011).

Experimental tests by Kodur et al. (2017)

Results from the residual capacity tests on two columns, designated as C1 and C2, were presented in (Kodur et al., 2017). Columns were first loaded, then heated and after complete cooldown, they were tested to failure, in order to determine the residual load capacity. Structural layout and reinforcement details can be seen in Figure 4.14, and they are identical to the columns tested by Raut and Kodur (2011). Columns had a length of 3350 mm but only the central portion of 1700 mm was exposed to fire. Both columns were built with NSC containing carbonate aggregate. Compressive strength at the test day was 50 MPa and 62 MPa for C1 and C2, respectively. Column C1 was loaded with a compressive force corresponding to 50 % of its factored ACI design capacity, while the load level of Column C2 was 55%. The load was maintained during both phases of the fire, heating and cooling. The two columns were exposed to design fires DF-1 and DF-2. The two design fires had the same cooling rate while the heating phase for DF-2 was 30 minutes longer than for DF-1. Peak temperatures reached in the rebars are around550 °C for C1 and around 600 °C for C2.

Structural behaviour is traced through the evolution of axial displacements, measured at the top of each column by LVDTs. Behaviour of the two columns is rather similar. Initially, the displacements increase due to thermal expansion caused by the increasing temperature. Then, it the second stage, axial deformation rapidly decrease and the columns start to contract, due to degradation of strength and stiffness in concrete and rebars. Once the temperatures in the member start to decrease, a recovery of the deflections takes place. Rate of recovery of the deflections is significantly slower than the rate of increase, due to nonlinear nature of the cooling phase and also irrecoverable damage that took place during heating and cooling. The residual deflection proved to be very sensitive to duration of the heating phase, as the residual deflection of Column C1 is about 50% greater than that of Column C2, though both columns pretty much

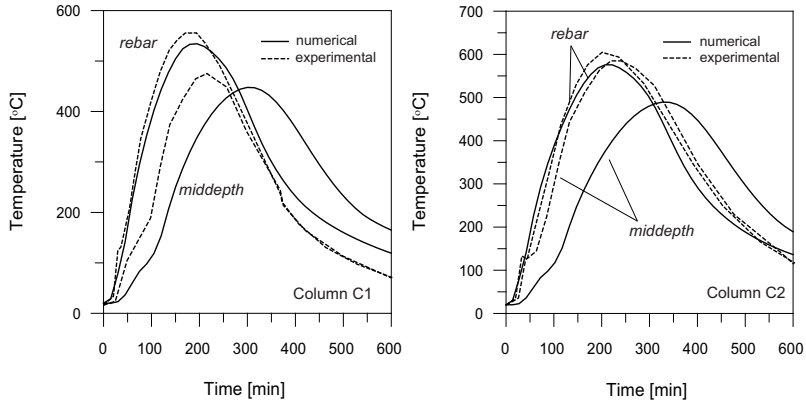

FIGURE 4.17: Rebar and concrete middepth temperature in column: (a) C1 and (b) C2 (Kodur et al., 2017).

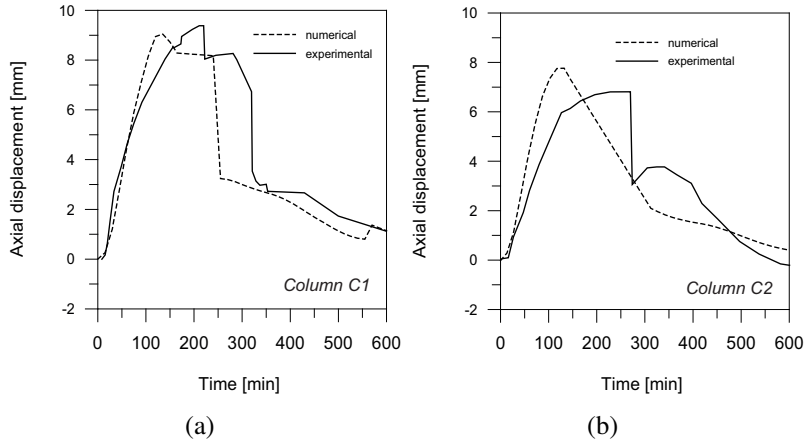

FIGURE 4.18: Axial deformation in column (a) C1 and (b) C2 (Kodur et al., 2017).

recovered their deflections to the initial state.

Chapter 5

3D Finite Element Analysis

Concrete modelling at high temperature is not an easy task due to the highly nonlinear material and structural behaviour. When irrecoverable deformation components at the material level are taken into account, it is often required to perform plastic analyses and, consequently, the use of advanced constitutive models implemented in finite element codes becomes mandatory. When beams and columns are at issue, numerical modelling via beam finite elements (Bamonte and Monte (2015)) can be carried out by using the uniaxial constitutive laws, such as those provided in the pertinent standards (European Committee for Standardization (2005b)). On the other hand, when more complex structural members (such as ceilings, walls and tunnel linings) are considered, 2D or 3D finite elements analyses must be carried out, thus requiring the definition of concrete behaviour for multiaxial states of stresses.
Numerical models that use 3D Finite Elements are the most complex models for structural analysis. They require significant computational and modeling effort and should be used with care. In the case where the local behaviour of RC structures exposed to fire is a principal study objective, a 3D element model can be a very efficient tool. In addition, non-uniform heating (e.g. localized heating), when the heat transfer along the length of the member is important, modeling the

bond slip or a localized spalling requires to consider the whole volume of the structural member and to model in the 3D space.
In this Chapter, procedure for performing the 3D finite element analysis in ABAQUS 6.16 software will be presented. At first, theoretical background with some indications on how the numerical models using 3D elements were built will be given. Focus will be put on the description of the material behaviour in cooling and stress-strain law definition in compression and tension for concrete and steel. Some words on the multiaxial concrete constitutive model available in the software will be given.
The 3D model is validated against the available experimental data on reinforced concrete beams. Parametric analyses were then performed on RC beams, and the influence of the various parameters (i.e. load ratio, concrete cover, duration of heating phase, cooling rate) on the global behaviour was studied. Besides RC beams, analyses were performed on the number of columns tested at University of Edinbourgh, to validate the ability of a 3D model to predict the deflections in case of exposure to a localized heating. Lastly, selected simply supported columns and beams, available in the literature were analysed and the results were compared with those obtained from sectional and beam element analysis, which were reported in the Chapter 3 and Chapter 4.

5.1 General characteristics of the numerical Analysis

Sequentially coupled thermo-mechanical analysis is performed by means of the commercial finite element software ABAQUS 6.16. First step consists in solving the pure heat transfer problem. Afterwards, the temperature solution is read into a stress analysis as a predefined field (ABAQUS, 2016).
Therefore, two sub-models are built: a model for thermal analysis and a model for mechanical analysis. Nodal temperatures are stored

as a function of time in the heat transfer results. The temperatures in the member act as thermal body-load in the structural model, being the initial condition for the subsequent mechanical analysis. Longitudinal reinforcing bars and stirrups are present in both thermal and mechanical model.

5.1.1 Thermal analysis

Heat transfer within the element is assumed to be governed by conduction. Thermal conductivity, specific heat and density are defined as temperature-dependent, with the assigned values as proposed in EN 1991-1-2. At the boundaries of the heat exposed surfaces, heat transfer takes place by convection and radiation. Convection with convective coefficient of α = 25 W/m^2K is assumed for fire exposed surfaces, while for the unexposed surfaces it is set to α = 9 W/m^2K, accounting therefore for the radiation. Radiation with ε = 0.7 is assumed for all the heat-exposed concrete surfaces. Thermal model is discretized into a number of finite elements (element side length h= 0.015m). Eight-noded linear brick elements (DC3D8) are used for concrete while reinforcing bars are discretized using two-noded link or truss elements (DC1D2). These elements have the nodal temperature as the only active degree of freedom. Concrete-rebar interface is modelled using a tie constraint, to enforce a unique temperature at the nodes shared between steel and concrete.

5.1.2 Mechanical analysis

Decay of the material mechanical properties at elevated temperature for concrete and reinforcing steel is taken as per EN 1992-1-2. In the cooling phase, the properties are considered as irrecoverable, to account for the thermal damage in the material. This has been done by implementing a FORTRAN user subroutine - UFIELD (ABAQUS, 2016), which updates the mechanical properties only in the heating phase, when the temperature in the current time increment has in-

creased with respect to the previous one. If the material is in the cooling phase, its properties keep the value they had at the maximum temperature, i.e. the behaviour is governed by the maximum and not by current temperature. Definiton of material properties in Abaqus software requires the definition of temperature dependent elastic properties as well as the definition of the plastic model. More words on this topic will be given in the next sections.
3D stress/displacements elements have been used for the discretization of concrete and steel rebars. Concrete is discretized using 8-node linear-brick elements (C3D8), with translations in three directions as active degrees of freedom at each node. This element type can be used for modeling of solids with or without reinforcement, and it is capable of accounting for cracking of concrete in tension and crushing of concrete in compression, creep and large strains (ABAQUS, 2016). Steel rebars are discretized with 2-noded linear displacement truss elements (T3D2), which deform by axial elongation only. They are pin jointed at their nodes. When the strains are large, the formulation is simplified by assuming that the trusses are made of incompressible material. This approach has been used to model the reinforcement where the nodes of reinforcement are coincident with the nodes of concrete (ABAQUS, 2016). Concrete-rebar interface is modelled with embedded region constraint, i.e. no slip is allowed.

5.2 Constitutive model for concrete

5.2.1 Concrete Damaged Plasticity Model

To define plastic behaviour of concrete in ABAQUS, Concrete Damage Plasticity (CDP) model (Lubliner et al., 1989, Lee and Fenves, 1998) is used. This model was originally set-up for modelling concrete behaviour under complex load cycles, featuring loading and unloading, development of irreversible deformations, as well as the ensuing degradation of the elastic properties. This model allows capturing the strong nonlinearity of concrete and different failure mecha-

nisms in tension (by cracking) and compression (by crushing), and is primarily intended for modelling reinforced concrete structures. CDP model assumes that the uniaxial tensile and compressive responses of concrete are characterized by a plastic behaviour, whereas the irreversible phenomena that characterize the unloading phase (if any) are treated by means of a damage mechanics approach (ABAQUS, 2016). Tension stiffening, i.e. the contribution of the tensile stiffness of uncracked concrete after to the reinforcement stiffness has to be defined. The temperature-induced decay of the mechanical properties of concrete is taken as per Eurocode 2 (European Committee for Standardization, 2005b). However, mechanical properties are considered as not recovered during cooling. Moreover, unloading is allowed to take place along the branch defined by the unloading stiffness, that is somewhat higher that the initial stiffness. In this way, the irrecoverable strain components (i.e. transient creep strain) are accounted for in an implicit and simple manner. The qualitative representation of the constitutive model for concrete can be seen in the Figure 5.1.

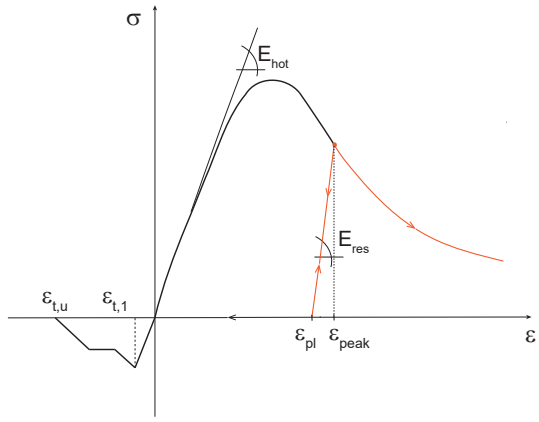

FIGURE 5.1: Constitutive model for concrete, implemented in ABAQUS.

5.2.2 Failure Criterion and Parameters of the CDP Model

In particular, in addition to the uniaxial mechanical properties (modulus of elasticity, compressive and tensile strength), in the CDP model two parameters must be defined in order to define the failure surface:

1. The ratio between biaxial and uniaxial compressive strength ($f_{c,b}/f_{c,1}$)
2. The ratio between the second stress invariant on the tension meridian and the second stress invariant on the compression meridian (k_c).

The first parameter defines the extension of the failure surface in the Haigh-Westergaard space, and is relevant for states of biaxial-triaxial compression, whereas the second parameter is related to the shape of the failure surface on any deviatoric plane, and is thus more relevant for states of combined tension and compression.

The most common values of these two quantities at ambient temperature are ${f_{bo}}^T / {f_{co}}^T$ = 1.16-1.20 and K_c = 0.667.

Failure model at ambient temperature

While well-established strength models for biaxially stressed concrete are available at room temperature (e.g. (fib, 2013)) it is not the case for high temperatures. However, failure criterion for concrete during heating or in residual conditions can be based on that for normal temperature, if properly modified.

In a very general form, assuming tension stress to be positive, yield function for frictional materials like concrete and rock can be written as in *Eq.* (5.1) (Lee and Fenves, 1998).

$$\overline{F}(\sigma) - c = 0 \tag{5.1}$$

where c is cohesion and $\overline{F}$ is a scalar function of invariants of stress tensor. Cohesion c represents material uniaxial compressive strength,

which is temperature dependent. In case of 3D stress states, yield function proposed in (Lubliner et al., 1989, Lee and Fenves, 1998) has the form of *Eq.* (5.2).

$$\overline{F}(s) = \frac{1}{1-a}[\sqrt{3J_2} + \alpha I_1 + \beta\langle\sigma_{max}\rangle\langle-\sigma_{max}\rangle] = f_c \qquad (5.2)$$

where $< a >$ = a if a is positive and 0 otherwise.

I_1 and J_2 are the first and second stress deviator, respectively, α and β are dimensionless constants depending on mechanical strength according to *Eqs. (4a,b)* and γ depends on the ratio K_c between second stress invariant on the tension meridian and second stress invariant on the compression meridian. They can be calculated using the Equations written below.

$$I_1 = \sigma_1 + \sigma_2 + \sigma_3$$

$$J_2 = \frac{1}{6}\left[(\sigma_1 - \sigma_2)^2 + (\sigma_2 - \sigma_3)^2 + (\sigma_1 - \sigma_3)^2\right]$$

$$\alpha = \frac{(f_{bo}/f_{co}) - 1}{2\,(f_{bo}/f_{co}) - 1}$$

$$\beta = (1-\alpha)\,(f_{co}/f_{to}) - (1+\alpha)$$

$$\gamma = \frac{3\,(1-K_c)}{2K_c - 1}$$

where f_{bo} and f_{co} are initial biaxial and uniaxial compressive yield stresses, respectively, and f_{to} is uniaxial tensile yield stress.

Parameter γ appears only in triaxial compression, since all principal stresses are negative (hence also σ_{max} is negative).

For biaxial compression (σ_{max} = 0), CDP matches the Drucker-Prager criterion (*Eq.* (5.3)).

$$\overline{F}(\sigma) = \frac{1}{1-\alpha}\left[\sqrt{3J_2} + \alpha I_1\right] \qquad (5.3)$$

Failure model at elevated temperature

Having the stresses measured in two principal planes and compressive strength at each test temperature, it is possible to calibrate the parameters α and β to fit the experimental data for each temperature. This will enable to study the variation of biaxial-to-uniaxial strength ratio with temperature.The main parameters of the CDP model were calibrated via inverse analysis (see LoMonte et al. (2017)), on the basis of the experimental data available in the literature regarding tests under multiaxial state of stress in hot (Ehm and Schneider, 1985, Kordina et al., 1986, Thienel and Rostasy, 1995, He and Song, 2009) and residual (He and Song, 2010, He and Song, 2016) conditions. The experimental tests results that served for the calibration will be briefly recalled in the following.

Experimental studies under multiaxial state of stress

Kordina et al. (1986) carried out biaxial compression tests on normal-strength concrete specimens, with a cube strength of 41 MPa. The tests were carried out in steady state and transient temperature conditions (hot tests). For each thermal level, the results of the tests were interpreted with a failure envelope in the plane of principal stresses σ_1 and σ_2 ($\sigma_3 = 0$ for biaxial state of stress). The strength under biaxial compressive stress turned out to be higher than the strength under uniaxial compression. The relative increase of strength under biaxial stress is more significant at higher temperatures than at ambient temperature. Moreover, the failure temperature of the specimens under biaxial stresses is higher than that of specimens in uniaxial compression.

Thienel and Rostasy (1995) studied the mechanical behaviour of NSC subjected to high temperature (hot conditions) and biaxial stress. The results concerning the biaxial compressive strength at different temperatures are reported for two different concrete mixes with an initial uniaxial compressive strength of 45 and 37 MPa respectively. The temperature-induced decrease of strength is affected by the com-

position of concrete in the entire range of biaxial compressive stress. The maximum aggregate size has a significant influence, while aggregate and w/c ratio are found to play a minor role. Moreover, strength values are affected by concrete composition up to a temperature of 450°C. At this temperature, the decomposition of portlandite begins and significantly alters the structure of the cement paste. After the decomposition of portlandite, the aforementioned tendencies change or become more pronounced.

Ehm and Schneider (1985) show that small load levels along the second axis significantly alter the mechanical properties of concrete at high temperature (hot conditions). Test results indicate an increase of ultimate biaxial strength at high temperature compared to uniaxial strength. Biaxial strength increase is comparatively larger at high temperatures with respect to residual conditions.

A series of tests were performed by He and Song (2016) for characterizing the strength and deformation behaviour of two High-Strength High-Performance Concretes (HSHPC) at 7 different stress ratios, after the exposure to high temperatures (residual conditions). The results showed that the uniaxial compressive strength of plain HSHPC after exposure to high temperatures does not decrease dramatically with the increase in temperature. The ratio of the biaxial to its uniaxial compressive strength depends on the stress ratios and brittleness-stiffness of HSHPC after exposure to different temperature levels. Moreover, the biaxial compressive strength is larger than its corresponding uniaxial compressive strength at all stress ratios for the same temperature level.

Results of the fitting procedure

Calibrating the parameter α to fit the available experimental data, biaxial-to-uniaxial strength ratio can be determined together with its evolution with temperature. As expected, this ratio increases with the temperature as clearly shown in Figure 5.2.

As for the fitting procedure results, it can be seen that the results

are satisfactorily fitted and with a small error margin for experimental data from residual tests, where the dependence of ratio ${f_{bo}}^T / {f_{co}}^T$ on temperature is less pronounced than in hot conditions and its value is not significantly increased with temperature. As for the hot tests, better fit is obtained at lower temperatures, when the values of ${f_{bo}}^T / {f_{co}}^T$ are still somewhat close to those at ambient conditions (α = 1.08-1.20). With significant increase in temperature and corresponding decay in uniaxial compressive strength, values of parameter α are sizably higher and the fitting accuracy is lower. The ratio ${f_{bo}}^T / {f_{co}}^T$ in hot conditions showed to be strongly dependent on the temperature, going from values in the range 1.1-1.3 at room temperature to values in the range 2.0-3.0 at 600°C. In residual conditions the variation is less evident, since at 750°C the ratio is around 1.8.

It is also shown as the biaxial yield function (failure dominium) described in CDP model satisfactorily represents the experimental evidences, even though with a lower accuracy in hot conditions.

As regards K_c, experimental data are available for residual conditions only. In such cases, K_c parameter proved to be far less temperature-sensitive than ${f_{bo}}^T / {f_{co}}^T$, remaining in the range 0.60-0.67 from 20 to 600°C, with only a slight decrease with temperature. For K_c is, thus, reasonable to keep a constant value (as for example the common value 0.667) for all the temperature range, at least in residual conditions. As for the triaxial tests, after performing fitting procedure on α, also the coefficient γ was calibrated for each test temperature. Its variation with temperature is far less pronounced (K_c = 0.660 at 20°C and K_c = 0.644 at 600°C).

5.2.3 Tension model

Cracking in the finite element models can be modelled using either discrete or smeared approach. In the discrete approach, cracks are modeled as a separation of elements while the smeared approach models solid cracked continuum (Pankaj, 1990). Given that discrete method requires a very fine mesh, it might be difficult to use it on

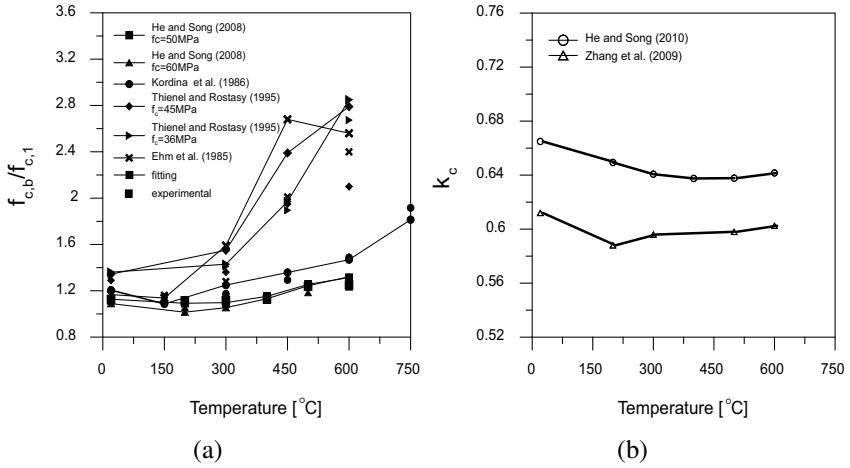

(a) (b)

FIGURE 5.2: Test results considered in the fitting procedure: a) normalized decay of the uniaxial compressive strength; and b) ratio between biaxial and uniaxial compressive strength as a function of temperature (LoMonte et al., 2017).

large scale arbitrary structures without facing a large computational effort.

Talking about the ambient temperature conditions, it is well known that the mesh insensitive results can be obtained through the implementation of a fracture energy based model. The concrete model implemented in ABAQUS software is a smeared crack model in the sense that it does not track individual ”macro” cracks. Constitutive calculations are performed independently at each integration point of the finite element model. The presence of cracks enters into these calculations by the way in which the cracks affect the stress and material stiffness associated with the integration point (ABAQUS, 2016). As a matter of fact, in ABAQUS software, the post-peak behavior in tension can be defined in three ways:

- Stress-strain relation (dependent on the element size)

- Stress-displacement formulation
- Tensile fracture energy

As stated in ABAQUS Technical Documentation (ABAQUS, 2016), the smeared cracking model is suitable for concrete modeling in all types of structures (beams, trusses, shells and solid). It is intended primarily for the analysis of reinforced concrete structures, but it can be used for plain concrete as well. The model is intended to model concrete behavior for relatively monotonic loadings under fairly low confining pressures. The concrete behavior is considered independently of the rebar. Effects associated with the rebar/concrete interface, such as bond slip and dowel action, are modeled approximately by introducing some "tension stiffening" into the concrete modeling to simulate load transfer across cracks through the rebar. As a matter of fact, tension stiffening allows to define the strain-softening behavior for cracked concrete, and, in a simplified manner, to account for the effects of the concrete-reinforcement interaction. The interaction between the rebars and the concrete tends to reduce the mesh sensitivity, provided that a reasonable amount of tension stiffening is introduced in the concrete model to simulate this interaction. The choice of tension stiffening parameters is important in Abaqus/Standard since, generally, more tension stiffening makes it easier to obtain numerical solutions. Too little tension stiffening will cause the local cracking failure in the concrete, introducing temporarily unstable behavior in the overall response of the model. Tenson stiffening, as a contribution of the uncracked concrete to the stiffness of the structure, decays as the stress increases, due to continued formation of cracks. Until the reinforcement start to yield, some tension stiffening is always present. Several tension stiffening models are available for modelling the concrete at ambient conditions (Model Code, 1993; Cervenka et al., 1990, Feenstra and de Borst, 1995). For instance, Cervenka et al. (1990) proposed that tension stiffening should be treated as a separate interaction contribution and not a part of the concrete constitutive model. Total stress in a member becomes a sum

of the three stress contributions: from the concrete, from the reinforcement and from the interaction. This makes it possible to define the concrete stress distribution, as well as tension stiffening effect, by the tensile fracture energy and the element side length, thus making the FE model mesh insensitive. The interaction contribution was defined as a trilinear function. However, in order to implement Cervenka Tension Stiffening Model, three criteria have to be satisfied: about minimum element size, maximum element size and reinforcement ratio (more details are given in Cervenka et al. (1990)). Model from Feenstra and de Borst (1995) is also based on the fundamental assumption of the tension stiffening as an interaction contribution. They defined modified fracture energy for RC tackled the issue of the limit on the minimum length of the element size.

Fracture Energy Based Tensile Model at Elevated Temperatures for Plain Concrete

Fracture energy based tensile model at elevated temperature is based on the material model by Terro (1998) for plain concrete. This model has a linear softening branch and assumes a constant value for the ultimate tensile strain at all temperatures equal to $\varepsilon_{ctuT} = 0.004$. Tensile fracture energy of a plain concrete is equal to the area under the stress-plastic displacement curve (triangular shape). For the element of constant size h, tensile fracture energy decays as the tensile strength of the concrete decreases. Fracture energy is equal to:

$$G_{fT} = \frac{1}{2} f_{ctT} \varepsilon_{ctuT} h \tag{5.4}$$

Tensile fracture energy at elevated temperatures can be expressed as a function of the tensile fracture energy at ambient temperature, G_f, by multiplying it with a reduction coefficient for tensile strength with temperatures.

$$G_{fT} = \zeta(T) \frac{1}{2} f_{ct,m} \varepsilon_{ctuT} h \tag{5.5}$$

Fracture Energy Based Tensile Model at Elevated Temperatures for Reinforced Concrete

The formulation for the plain concrete is expanded to include the interaction contribution as per Cervenka et al. (1990). Interaction contribution is still considered to be a trilinear function and it is defined by four strains: the strain at peak stress ε_{0tT}, the ultimate concrete strain ε_{cuT}, the ultimate strain ε_{uT} and finally the yield strain of the reinforcement ε_{yT}. These strains are computed using the formulations valid at ambient temperature but with the material properties of concrete and steel being temperature dependent. These strains are computed as:

$$\varepsilon_{0tT} = \frac{f_{ctT}}{E_{ciT}} \tag{5.6}$$

$$\varepsilon_{cuT} = \frac{2G_{fT}}{hf_{ctT}} \tag{5.7}$$

$$\varepsilon_{uT} = \varepsilon_{yT} - \frac{\alpha_{ts} f_{ctT}}{\rho_{s,eff} E_{sT}} \tag{5.8}$$

$$\varepsilon_{yT} = \frac{f_{yT}}{E_{sT}} \tag{5.9}$$

where α_{ts} is the strength level of the interaction contribution (assumed as 0.7).

A care should be taken concerning some limitations regarding the element size and minimum reinforcement ratio that can be considered for the interaction formulation (Cervenka et al., 1990).

5.3 Constitutive model for steel

Plasticity model that uses Mises yield surface with associated plastic flow and isotropic hardening was used to model the steel in tension and compression (ABAQUS, 2016). Eurocode-proposed model with

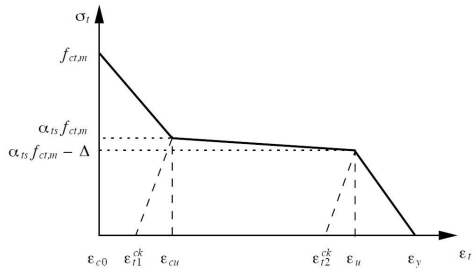

FIGURE 5.3: Tension stiffening models defined in ABAQUS software - combination of the concrete and interactions contributions (from Carstensen (2011) and based on Cervenka et al. (1990)).

distinct elastic and yield strength was used. Variation of the mechanical properties, namely strength and elastic modulus, is taken as per Eurocode. Limiting criteria for the irrecoverable damage in steel was the maximum temperature. Strength and stiffness of the steel rebars are considered as not recovered upon cooling only if the maximum temperature in the rebars exceeded 500°C. Otherwise, influence of irrecoverable creep can be neglected and steel can be considered to recover its strength and elastic modulus upon cooling down (Neves et al., 1996). The qualitative representation of the constitutive model for the reinforcing steel can be seen in the Figure 5.4.

5.4 Validation of the numerical model

Model validation was carried out on two beams tested by Dwaikat and Kodur (2009). The first beam, designated as B1, was a simply supported beam and subjected to a standard fire (ASTM E-119). The second beam, designated as B2, was axially restrained and subjected to a short design fire (SF). Details of the beam geometry and cross

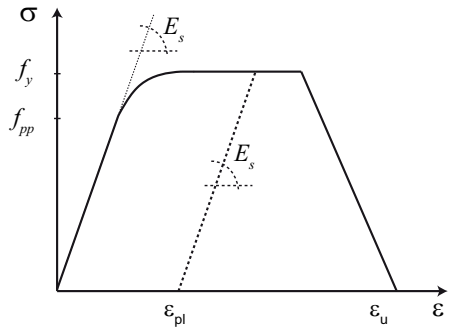

FIGURE 5.4: Constitutive model for steel, according to EN 1992-1-2.

section can be found in Dwaikat and Kodur (2009). The two beams had identical reinforcement, with rebars having a yield strength of 420 MPa. The beams were made of NSC, having average compressive strength of 55 MPa. Both beams were tested under two point loads of 50 kN, applied 30 minutes before the start of the fire and maintained constant throughout the fire exposure. The applied loads produced a bending moment equal to 55% of the flexural capacity of the beam. There was no spalling during the test.

Temperature distribution

For the beam B1, temperatures monotonically increase during fire exposure. Comparison between measured and calculated temperatures in the bottom corner rebar as well as the quarter and mid-depth can be seen in Figure 5.5(a). This beam failed during the test, after around 180 minutes into fire exposure, when rebar temperature reached 577°C. On the other hand, maximum temperature in the rebar predicted by the model is slightly higher, 597°C. Generally, temperatures are in a good agreement.

For the beam B2, rate of temperature rise at the beginning is rather high, due to steeper temperature rise of SF fire. Maximum temperature both in the rebar and concrete core is reached during the cooling

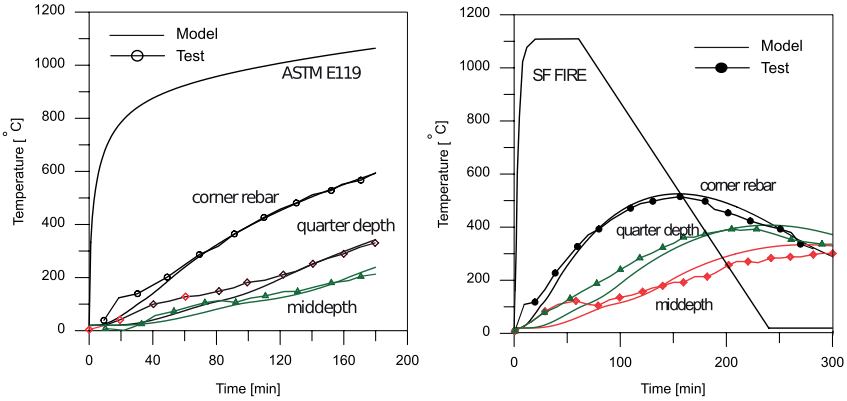

(a) (b)

FIGURE 5.5: Comparison between measured and calculated temperatures for the beam (a) B1 and (b) B2 (Dwaikat and Kodur, 2009).

phase of the fire. After reaching the maximum temperature, decrease in temperature takes place due to decay phase of fire exposure, as it can be seen in Figure 5.5(b).

Structural behaviour

Given that the behaviour of RC members in flexure is governed primarily by the temperature in the rebars, midspan deflections are increasing as long as the rebar temperature is increasing. As the rebars start to cool down, the trend of the deflection response reverses, leading to a certain recovery and a residual deflection smaller than the maximum one (Figure 5.6(b)).

For beam B1, midspan deflections increase during early stages of fire exposure due to temperature induced degradation of strength and stiffness of concrete and reinforcing steel. Following the monotonic increase of temperature, the beam fails due to excessive deflections caused by significant degradation of strength and stiffness. The trend

is captured correctly by the numerical model. On the other hand, beam B2 did not fail during heating-cooling cycle. Given that the behaviour of RC members in flexure is governed primarily by the stiffness in the rebars, it is clear that the midspan deflections are increasing as long as the rebar temperature is increasing. As the rebars start to cool down, the trend of the deflection response reverses, leading to a certain recovery and a residual deflection smaller than the maximum one. Overall, the agreement between the numerical and experimental values is good, both for the temperatures and the midspan deflection.

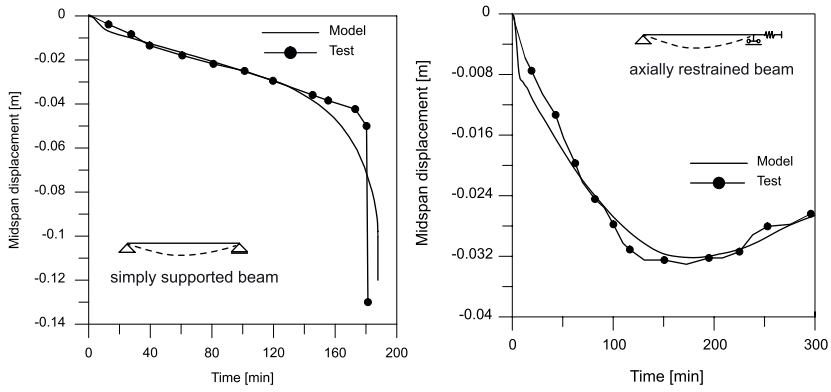

FIGURE 5.6: Comparison between measured and calculated displacements for the beam (a) B1 and (b) B2 (Dwaikat and Kodur, 2009).

5.5 Parametric analyses

Parametric analyses were performed on two RC beams, with a span L=5 m (Kalaba et al., 2018). Central portion of the span was exposed to fire. Beam geometry and cross-section details can be seen in Figure 5.7. Reinforcement ratio for both beams was 1.2%. Section BX2

is more massive than BX1; in this way, the role of the section size in the overall structural response can be highlighted.

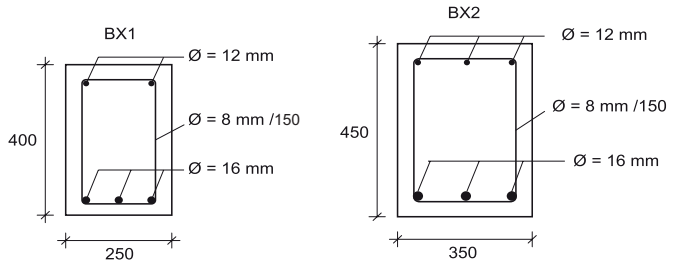

FIGURE 5.7: Cross-section details of the beams BX1 and BX2.

Concrete compressive strength is f_c=50 MPa while the steel yield strength is f_y=450 MPa. Bending capacity of the two beams at ambient temperature is M_{rd}=126 kNm for BX1 and M_{rd}=191 kNm for BX2. Uniformly distributed load acting on both beams caused maximum bending moments equal to 50% of the capacity at ambient temperature (load level 0.5). Parameters such as duration of the heating phase, cooling rate and concrete cover were varied. All the fire scenarios correspond to the parametric fire of Eurocode 2. The amount of fuel load varied from 250 to 750 MJ/m^2, resulting in the heating phase duration of 1h for fire scenario PF1, 2h for fire scenario PF2 and 3h for fire scenario PF3. Cooling took place along a linear branch, with cooling rate computed according to Eurocode - faster cooling (European Committee for Standardization, 2005b)) and "Buchanan" - slower cooling (Feasey and Buchanan, 2002). The initiation of the cooling phase of fire is also indicated in the figures. Concrete cover varied from 20 to 40 mm. Reference parameters are PF1 fire scenario with Eurocode cooling rate and concrete cover of 4 cm.

TABLE 5.1: Parameters defining three fire scenarios for parametic analyses

Fire Scenario	$q_{t,d}[MJ/m^2]$	Opening Factor O	Cooling rate EC [°C/h]	Cooling rate Buchanan [°C/h]
PF1	250	0.056	580	325
PF2	550	0.056	550	305
PF3	750	0.056	606	320

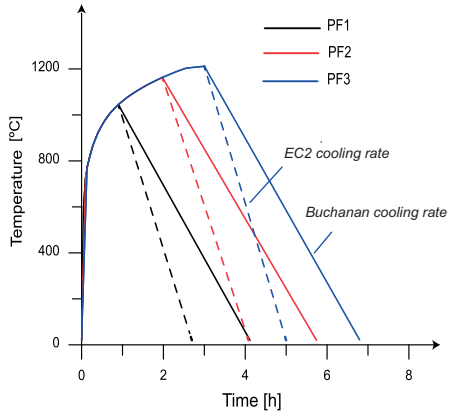

FIGURE 5.8: Three fire scenarios used for parametric analyses of the RC beams.

5.6 Role of thermal field

Given that almost the full moment capacity of the RC beam is provided by the reinforcing steel, it is more than clear that a sizable loss of rebar stiffness and strength has to be prevented in order to minimize the residual deflections and eventually avoid failure. However, since the reference concrete cover depth is 4 cm, very high temperatures are likely to be attained in most cases. In Figure 5.9(a) the average temperature in the corner rebars is plotted as a function of the fire duration, for the beam BX1. It is worth noting that the tempera-

ture continues to increase for some time after the onset of the cooling phase: as a matter of fact, the maximum temperature is reached at approximately 120, 180 and 270 minutes for heating phase durations of 60, 120 and 180 minutes, respectively. As previously mentioned, this can be attributed to the low conductivity and high thermal capacity of concrete, which delay the heat transfer towards the inner layers of the section.
Maximum temperature varies significantly with the duration of the heating phase, from 484°C for 1h fire duration to 791°C for 3h fire duration. Note that failing to account for the cooling phase can lead to a significant underestimation of the maximum temperature (from -20 to -50%). Similar trends are followed also for beam BX2, but given that it is more massive, the temperatures are somewhat lower (Figure 5.10). In Figure 5.9(b), the average temperature in the rebars is plotted as a function of the cooling rate, for the duration of the heating phase of 60 min (PF1). Cooling rate has a significant influence on the temperature in both the concrete core and the rebars, with slower cooling leading to higher temperatures. Moreover, better protected steel rebars experience lower temperatures (Figure 5.10(b)).

5.7 Structural response

In Figure 5.12, the evolution of the deflection at midspan is shown for fire durations of 1, 2 and 3 hours. Increasing the fire duration increases the temperature in the rebars which then leads to higher peak deflections and also higher residual deflections. The deflections continue to increase also in the cooling phase of the fire; therefore neglecting the cooling phase of fire can lead to a significant underestimation of the maximum deflection (up to 40%). Upon cooling, the deflection trend reverses, leading to a limited recovery. In Figure 5.13(a) the effect of the cooling rate on the evolution of the midspan deflection can be noticed. Slower cooling leads to higher maximum deflection, due to prolonged increase of the temperatures

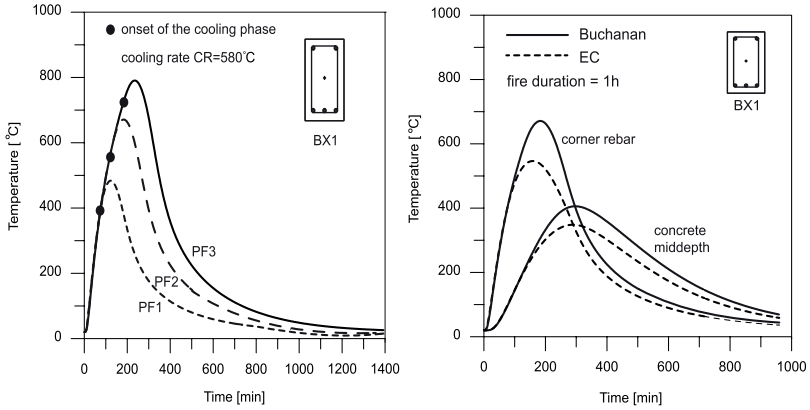

(a) (b)

FIGURE 5.9: Temperature in the corner rebar in the beam BX1 for: (a) different fire duration; (b) different cooling rates.

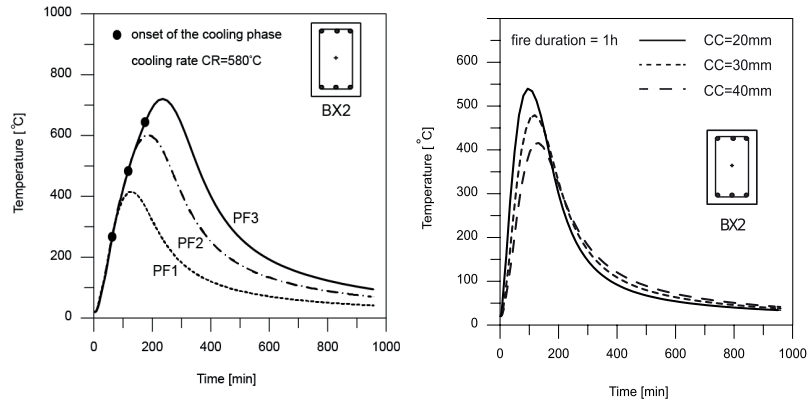

(a) (b)

FIGURE 5.10: Temperature in the corner rebar in the beam BX2 for: (a) different fire duration; (b) varying concrete cover to steel bars.

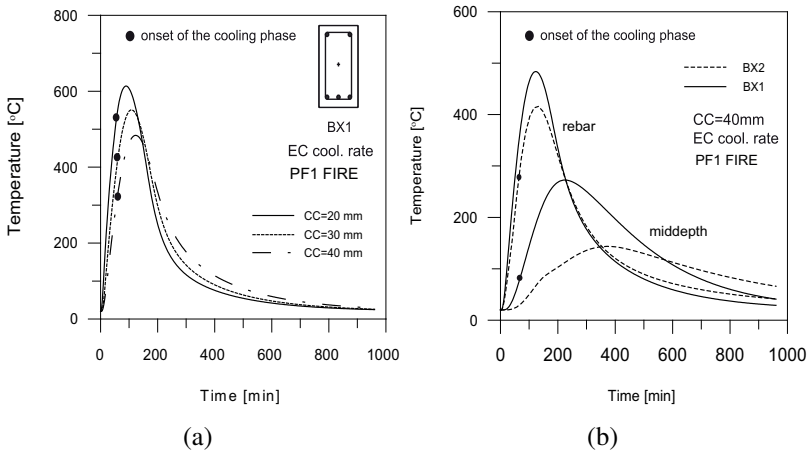

(a) (b)

FIGURE 5.11: Temperature in the corner rebar in: (a) Beam BX1 and varying concrete cover; (b) comparison between BX1 and BX2.

inside the member. The recovery of the deflection, however, is more pronounced than in the case of faster cooling, with the residual deflection being around 75% of the maximum value. Nevertheless, faster cooling is more beneficial, given that it leads to lower both peak and residual deflections. Effect of the concrete cover can be seen in Figure 5.13(b). Poorly protected rebars experience higher temperatures, which then leads to higher maximum deflection at midspan and almost no recovery after cooling down.

The beams were also exposed to a varying load levels (Figure 5.14). Increasing the load level does not affect the general trend, but it amplifies the response. Both peak and residual displacements increase with higher load level (Figure 5.14(a)) and the more loaded beam will collapse in the earlier stage of fire (Figure 5.14(b)). As for the effect of the dimension of the section, in the Figure 5.15(a) and Figure 5.15(b) it can be seen that more massive beam (BX2), for the fire duration of 2h, experiences more recovery in the deflections during the cooling down phase, eventually leading to lower residual de-

flections than in beam BX1. Moreover, for the fire duration of 3h, more massive beam did not fail while beam BX1 failed in the heating phase.

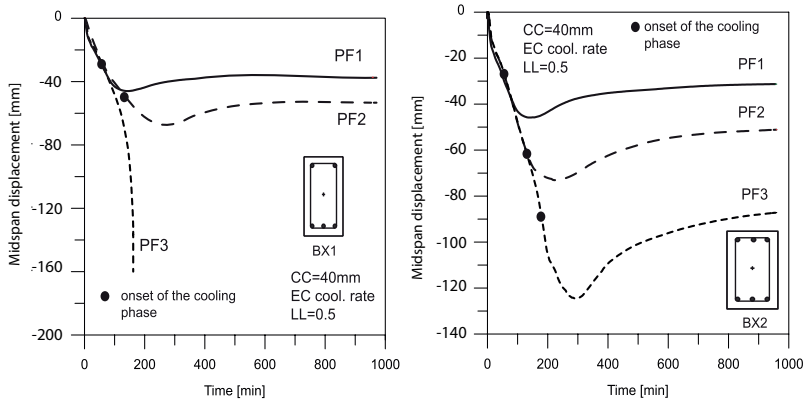

(a) (b)

FIGURE 5.12: Midspan deflection in time for varying fire scenario for: (a) beam BX1; (b) beam BX2.

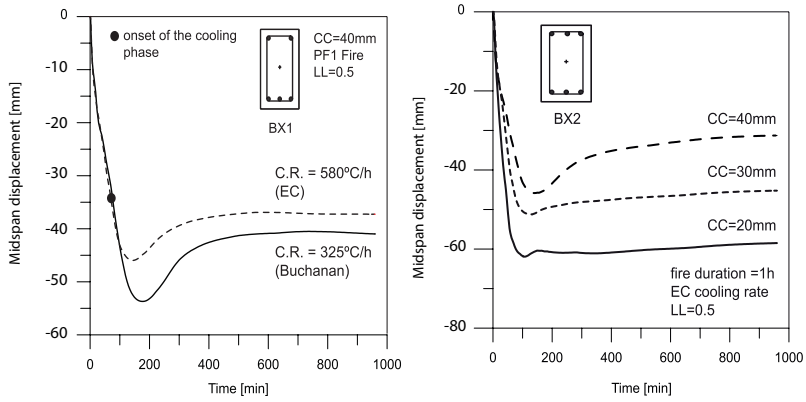

(a) (b)

FIGURE 5.13: Midspan deflection in time for varying fire scenario for: (a) beam BX1 and varying cooling rate; (b) beam BX2 and varying concrete cover to steel bars.

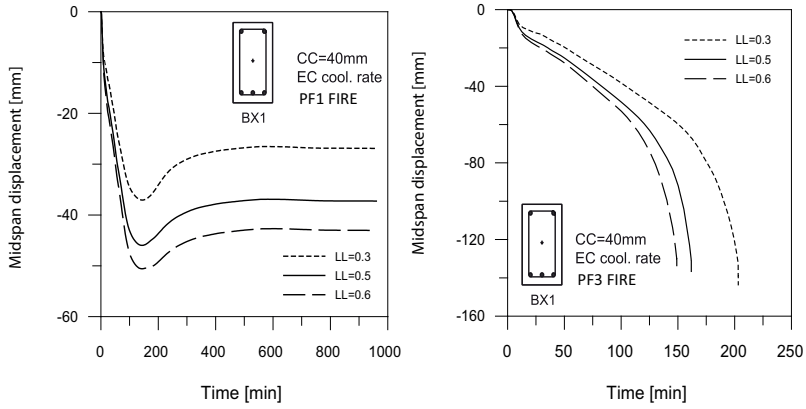

(a) (b)

FIGURE 5.14: Midspan deflection in time for beam BX1 for varying load level: (a) fire scenario PF1; (b) fire scenario PF3.

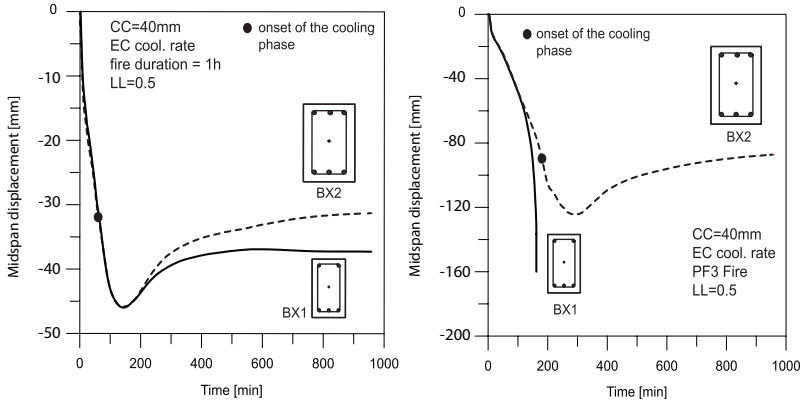

FIGURE 5.15: Midspan deflection in time for different cross-sections for: (a) fire scenario PF1; (b) fire scenario PF3.

TABLE 5.2: Summary from the parametric analyses on the beam BX1 and BX2

PARAMETER	Beam	Fire scenario	Load ratio (%)	Concrete cover [mm]	Cooling rate	Peak rebar temperature (°C)	Peak deformation [mm]	Residual deformation [mm]	RESIDUAL/PEAK DEFORMATION
Fire scenario	BX1	PF1	50	40	EC	484	46	37	0.80
		PF2				670	74	54	0.73
		PF3				791	160	-	-
	BX2	PF1	50	40	EC	415	46	32	0.70
		PF2				602	73	51	0.70
		PF3				720	125	86	0.69
Cooling rate	BX1	PF1	50	40	EC	484	46	37	0.80
					Buchanan	547	54	41	0.76
Load ratio	BX1	PF1	30	40	EC	484	37	27	0.73
			50				46	37	0.80
			60				51	42	0.82
		PF3	30			791	-	-	tf=150 min
			50						tf=160 min
			60						tf=200 min
Concrete cover	BX1	PF1	60	20	EC	614	51	42	0.71
				30		551	59	49	0.72
				40		484	68	58	0.94
	BX2	PF1	50	20	EC	540	62	42	0.82
				30		475	51	49	0.96
				40		415	46	32	0.70
Beam size	BX1	PF1	50	40	EC	484	46	37	0.80
		PF2				670	74	54	0.73
		PF3				791	160	-	-
	BX2	PF1				415	46	32	0.70
		PF2				602	73	51	0.70
		PF3				720	125	86	0.69

5.8 Experimental campaign at University of Edinburgh

A total of 46 geometrically identical RC columns have been tested at the University of Edinburgh (MacLean, 2018). 36 columns have been tested while exposed to fire, while 10 columns have been tested at ambient temperature, to determine their load capacity.
Dimensions of the specimen and a general test set-up can be seen in the Figure 2.12. Conditions at the boundaries of the member are pin-pin. To restrain the translations at the base (in x, y and z- direction) and the top (x and y-direction) of the column, two reference points are created, at a small distance from the column member, and then kinematically coupled with the surface of the column. Restraint conditions are applied to the two reference points, RP-1 and RP-2 (Figure 5.17). All of the tested columns had identical geometry, with dimensions of the cross section of 150 mm x 150 mm and length of 1400 mm. Reinforcement details can be seen in the Figure 5.16. Concrete strength at the test day were 30 MPa and 50 MPa for the two mixes. Both mixes contain 2 kg/m^3 of polypropylene fibers, to minimize the probability of spalling.

Heating of the columns

Columns were heated by using radiant panels, and a heat flux is applied to the heat-exposed face. The panels could be placed to a specified distance from the target member, in order to achieve desired incident radiant heat flux. Only a portion of the column was directly heated, while in the areas of concrete member away from the heated surface area, heat transfer was governed by conduction through the concrete itself, rather than radiation from exposure to the radiation from the panels (as well as convective losses from exposed surfaces) (MacLean, 2018). However, such setup leads to the non-uniform distribution of incident heat flux over the exposed surface of the column, which is due to the variation in radiation view factor at any particu-

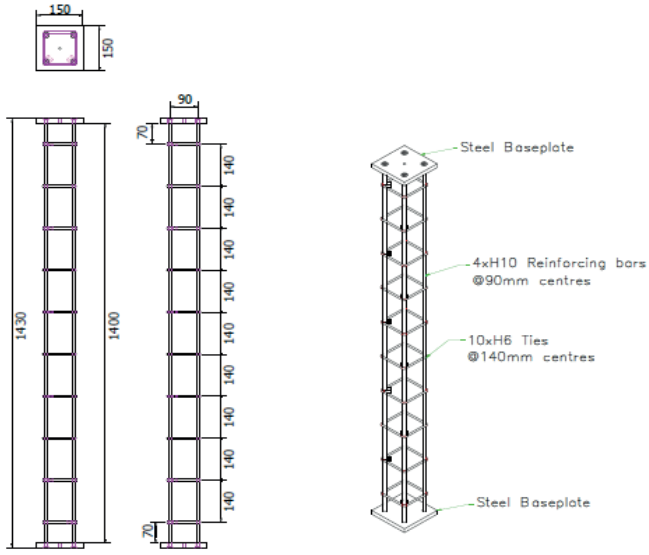

FIGURE 5.16: Schematic representation of the reinforced columns, from (MacLean, 2018).

lar location on the heated surface and the interaction of the surface with convective currents generated both by the radiant panels themselves and by the hot surface of the column (MacLean, 2018). Radiant panel has a rectangular shape, therefore the plane of incident radiant heat flux which represents a specific desired peak value (for example, $50kW/m^2$ or $70kW/m^2$ in this case) at the location of maximum heat flux at a specified offset distance will actually represent a variable incident radiant heat flux distribution over the target surface (MacLean, 2018).

User subroutine DFLUX was used to calculate net incident heat flux on the heat-exposed surface of the member, as a function of time (in the cooling phase, applied heat flux is equal to zero). The subroutine will be called at each integration point for surface-based nonuniform distributed flux definition in the analysis (ABAQUS, 2016). Net

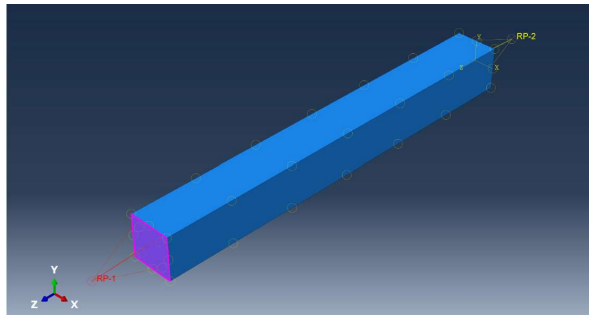

(a)

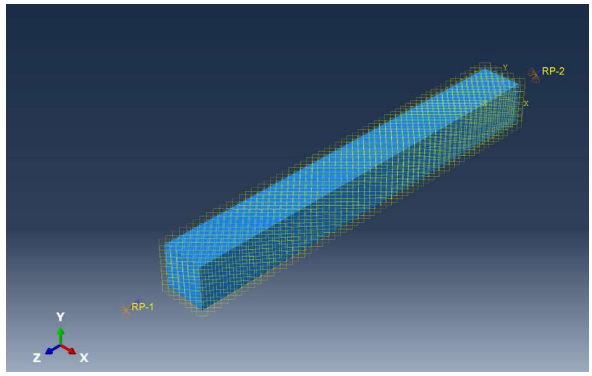

(b)

FIGURE 5.17: Definition of the mechanical boundary conditions for the columns; (a) reference points kinematically coupled with the column surface; (b) restraints applied to the reference points. Note- the axis along the column length is z-axis

incident heat flux is calculated according to the Equation C.9 of EN 1992-1-2 (European Committee for Standardization (2005b)):

$$\dot{h_{net}} = \dot{h} - \dot{\alpha_c}(\dot{\theta_m} - 20) - \Phi\varepsilon_m\varepsilon_t\sigma[(\theta_m + 273)^4 - (293.15)^4] \quad (5.10)$$

Where $\dot{h}$=50 kW/m^2 or $\dot{h}$=70 kW/m^2; Φ=0.7; α_c=9 and ε_m=0.7.

Subroutine DFLUX requires the definiton of the two FLUX values: FLUX(1) is the value of applied heat flux, magnitude of the flux flowing into the point, while FLUX(2) is the derivative of the heat flux with respect to surface temperature.

As already being said, the incident heat flux varies over the exposed surface. The maximum incident radiant heat fluxes to which the columns were exposed are 50 kW/m^2 and 70 kW/m^2 but these values are not constant over the exposed surface. This variable spatial distribution of the heat flux on the exposed surface was not taken into account in the model, neither the radiative losses in the environment - the applied heat flux on the exposed surface was constant in the model (Figure 5.18). For this reason, 50 kW/m^2 and 70 kW/m^2 were reduced to 42 kW/m^2 and 60 kW/m^2, respectively, to obtain a reasonably accurate fit between the numerically predicted temperature at the heat exposed side and the experimentally measured value.

Heat transfer inside the member takes place through conduction. At the boundaries of the heat exposed surfaces, convection with convective coefficient of 25 W/m^2K is assumed, while for the unexposed surfaces, convective coefficient is set to 9 W/m^2K, accounting for the radiation. Radiation with ε = 0.7 is assumed for all the heat-exposed concrete surfaces. Thermal properties of concrete and steel are assumed as per Eurocode 2. Temperature distribution in the column at the end of the heating phase (after 90 minutes) can be seen in (Figure **??**).

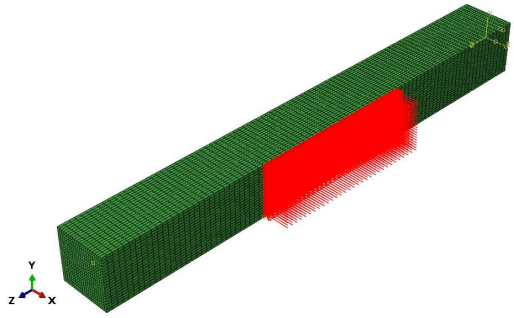

FIGURE 5.18: Applied heat flux on the portion of the column model.

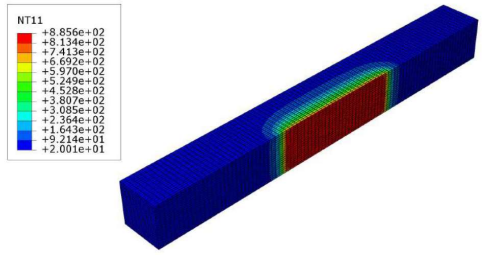

FIGURE 5.19: Temperature distibution in the column.

Investigated parameters

In the experimental campaign by MacLean (2018), the influence of the various parameters on the columns' performance during heating

and during/after cooling has been investigated:

- Load magnitude: severe loading and low loading were considered - 60 % of the ambient load capacity or a constant load of 10kN (equivalent to 1-2% of the columns ambient capacity)
- Eccentricity of the applied load: 5, 15 or 25mm
- Concrete compressive strength: 30 or 50 MPa
- Magnitude of applied initial incident radiant heat flux: 0, 50 or 70 kW/m^2
- Overall length of the heated area- 33% of the length (middle third) or 66% of the column length
- Number and sides exposed to fire (one side or two sides) - the heated sides were front and back of the columns

Before presenting the results, it is important to explain denomination of the tested columns, that here follows the same principle as in (MacLean, 2018). For instance, the test HF70-F30-L60-E25-C stands for the column exposed to a Heat Flux of 70 kW/m^2 (HF70), having a compressive strength f_c=30 MPa (F30), loaded with an axial force equal to the 60% of its axial capacity (L60) and applied with the eccentricity of 25 mm (E25) and finally, C (C) denotes the side heated - compression or tension heated side. As explained in detail in (MacLean, 2018), denomination of the heated faces (i.e. tension face or compression face) does not necessarily reflect the state of stress on the column sides. In case both sides are compressed (for example columns tested with 5 mm eccentricity), ”compression” face is the most compressed face, while ”tension” face is less compressed face. For a detailed list of simulated columns and their parameters, see the Table 5.3. In the following, the results from the numerical analyses performed on the selected columns will be presented (Table 5.4). In order to present the results in a simple way, the columns were divided into three groups. In each group, compressive strength and/or

the heat flux were constant, while other parameters varied. Experimentally measured lateral deflections at the midspan of the column were compared against the deflections obtained numerically. As for the sign convention, negative displacement means deflection towards the heat source, while positive is in the direction away from the heat source.

5.8.1 Columns of the 1st group

All the columns that belonged to this group had a compressive strength f_c=30 MPa and were exposed to a heat flux 70 kW/m^2. Load level, side exposed to fire and eccentricity of the applied load varied.

Low load

Applying the low load on the columns helps to understand the extent of the irrecoverable deformation that takes place upon cooling back to ambient temperature (MacLean, 2018). In case that a low load, equal to 1-2 % of the load capacity, is applied, it would be expected that the thermal expansion governs the deflection response. In case of low load eccentricity, lateral deflection and bowing take place due to thermal expansion.
Looking at the Figure 5.20, the displacement response can be somewhat divided into three stages: initial bowing towards the heat source, governed by the thermal expansion, followed by the contraction of the columns, and the bowing direction reversal. Last stage of cooling phase brings in some stabilization of the deflections, when the values keep almost constant values (from around 200 minutes onwards). Maximum deflection is reached soon after heating phase has ended (after 90 minutes).

Slight difference in the response can be observed for a varying eccentricity (Figure 5.20(b)). For a 25 mm load eccentricity, ”tension heated” columns deflect more than ”compression heated” columns.

There is no full recovery to initial values upon cooling: experimentally measured residual deflection is around 1 cm.
The general trend is well reproduced by the numerical model. However, the displacements are very conservative in the later stages of the heating phase and then in the subsequent cooling phase of fire. Numerical model predicts the certain amount of irrecoverable deformation which was not measured in the experiments. As pointed out by MacLean (2018), thermal expansion of ”tension heated” columns together with the moment induced by the eccentrically applied load, increases the deflection of the column. This increase in the deflection would then induce secondary moments, increasing the moment in the section even farther. In ”compression heated” columns the opposite is valid - deflections due to thermal expansion reduce the moment in the section, resulting in smaller deflections in comparison to ”tension heated” columns. Still, the fact that ”tension heated face” columns deflect more than ”compression heated” columns might have been caused by higher temperatures experienced in those members, given that during the fire they deform towards the heat source which makes them more ”hot” on the exposed side than ”compression heated” specimen. This effect is not captured in the numerical analyses, as the basic premise of the sequentially-coupled thermo-mechanical analysis is that the thermal field is not dependent on the displacement/stress field.

Higher load

Columns tested under higher loads exhibit quite different structural response than the columns tested under low loads (Figure 5.21).
At the start of the test, the ”compression heated” columns bow away from the heat source, as the effect of the load dominates the response (Figure 5.21(c)). Unexpectedly, the column continues to deflect away from the heat source even after being exposed to high temperatures. This can be explained with the effect of transient creep strain, resulting in contraction rather than expansion. Upon removal of the heating

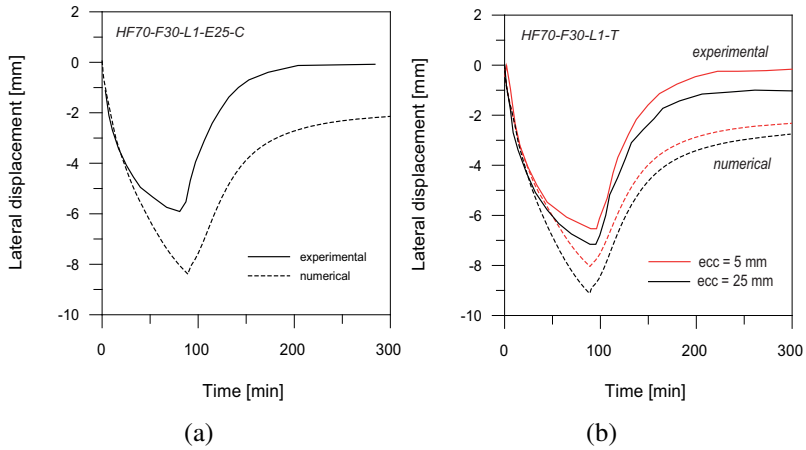

FIGURE 5.20: Comparison between experimental and numerical midspan displacement evolution in: (a) "compression heated" with $e = 25mm$ and (b) "tension heated" column with $e = 25mm$ and $e = 5mm$ - note: continuous lines are experimental curves while numerical results are represented with dashed lines.

panels (after approximately 90 minutes), the columns deflect rapidly away from the heat source, until failure or until reaching the new state of equilibrium. Deflections are not recovered during cooling. Instead, after around 3h into fire, the deflections stabilized and kept almost a constant value until the end of the test. Numerically, the general trend is well reproduced. The column failed for the eccentricity $e = 25mm$, after around 260 minutes (in the cooling phase of fire), which is slighly unconservative in comparison to the failure time from the experiment. On the other hand, column survived the fire for lower eccentricity, thanks to the smaller bending moments and thus smaller deflections and less pronounced second-order effects; the predicted displacements follow closely the experimental curve. Residual deflection obtained numerically is around 16 mm while experimentally measured value was 14.7 mm.

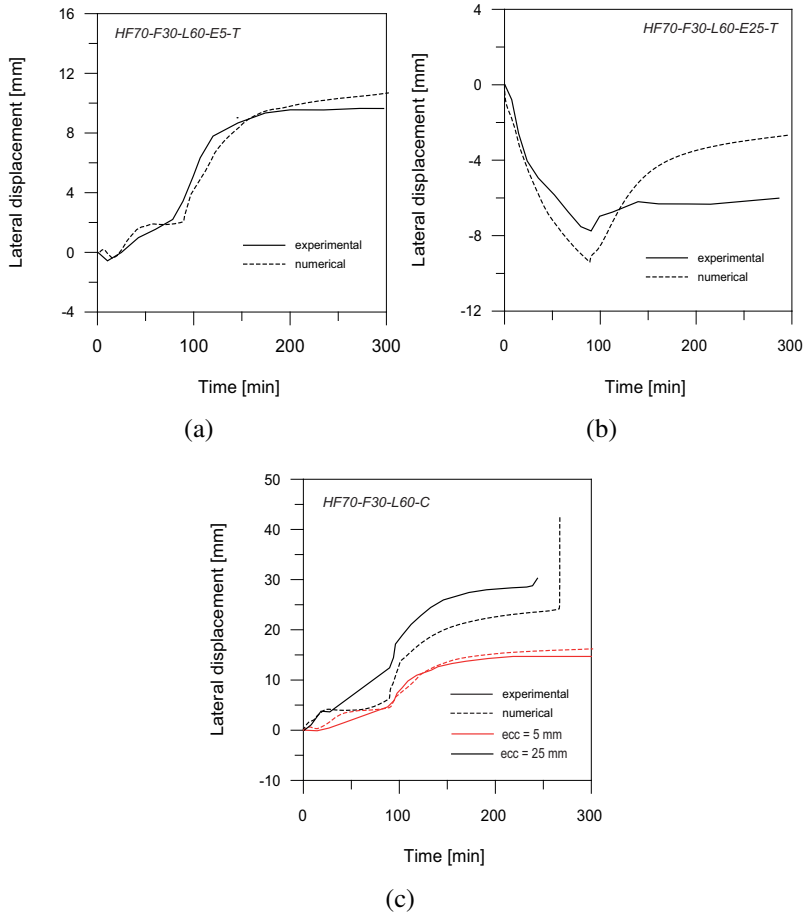

FIGURE 5.21: Comparison between experimental and numerical lateral midspan deflection evolution for heavily loaded columns and: (a) "tension heated" for $e = 5mm$; (b) "tension heated" for $e = 25mm$ and (c) "compression heated" for: $e = 5mm$ and $e = 25mm$.

Tension heated columns with low load eccentricity (Figure 5.21(a)) behave in a similar way to "compression heated" columns (Figure 5.21(c)). The behaviour during heating phase and the stabilization of the de-

flection in the later stages of cooling phase is correctly captured by the model. However, the same cannot be said for the tension heated column with the higher load eccentricity (Figures 5.21(b). In this column, the effect of thermal expansion prevails, due to low compressive stresses at the heated face, resulting in overall smaller deflections that for the lower load eccentricity case. Numerical model was not able to capture the experimentally observed behavior during the cooling phase, where there was almost no recovery in the deflections (Figure 5.21(b)). Numerical model underestimated the residual deflection measured during the test, while the maximum deflection measured at the end of the heating phase was somewhat conservative.

5.8.2 Columns of the 2nd Group

All the columns that belong to this group had a compressive strength f_c=30 MPa, were exposed to a heat flux 50 kW/m^2 and loaded with an axial force equal to 60% of axial load capacity. Side exposed to fire and eccentricity of the applied load varied.

During the experiments, it was observed that decreasing the heat flux to 50 kW/m^2 does not change the general trend in the deflection evolution; it produces similar but less severe and less pronounced response compared to a higher heat flux of 70 kW/m^2. This is expected because increasing the heat flux will lead to the similar thermal field inside the member, with the difference that the maximum experienced temperature will be higher and thus the damage inside the member will be higher.

"Compressive heated" columns deflect away from the heat source during whole fire duration (Figure 5.22(b)). Columns from Group 1, exposed to a heat flux of 70 kW/m^2, sustained greater damage and deflections than columns from the Group 2. This is probably due to transient thermal creep caused by the higher temperatures at the heat exposed side. Predicted displacement is slightly underestimated in the case of compression heated columns loaded with the eccentricity of $e = 25mm$, while in the case of lower eccentricity, the displace-

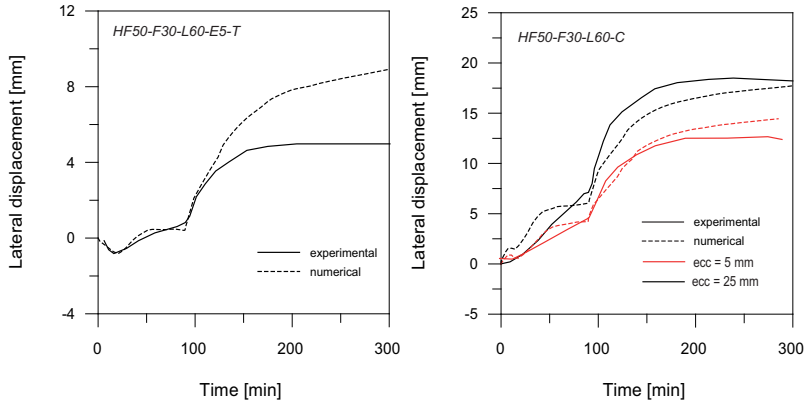

(a) (b)

FIGURE 5.22: Comparison between experimental and numerical midspan displacement evolution for the heavily loaded columns heated, with a heat flux of 50 kW/m^2 for: (a) "tension heated" with $e = 5mm$ and (b) "compression heated" column with $e = 5mm$ and $e = 25mm$.

ments are well predicted, during both heating and cooling phase of the fire (Figure 5.22(b)).
"Tension heated" specimen bows towards the heat source in the first 20 minutes of fire, and then the deflection trend reverses, and the columns bow away from the heat source for the remaining duration of fire. Displacement of tension heated columns is overestimated by the model. General trend suggests that the displacements are monotonically increasing (though at a lower rate during cooling phase, i.e. after 150min), while during the experiment, displacements were almost constant after 150 min of fire.

5.8.3 Columns of the 3rd Group

All the columns that belonged to this group had a compressive strength f_c=50 MPa and were exposed to a heat flux 70 kW/m^2. Load level,

side exposed to fire and eccentricity of the applied load varied.

Low load

The columns deform towards the heat source for the whole duration of heating-cooling cycle. In the first 90 minutes of heating, the displacement is increasing towards the heat source. Upon cooling, the deflection trend reverses, and the columns deform far away from the heat source. Both "compression heated" and "tension heated" columns behave in a similar way, except that "compressive heated" columns recovered the deflections to the initial values, while tension heated columns had some residual deflection left. Comparing the response of the columns with different compressive strength shows great variation, as expected. As pointed in (MacLean, 2018), it is difficult to draw direct comparison on heavily loaded specimen, given that the load level in the tests is expressed as a function of the axial capacity. Therefore, the columns with different compressive strength will have a different axial capacity, and consequently will be exposed to a different load.
Still, the comparison can be done for columns loaded with low load, where the influence of load is minimal and the deflections are expected to be fully recovered upon cooling (transient strain is not taking place). In the experiments, columns with compressive strength $f_c = 30MPa$ deflected less than columns with compressive strength $f_c = 50MPa$, which is somewhat counter-intuitive, especially given the fact that same low load was applied to all the columns. This may suggest that stronger columns suffered more pronounced thermal expansion but this cannot be verified MacLean (2018). However, an opposite trend is obtained by the model - stiffer and stronger columns indeed deformed less, both in terms of peak deflection and also in the residual stage (Figure 5.23).

Columns exposed to low load exhibited lateral deflections and bowing almost immediately after being exposed to fire, due to thermal gradients developing through the depth of the column section. While

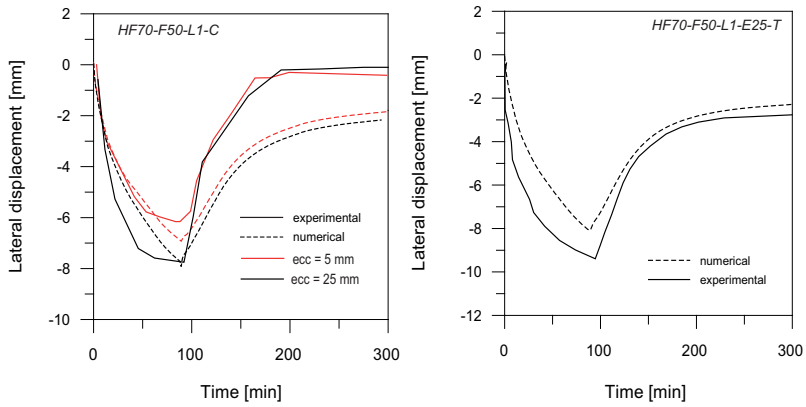

(a) (b)

FIGURE 5.23: Comparison between experimental and numerical lateral midspan displacement evolution for the low loaded columns, with compressive strength $f_c = 50MPa$ for: (a) "compression heated" with $e = 5mm$ and $e = 25mm$ and (b) "tension heated" column with $e = 25mm$.

numerical model has been able to capture the general trend as well as to predict the maximum deflection at the end of the heating phase, it proved to be more conservative during the cooling phase. It predicted certain amount of residual deflections of compression heated columns, while in the experiments almost complete deflection recovery was observed (Figure 5.23(a)). On the other hand, deflections during cooling for "tension heated" columns are well predicted, while during heating phase they are underestimated (Figure 5.23(b)).

Higher load

While the load level proved to be a significant factor, compressive strength proved to play less important role in view of the deflection evolution. It is true that the columns of different strength deform

to a different extent but this is in part due to the different load applied. "Compression heated" specimen deflect away from the heat source due to the transient creep strain while "tension heated" specimen bend towards the heat source due to thermal expansion of the extreme fibre of the heated face. Behaviour of the "compression heated" columns is well simulated and failure time is predicted well, though slightly on the unconservative side (Figure 5.24). Deflection of the "tension heated" column is predicted accurately for lower eccentricity, when the columns bows away from the heat source, due to the influence of applied load and stresses on the heated side. On the other hand, for higher eccentricity the influence of thermal expansion dominates the response, because compressive stresses in the heat exposed side are low and cannot counteract the thermal expansion. Thus, the column bows towards the heat source.
General trend is well predicted by the model, but the displacements in the cooling phase are underestimated (Figure 5.25). "Compression heated" columns are heated on the most stressed section, the extent of the transient creep and therefore the magnitude of the deflections depends on the magnitude of the load - higher loads lead to higher compressive stresses and thus to higher deflections (away from the heat source) due to transient thermal creep strain. Being exposed to higher loads than corresponding columns from the Group I (with f_c=30 MPa), they deflect more and their deflection response is more severe. "Tension heated" columns are subjected to elevated temperatures on the less stressed section of the column, thus the columns deflect toward the heat source. In the case of ecc=25 mm, induced compressive stresses are not enough to counteract the effect of thermal expansion through the development of transient thermal creep. Still, the heat penetrates deeper into the concrete layer during time, so when the heat gets closer to the "compression face" where the compressive stresses are higher, transient thermal creep appears, which changes the deflection evolution. Differently from "compression heated" specimen, higher load in "tension heated" columns results in lower stresses on the "tension face", resulting in smaller deflections.

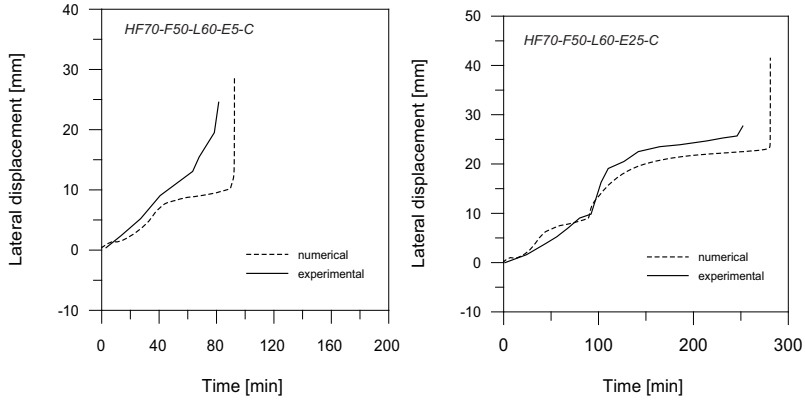

(a) (b)

FIGURE 5.24: Comparison between experimental and numerical midspan displacement evolution for the heavily loaded columns heated with compressive strength fc=50MPa for: (a) "compression heated" with e=5mm and (b) "compression heated" column with e=25mm.

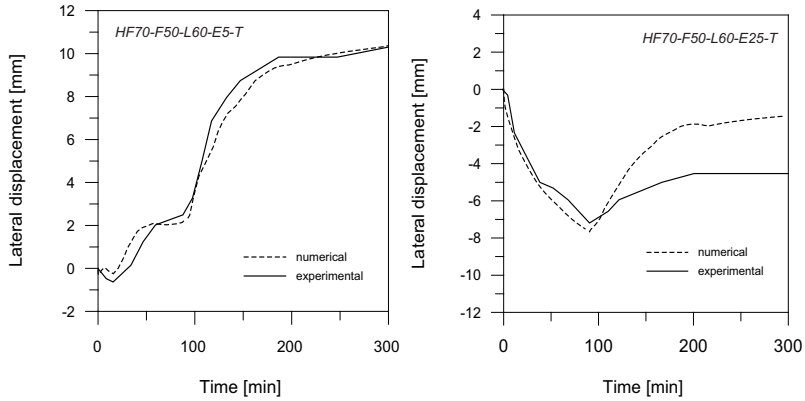

(a) (b)

FIGURE 5.25: Comparison between experimental and numerical midspan displacement evolution for the heavily loaded columns heated with compressive strength fc=50MPa for: (a) "tension heated" with e=5 mm and (b) "tension heated" column with e=25 mm.

5.8.4 Influence of parameters

Influence of the recoverable concrete and steel properties

In the following, the influence of the recoverability of the strength and stiffness of concrete and steel on the deflections is presented, for columns from the Group I (Figure 5.26), Group II (Figure 5.27) and Group III (Figure 5.28). By default, mechanical properties of the concrete and steel are considered as irrecoverable during cooling, keeping the value reached at maximum temperature throughout the cooling phase (curve "numerical" in the plots). Complementary analyses have been done, by considering the steel and concrete properties as fully recovered during cooling, i.e. governed by the current and not maximum temperature (curve "numerical-recoverable" in the plots).

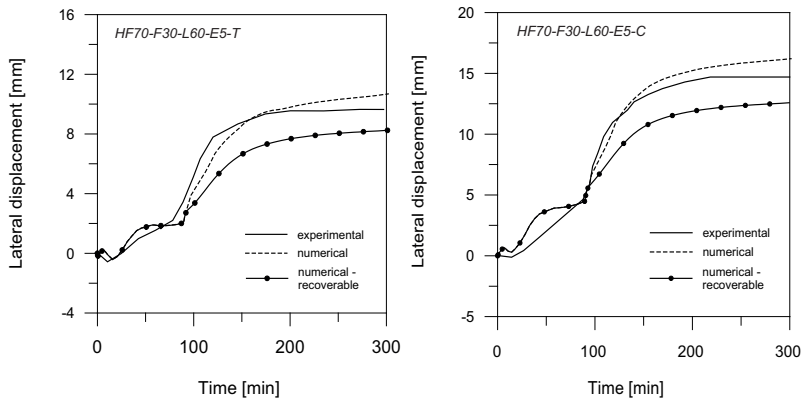

(a) (b)

FIGURE 5.26: Influence of the recoverability of the concrete and steel mechanical properties on the lateral displacement of heavily loaded columns for the cases of: (a) "tension heated" with $e = 5mm$ and (b) "compression heated" column with $e = 5mm$.

Looking at the Figure 5.26(a) and Figure 5.26(b), deflection re-

sponse during cooling is better predicted if the material strength and stiffness are considered as irrecoverable. This means that the behavior in cooling is governed by the maximum experienced temperature, and not by the current temperature. Considering mechanical properties as recovered leads to somewhat unconservative displacement prediction, underestimating the residual deflection for approximately 15% with respect to experimental value (d_{max}=8.2 mm against d_{max}=9.6 mm measured in the test for tension heated columns and d_{max}=12.6 mm against d_{max}=14.2 mm measured in the test for compression heated column).

As regards the structural response of compression heated specimens during cooling down phase, similar conclusions can be found: better prediction of the displacement is obtained by considering the material strength and stiffness as irrecoverable (Figure 5.27). Not considering the properties as irrecoverable leads to the underestimation of the displacements, which is particularly obvious for the lower eccentricity case. This means that the behavior is governed by the maximum experienced temperature, and not the temperature in the current time step. On the other hand, for tension heated specimen, "locking" the mechanical properties at maximum temperature leads to the displacements prediction that is too safe (Figure 5.27(c)).

Looking at the columns from Group III, the deflection evolution of compression heated and low loaded specimens during cooling phase shows small differences in the predicted deflection between the model that considers the material strength and stiffness as irrecoverable and the one that does not. This is expected, because the behavior of the low-loaded specimens is governed by the thermal expansion, and the mechanical parameters have less pronounced influence on the structural response (Figure 5.28(a) and Figure 5.28(b)).

Regarding the deflection evolution of tension heated and heavy loaded specimens during cooling, a common conclusion cannot be drawn. In the case of eccentricity e=5mm, a model with irrecoverable properties leads to more accurate prediction of displacements. On the other hand, for the higher eccentricity case, the displacement predic-

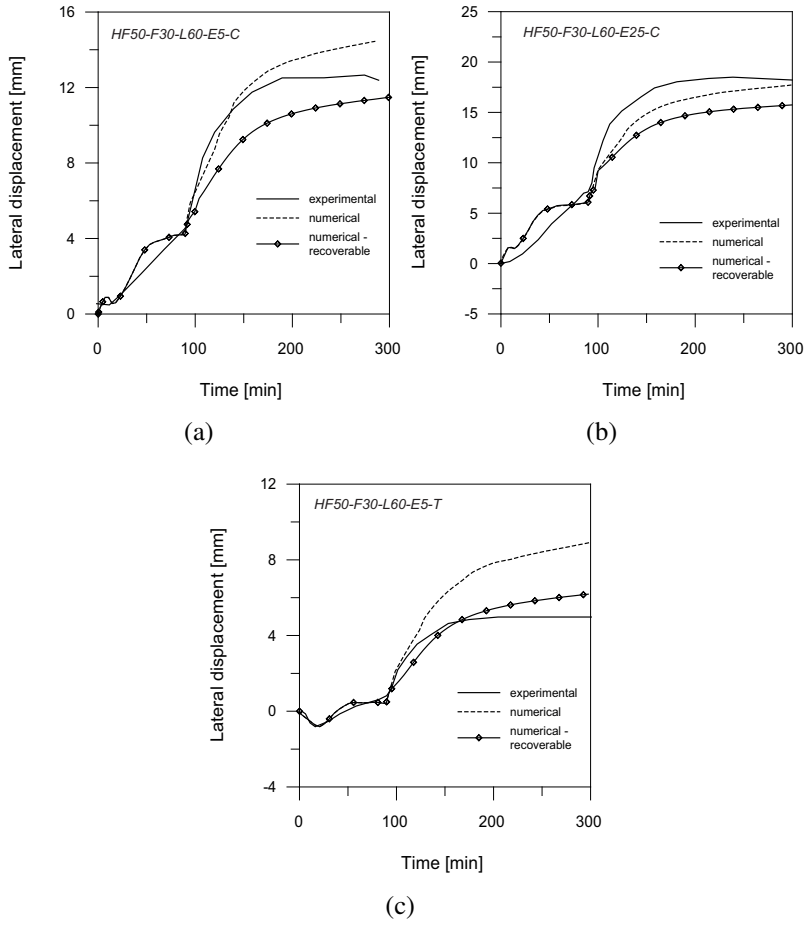

FIGURE 5.27: Influence of the recoverability of the concrete and steel mechanical properties on the lateral displacement of heavily loaded columns for the cases of: (a) "compression heated" with $e = 5mm$ and (b) "compression heated" column with $e = 25mm$ and (c) "tension heated" column with $e = 5mm$.

tion is on the unsafe side, predicting more significant recovery of the deflections during cooling phase (Figure 5.28(c) and Figure 5.28(d)).

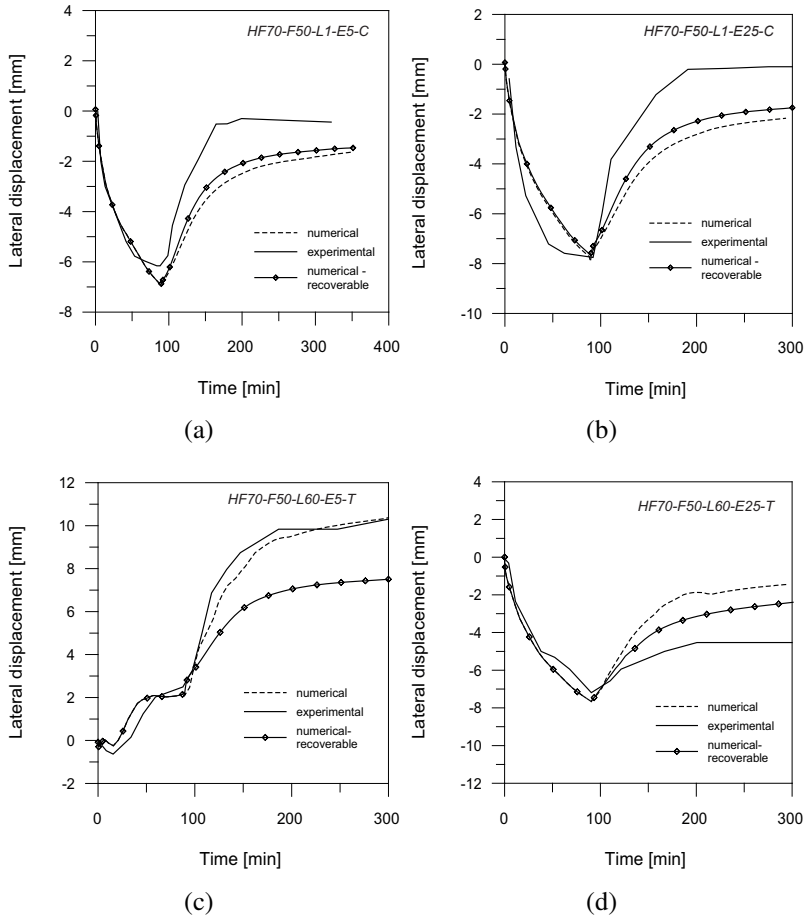

FIGURE 5.28: Influence of the recoverability of the concrete and steel mechanical properties on the lateral displacement of: (a) low loaded and "compression heated" columns for $e = 5mm$ load eccentricity; (b) low loaded and "compression heated" columns for $e = 25mm$ load eccentricity; (c) heavy loaded and "tension heated" columns for $e = 5mm$ load eccentricity and (d) heavy loaded and "tension heated" columns for $e = 25mm$ load eccentricity.

Influence of the additional reduction of compressive strength during cooling phase

Concrete not only does not recover to its original strength upon cooling, but it also suffers damage that results in additional loss of strength with respect to the value it had at the end of the heating phase or when it reached the maximum temperature. As suggested by European Committee for Standardization (2005a), an aditional loss of 10% of the compressive strength during cooling phase should be considered. Results from numerical simulations on ”tension” and ”compression heated” columns, under low load and eccentricity of 25mm, suggest that the influence of the additional compressive strength reduction of 10% during cooling phase leads to the results somewhat closer to the experimentally obtained values, but the difference is not drastical. Losing the strength to a greater extent leads to the slightly bigger deflection (contraction) rate (Figure 5.29). In case of heavily loaded concrete columns with the axial load eccentricity of 5mm, it can be seen that the influence of the additional compressive strength reduction of 10% during cooling causes similar effects as in low loaded columns - it accelerates the deflection rate and it leads to the displacement prediction that is more conservative with respect to the experimental values (Figure 5.30).

Conclusions from the parametric study

From the extensive experimental campaign (MacLean, 2018) and the numerical analyses of the selected tested columns, several meaningful conclusions can be drawn about the structural behaviour of eccentrically loaded columns exposed to a localized heating. It was concluded, or to say confirmed, that the thermal gradient and stress state within the section are the two most important factors governing the response. In that regard, the most significant tested parameters are:

- Load eccentricity: Increasing the eccentricity of the applied

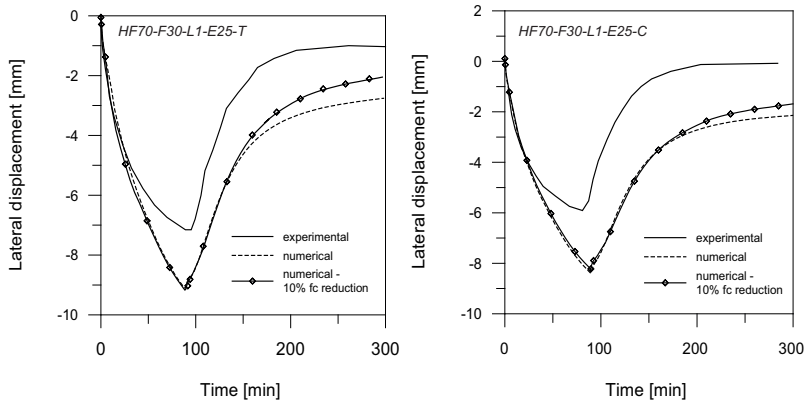

(a) (b)

FIGURE 5.29: Influence of the additional 10% f_c reduction on the lateral displacement of low loaded columns for the cases of: (a) "tension heated" with $e = 25mm$ and (b) "compression heated" column with $e = 25mm$.

load increases the moment induced by the load. If the stress on the heated face is large enough to cause a transient thermal creep, the column will deflect away from the heat source during whole fire duration. Otherwise, the influence of thermal expansion will dominate the response and the columns will bow towards the heat source.

- Load magnitude: Magnitude of the imposed load will determine the stress state within the section and this will determine the extent of transient thermal creep through the depth of the section. This directly influences direction in which the column will deflect: towards the heat source, in case the thermal expansion governs the problem (compressive stresses on the heat exposed sides are low) or away from the heat source (in case the compressive stresses at the heat exposed side are large enough

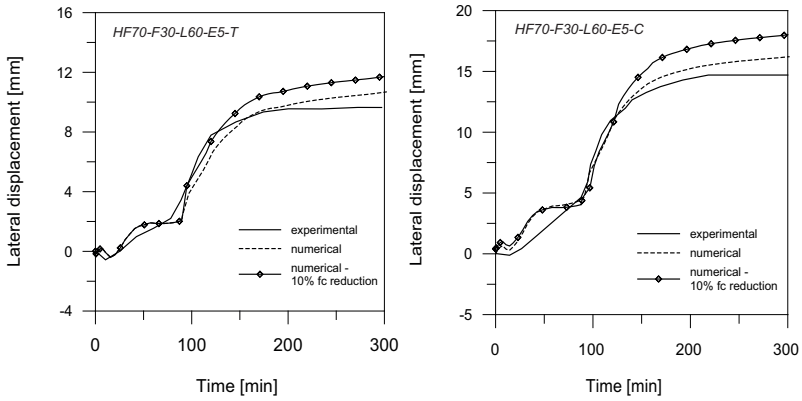

(a) (b)

FIGURE 5.30: Influence of the additional 10% f_c reduction on the lateral displacement of low loaded columns for the cases of: (a) "tension heated" with $e = 5mm$ and (b) "compression heated" column with $e = 5mm$.

to counteract the effect of thermal expansion).

- Heat flux: Heat flux is a parameter of utmost importance, as it determines the temperature gradient within the structural element and thus it has a strong impact on the structural response. The higher the temperature inside the member, the more the concrete will be weakened and the greater non-recoverable deformations as a result of increased transient thermal creep resulting both from the elevated temperature and stress distribution through the section.

- Side heated: The structural response can be very different depending on which side of the member is heated - the most stressed side or the least stressed side. This can even determine if the column will survive heating and cooling or will collapse.

TABLE 5.3: Simulated columns from the experimental campaign (MacLean, 2018)

	LOAD LEVEL (%)		COMPRESSIVE STRENGTH (MPa)		ECCENTRICITY (mm)		HEAT FLUX (kW/m2)		FACE HEATED	
TEST	1	60	30	50	5	25	50	70	C	T
HF70-F30-L1-E25-C	x		x			x		x	x	
HF70-F30-L1-E25-T	x		x			x		x		x
HF70-F30-L1-E5-T	x		x		x			x		x
HF70-F30-L60-E25-C		x	x			x		x	x	
HF70-F30-L60-E5-C		x	x		x			x	x	
HF70-F30-L60-E5-T		x	x		x			x		x
HF70-F30-L60-E25-T		x	x			x		x		x
HF50-F30-L60-E5-T		x	x		x		x			x
HF50-F30-L60-E25-C		x	x			x	x		x	
HF50-F30-L60-E5-C		x	x		x		x		x	
HF70-F50-L1-E25-C	x			x		x		x	x	
HF70-F50-L1-E5-C	x			x	x			x	x	
HF70-F50-L1-E25-T	x			x		x		x		x
HF70-F50-L60-E5-C		x		x	x			x	x	
HF70-F50-L60-E25-C		x		x		x		x	x	
HF70-F50-L60-E5-T		x		x	x			x		x
HF70-F50-L60-E25-T		x		x		x		x		x

TABLE 5.4: Predicted vs experimentally measured deflections at mid-height

		Peak lateral deflection [mm] OR deflection at 90 minutes		Residual lateral deflection [mm]			
	TEST	experimental	numerical	experimental	numerical	recoverable properties	additional 10% fc reduction
Group 1	HF70-F30-L1-E25-C	-6.0	-8.3	0.0	-2.1	-	-1.7
	HF70-F30-L1-E25-T	-7.1	-9.0	-1.0	-2.8	-	-1.6
	HF70-F30-L1-E5-T	-6.5	-8.0	-0.2	-2.3	-	-
	HF70-F30-L60-E25-C	t_f=243 min	t_f=267 min	-	-	-	-
	HF70-F30-L60-E5-C	4.0	4.1	14.7	16.2	12.6	18.0
	HF70-F30-L60-E5-T	3.4	2.6	9.6	10.7	8.2	11.7
	HF70-F30-L60-E25-T	-9.5	-8.0	-6.0	-3.0	-	-
Group 2	HF50-F30-L60-E5-T	0.7	0.5	4.9	8.9	6.2	-
	HF50-F30-L60-E25-C	7.1	6.1	18.3	17.8	15.7	-
	HF50-F30-L60-E5-C	4.3	4.2	12.6	14.4	11.5	-
Group 3	HF70-F50-L1-E25-C	-7.8	-7.6	0.0	-2.2	-1.75	-
	HF70-F50-L1-E5-C	-6.2	-6.9	-0.4	-1.6	-1.8	-
	HF70-F50-L1-E25-T	-9.2	-8.0	-2.8	-2.3	-	-
	HF70-F50-L60-E5-C	t_f = 82 min	t_f = 92min	-	-	-	-
	HF70-F50-L60-E25-C	t_f = 252min	t_f = 282min	-	-	-	-
	HF70-F50-L60-E5-T	2.7	2.1	10.4	10.4	7.5	-
	HF70-F50-L60-E25-T	-7.2	-7.7	-4.5	-1.5	-2.4	-

5.9 Comparison of the different analysis methods

In the Chapter 3 and Chapter 4, the RC members exposed to fire were studied via sectional analysis and structural analysis with beam elements. Several experimentally tested beams and columns were numerically simulated and the influence of various parameters on the global behaviour has been studied. Herein, the results from the analysis using 3D elements on two experimentally tested beams and six columns will be confronted againts the results obtained using the two previously mentioned methods - sectional and beam element analysis. The overview of the results obtained using different methodologies will be done, though without entering into details about the test setup and specimens, as that has already been done previously. It has to be highlighted that the chosen members are simply supported at the boundary. It is clear that changing the restraint conditions would lead to conclusions different than those obtained here, given that increasing the complexity of the structural member favors the use of more complex methods. The main objective of this comparison is to show the ability of simple methods to predict the structural behaviour of simple structures exposed to fire, such as simply supported beams and columns. Looking at these results, it can be seen if and how the increase in computational and modeling effort affects the accuracy of the predicted response of RC members exposed to full heating-cooling cycle.

5.9.1 Eccentrically loaded columns exposed to standard fire

The columns tested by Hass (1986), though exposed to standard fire, are significant because they are eccentrically loaded. Comparison in terms of axial and lateral displacement is presented for the two Hass columns: Hass 1 (Figure 5.31) and Hass 21 (Figure 5.32). Hass 1 col-

umn is simply supported while Hass 21 is fixed at the bottom. Focus was on the prediction of experimentally measured failure time for eccentrically loaded columns with different restraint conditions. Both columns failed during the experiment, due to excessive lateral deflection: Hass 1 column after 86 minutes and Hass 21 after 125 minutes. In the Figures below, the predicted axial and lateral displacement evolution in time is presented, using sectional, beam element and 3D element analysis.

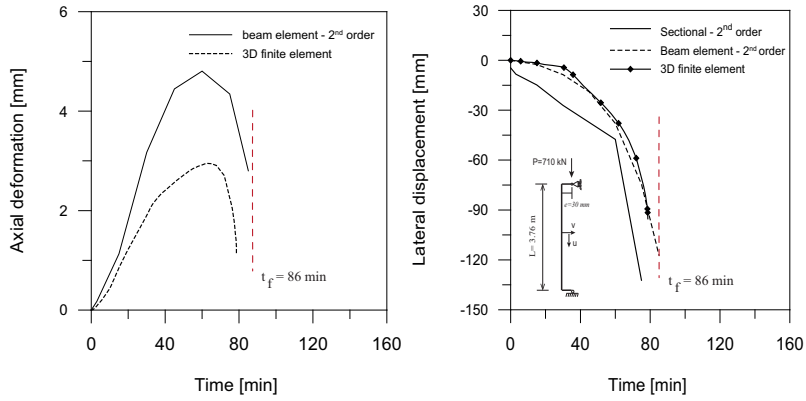

FIGURE 5.31: Comparison of the different analysis methods for Hass 1 column: (a) axial deformation and (b) lateral deflection (Hass, 1986).

It can be concluded that for both columns, 3D model was the most accurate to predict the failure time. On the other hand, the failure time from sectional analysis was conservative for both columns, underestimating the failure time, especially for the column Hass 21 fixed at the bottom. With 3D element and 2D beam element model very similar results have been obtained.

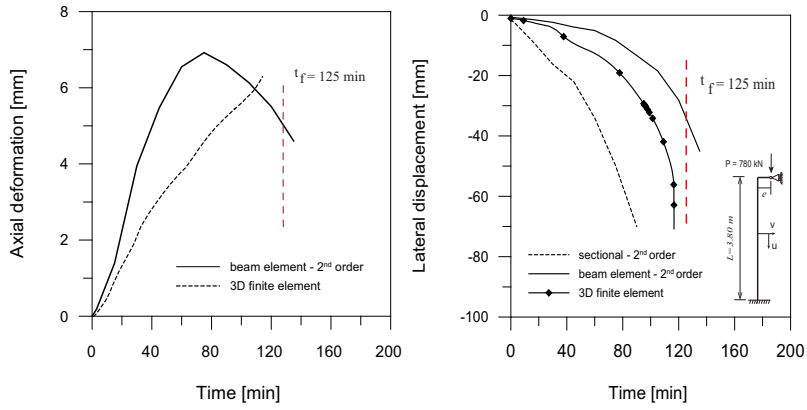

(a) (b)

FIGURE 5.32: Comparison of the different analysis methods for Hass 21 column: (a) axial deformation and (b) lateral deflection (Hass, 1986).

5.9.2 Concentrically loaded columns tested in residual conditions

Columns tested by Kodur et al. (2017) were analysed in the previous Chapters by sectional method and 2D beam element analysis and here the results will be presented, together with the results from 3D element analysis (Figure 5.33). These columns were exposed to a design fire, with the heating phase lasting 90 and 120 minutes for the Columns C1 and C2, respectively, and then cooled down. Generally, all the methods lead to similar results. Sectional analysis gave the most conservative axial deformation prediction, while 3D analysis is the least conservative among the three methods studied, .

Results from the analyses of columns tested by Raut and Kodur (2011) are presented in Figure 5.33. Column NSC was concentrically loaded and exposed to standard fire. Column HSCP2 was made of high strength concrete and exposed to a long duration fire. This

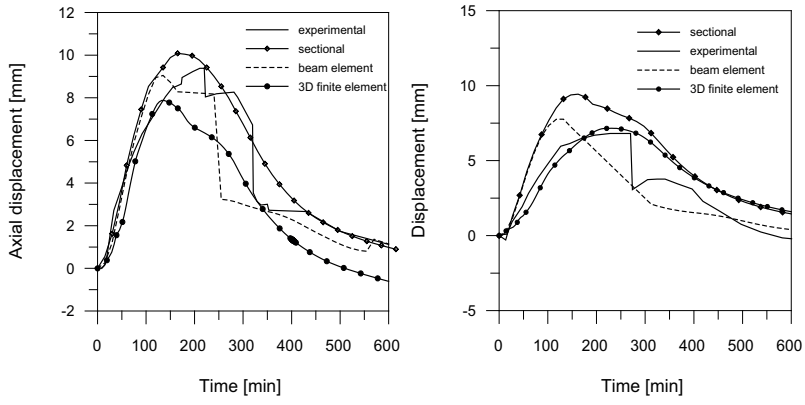

(a) (b)

FIGURE 5.33: Comparison of the different analysis methods for column: (a) C1 and (b) C2 (Kodur et al., 2017).

column was chosen in order to compare the failure time predicted by the three methods. Column NSC failed after 183 minutes into the test, while HSCP2 failed after 220 minutes, which is in the early stage the cooling phase of fire.

It can be seen that failure time is predicted well, whichever the method used. When looking at the axial deformation in time, it is most accurately predicted by the 3D model, though with both sectional and 2D beam element method, the deformations are conservative.

5.9.3 Case of simply supported beams tested in residual conditions

Two beams tested at Michigan State University were simulated both by a sectional analysis and by the 3D model. Two simply supported beams were exposed to a design fire, with heating phase duration of 120 and 90 minutes for beams B1 and B2, respectively. Both beams were loaded with the laod equal to around 55-60% of their capacity.

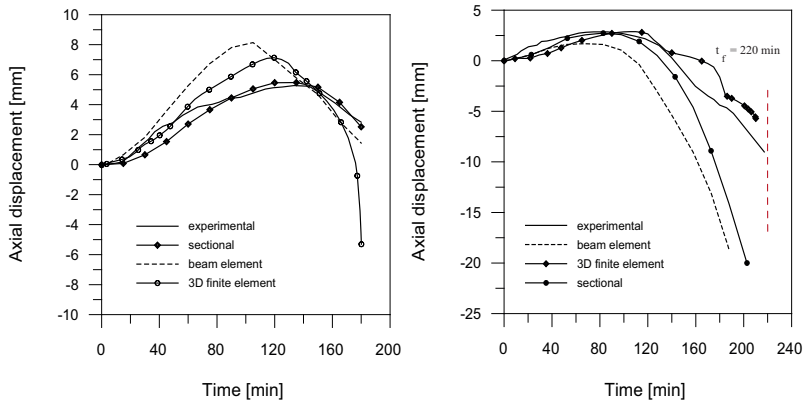

FIGURE 5.34: Comparison of the different analysis methods for column: (a) NSC and (b) HSCP2 Raut and Kodur (2011).

For the beam B1, the load was removed after 300 minutes. 3D model midspan deflection prediction for beam B1 proved to be very conservative, while for the beam B2, 3D model predicted the midspan displacement very accurately; both in heating and cooling phase. On the other hand, sectional analysis overestimated the peak displacement while the residual displacement is somewhat underestimated.

To sum up, all the three methods generally predict well the structural response of columns and beams exposed to fire. To study the simply supported members, sectional analysis, as a very simple mean, is generally a good approach. It predicts the failure time in a conservative manner, which is rather expected, given that it considers that the member fails as soon as the most stressed section fails. Displacement evolution in cooling phase is in general better predicted by the more complex methods. Though from the obtained results it is not simple to give a unique conclusion, it can be said that the sectional analysis is an efficient tool to analyse structural members with a simple geometry and boundary conditions, and that generally gives safe

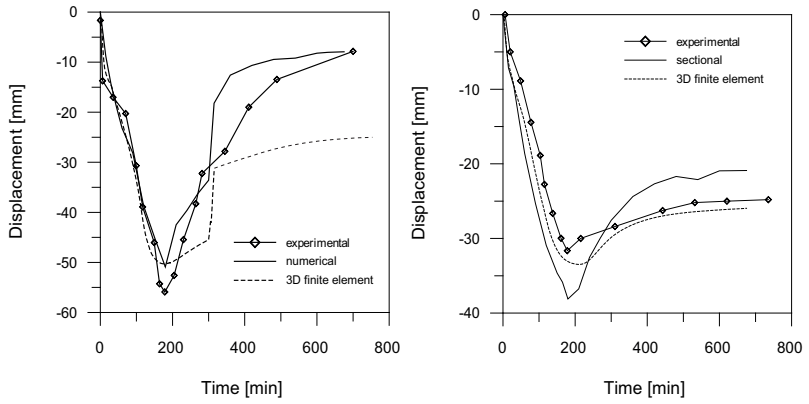

FIGURE 5.35: Comparison of the different analysis methods for the beam: (a) B1 and (b) B2 Agrawal and Kodur (2018).

predictions, even in the cooling phase of fire. If however, the focus is on the more precise evaluation of the residual displacements, one can resort to the 2D beam element and 3D element analysis, which are definitely more general methods and with wider field of application. Increasing the complexity of the method usually increases the accuracy of the predicted displacement, to a lesser or greater extent, depending on the case, but on the other hand, it increases the computational time and modelling effort. The choice of the method can be based on the final objective of the study - investigation of the possibility of failure or residual behaviour, local or global behaviour - and also on the type of the studied structure.

TABLE 5.5: Comparison between the three models-summary of the results

		peak deformation [mm] / time to failure [min]				residual displacement [mm]			
		sectional	Beam element	3D finite element	experimental	sectional	Beam element	3D finite element	experimental
RC Columns									
Hass (1986)	HASS 1	78 min	85 min	80 min	86 min	-	-	-	-
	HASS 21	90 min	135 min	115 min	125 min	-	-	-	-
Raut and Kodur (2011)	NSC	180 min	180 min	180 min	183 min	-	-	-	-
	HSCP2	200 min	190 min	210 min	220 min	-	-	-	-
Kodur et al. (2017)	C1	10.1	9.04	7.8	9.38	0	1.41	-0.5	1.12
	C2	9.4	7.76	7.2	6.8	2	0.37	2.1	-0.2
RC Beams									
		sectional	Beam element	3D finite element	experimental	sectional	Beam element	3D finite element	experimental
Agrawal and Kodur (2018)	B1	51	-	50	57	7	-	25	7
	B2	38	-	34	32	22	-	26	25

Chapter 6

Concluding remarks

6.1 Summary of the results

In this work, the structural behaviour of reinforced concrete members exposed to natural fires was studied using three different modelling approaches: sectional analysis, finite element analysis via beam elements and finite element analysis via three-dimensional elements. For the first two methods, an ad-hoc code in *VisualBasic* was developed, while the 3D analysis was performed by means of the commercial software ABAQUS 6.16. All the three models were validated against relevant test results available in the literature.
The preliminary numerical analyses carried out on the prestressed and reinforced concrete sections allow drawing some general conclusions on the structural behaviour of members exposed to natural fire, contributing to more general and complex methods that will follow. The influence of section geometry is determined mainly by the concrete cover and available ”thermal mass”. Less massive section exhibited the worst performance in terms of fire resistance. The results from the thermal analyses clearly indicate that heating of the prestressing and reinforcing steel continues long after the onset of the cooling phase, especially for lower fire durations. As a consequence, depending on fire duration, cooling rate and load level, failure can

take place also in the cooling phase. Cooling rate and load level both proved to be important factors. With longer durations of the cooling phase, higher temperatures can be reached in the reinforcing bars, especially in more massive sections. Faster cooling, by contrast, brings in a sizable reduction of the residual displacements. The role of several parameters, namely the irrecoverable damage, residual thermal strain, irrecoverable strain components and the explicit consideration of transient creep strain, on the structural response were studied. The results showed that neglecting the thermal damage in the steel bars (i.e. considering the mechanical properties as recoverable upon cooling) leads to non-conservative displacement predictions and significantly underestimated residual deflections. In order to study the effect of the transient creep consideration, two models have been compared - Eurocode model that considers the transient creep implicitly and the explicit model by Gernay and Franssen (2012). Slight difference in the deflection response for these two models can be seen in the cooling phase, with the explicit model yielding results that are slightly closer to the experimental ones, but on overall, the difference is of minor importance. In addition, a set of analyses has been performed by considering the thermal strain of concrete as fully recovered upon cooling: focusing on statically determined members, such as simply supported beams, no significant difference in the midspan deflection have been observed. Finally, the influence of the unloading modulus has been studied. The results obtained by the variation of the residual unloading modulus and by describing the behaviour as nonlinear-elastic are very similar. These findings are rather expected, given that the midspan deflections of beams are governed by the strength and deformability of the steel bars, while the role of the concrete in the structural response is less important. Finally, a numerical procedure for the investigation of slender reinforced concrete columns exposed to standard and natural fires was presented. The procedure is based on sectional analysis and nominal curvature method (Annex B3 of EN 1992-1-2). It must be highlighted that this method, while being very robust at the sectional level, is very simplified for the structure

as a whole. The method was applied on several reinforced concrete columns, available in the literature, and it can be seen that in the cases where second order effects play a role, it gives very conservative failure time prediction. On the other hand, sectional analysis was quite accurate in displacement prediction where second order effects did not play a role, both during heating and cooling phase of fire. Irrecoverable damage in the concrete and steel proved to be a parameter of great importance, as it was observed in the case of beams. Considering the mechanical properties as fully recovered upon cooling leads to a structural response that is quite different from what was observed in the experiments - rate of deformation in the cooling phase is much slower and the amount of contraction is significantly underestimated. Moreover, the influence of concrete is dominant over steel. Unloading modulus did not prove to play a role - it could be that unloading mainly takes place during cooling, when the stresses inside the section are quite low (compressive strength is ”locked” at the value attained at the maximum temperature). It can be seen that residual thermal strain plays a role, especially in the later stages of cooling phase. Contraction in the later stages is underestimated if no residual strain is considered.

Generally speaking, irreversible effects, such as residual thermal deformation and accumulation of plastic deformations, are definitely of minor importance as regards the failure. Failure of statically determinate flexural members is governed by the load level acting on the member and the maximum temperature in the steel rebars. Influence of the residual thermal strain is more pronounced in columns than in beams. With the aim to overcome intrinsic limitations of the sectional analysis and to offer a more general approach for studying simple structural members exposed to fire, a code was developed for the structural analysis using beam finite element. Both material and geometric nonlinearity are taken into account. A number of significant examples based on real-scale fire tests on columns were modelled, taking into account different heating, loading and boundary conditions. It is worth noting that performing a second-order anal-

ysis causes very strong decrease of fire resistance and brings the predicted values closer to the experimentally measured ones. Axially restrained columns were simulated as well, while checking the influence of the explicit consideration of transient creep strain. Explicit model (Gernay and Franssen, 2012) gives closer prediction of the residual deformations with respect to the experimental values, while implicit model overestimates the deflection recovery, leading to lower residual deflections in comparison to the measured ones. In general, the numerical models were able to predict the axial deformation evolution in time quite well, both during the initial stage of thermal expansion due to thermal gradients, and also in the contraction phase and cooling. Finally, in Chapter 5, the procedure for sequentially coupled thermo-mechanical analysis by means of the commercial finite element software ABAQUS 6.16 was described. First step consists in solving the pure heat transfer problem. Afterwards, the temperature solution is read into a stress analysis as a predefined field (ABAQUS, 2016).

From the preliminary analyses performed at the sectional level, it was very clear that the definition of the irrecoverable mechanical properties in the constituent materials - concrete and steel- are of utmost importance if the behaviour in cooling is at issue. This feature may not be embedded in the material definition in commercially available finite element codes. Therefore, a further effort should be taken in modifying the mechanical behaviour in cooling. In ABAQUS software, this can be done through the implementation of the user subroutine UFIELD, which allows to define steel and concrete mechanical properties as dependent on a suitably defined field variable, namely the maximum temperature. The numerical investigations were carried out on reinforced concrete beams exposed to three different fire scenarios, all featuring heating and cooling. Influence of several parameters was investigated, such as load level, concrete cover, duration of heating phase and rate of cooling, as well as massivity of the section. In addition, a recent extensive experimental campaign at University of Edinburgh on 46 reinforced concrete columns pro-

vided a very valuable database for the numerical models validation. Columns were eccentrically loaded and were exposed to a localized heating on one portion of the column's side. Selected columns were modelled and the model was generally able to predict well the evolution of the lateral displacement in time. The obtained results once again highlighted the importance of the correct definition of the mechanical properties in cooling, and particularly for the columns whose behaviour was governed by the compressive stresses on the heat exposed side (and not by the thermal expansion). As demonstrated in the more simple approaches, the role played by the irreversible variation of concrete strength and deformability upon cooling is important, and this should be adequately taken into account in the model, in order to accurately predict the residual response of the member. Concluding Chapter 5, the results from the analysis using 3D elements on two experimentally tested RC beams and six columns are confronted against the results obtained by using sectional and finite element analysis with beam elements. The main objective of such a comparison is to show the ability of simple methods to predict the structural behaviour of simple structural members, exposed to standard and natural fire. To sum up, all the three approaches, despite having a different complexity level, generally predict well the structural response of columns and beams exposed to fire. Sectional analysis is an adequate approach if the objective is to study statically determinate members. It predicts the failure time in a conservative manner, while the displacement evolution in cooling phase is, in general, better predicted by the more complex methods.

6.2 Principal conclusions

Behaviour of RC members exposed to natural fires has been studied with a sectional and structural approach, via beam finite elements and 3D finite elements. The main conclusions are outlined here:

- Maximum temperature, as one of the most significant factors

affecting the performance of the structural members in fire, is reached in the cooling phase of fire. Realistic representation of the fire scenario, a basis for the performance based design, is fundamental for the correct prediction of the maximum temperatures reached in concrete and steel.

- Ensuring the structural safety only until the maximum fire temperature is reached is not enough - structural members can survive the heating phase of fire but fail in the cooling phase. This delayed failure is governed by increasing temperatures in the inner zones of concrete and in the rebars, even after onset of the cooling phase to an extent that depends on the ”thermal mass” and concrete cover.

- Behaviour of structural members in cooling is not governed by the current temperature but by the maximum experienced temperature - mechanical properties are not completely recovered during cooling and this should be properly taken into account in any numerical model or code.

- All three models/approaches demonstrated that they can predict the structural response accurately enough, during both heating and cooling.

- Sectional analysis, as the most simple method, showed to be generally very conservative in failure time prediction, and sufficiently accurate (though less accurate than the other two methods) in the prediction of the response during cooling - this, of course, under the condition that material and geometrical nonlinearity and irrecoverable damage are accounted for.

- Structural analysis using beam finite elements is a way in the middle between sectional and 3D model in terms of complexity, but with larger field of application in comparison to sectional.

- While 3D models do not have intrinsic limitations in terms of applicability and may look very appealing to the researchers,

their complexity might not be justified for the use in studying simple structural members, as these can be effectively studied with more simple methods. Their application is, however, necessary in the cases where local effects are to be examined, where heat transfer along the length of the member cannot be neglected or for the more complex structural members whose behaviour is governed by multi-axial stress states.

- Increasing only the model complexity itself does not bring many improvements in the prediction of the structural response - instead, the focus should be put on the realistic definition of fire scenario (in view of the estimation of the maximum temperature) as well as on the proper definition of the material properties during cooling (irrecoverable damage).

6.3 Outlook

Most of the current knowledge on the behaviour of reinforced/prestressed concrete structures comes from standard tests, where the fire scenario is not defined in a realistic way. On the other hand, the behaviour of structures exposed to heating and cooling is, despite gaining more attention in the recent years, still an open issue. The present study tries to contribute to answer several open questions on the behaviour of reinforced concrete structures exposed to natural fires. Nevertheless, a number of questions are still open to discussion and can provide some indications for future work.

- More systematic and accurate study on the materials properties to be used in cooling should be performed. So far, clear indications about the evolution of strength/deformability in the cooling phase are missing, with only few available research works on this topic. Moreover, slightly contradictory provisions are given in EN1992-1-2 and EN1994-1-2, where in the latter a set of equations for determining the residual compressive strength is given, but the basis for the equations is not known.

- Residual thermal properties of concrete are still an open topic, given that little or no information is available.

- The important role of the thermal strain upon cooling on the structural response of members in compression requires further research - not many experimental data are available. Permanent strains in the structure caused by the residual thermal deformation can lead to a structure that is in prestrained/predeformed condition after fire - it can be a problem for the failure modes where the behaviour is not ductile, such as in the case of columns.

- Most of the current works (experimental and numerical) are based on testing/modeling only the single structural member, without accounting for the interaction between the structural members/components. The point of view should be enlarged to structural assemblies and full structural context could be studied instead. Consideration of the structural member as isolated cannot capture the effects of thermal restraint provided by the surrounding members, leading eventually to the inaccurate prediction of residual displacements, which are an important indicator for assessing the damage in the member and undertaking suitable post-fire measures (demolition or repair). Moreover, considering the structure as a whole could provide indications as to whether focusing on single members (as it is usually done in common design applications) remains a safe approach also in the presence of natural fires.

Bibliography

209 A. (1992). "State of the Art Report - Time dependent Effects in Concrete Structures." *Report 209*, American Concrete Institute.

ABAQUS (2016). "ABAQUS Version 6.16 Documentation." *User's manual*, Dassault Systems Simulia Corp., Providence (Rhode Island, USA).

Abramowicz M. and Kowalski R. (2007). "Residual mechanical material properties for the reassessment of reinforced concrete structures after fire." *Proceedings of the 9th International Conference, Modern Building Materials, Structures and Techniques*. 1147–1151.

Abrams M. S. (1971). "Compressive Strength of Concrete at Temperatures to 1600F." *Temperature and Concrete. ACI Special Publication No. 25*, American Concrete Institute, Detroit (Michigan, USA). 33–58.

Agrawal A. and Kodur V. (2018). "An experimental approach for evaluating residual capacity of fire damaged concrete members." *The 10th International Conference on Structures in Fire FireSERT*, Belfast (UK). 949–957.

Aguado J., Espinos A., Hospitaler A., Ortega J. and Romero M. (2012). "Fire Resistance of Hollow-Core Slabs. Influence of Reinforcement Arrangement." *Proceedings of the 7th Interna-*

tional Conference on Structures in Fire, Structures in Fire, Zurich, Switzerland. 699–708.

Anderberg Y. (1988). "Modelling steel behaviour." *Fire Safety Journal*, 13(1), 17–26.

Anderberg Y. and Thelandersson S. (1973). "Stress and Deformation of Concrete at High Temperatures-General Discussion and Critical Review of Literature." *Bulletin 34*, Division of Structural Mechanics and Concrete Construction, Lund Institute of Technology.

Anderberg Y. and Thelandersson S. (1976). "Stress and Deformation Characteristics of Concrete at High Temperatures - 2. Experimental Investigation and Material Behaviour Model." *Report No. 54*, Division of Structural Mechanics and Concrete Construction, Lund Institute of Technology, Lund (Sweden).

Annerel E. (2010). "Assessment of Residual Strength of Concrete Structures after Fire Exposure," PhD thesis, University of Ghent.

ASCE Committee on Fire Protection (1992). *ASCE Manual of Practice No. 78, Structural Fire Protection*. New York, USA.

Bamonte P. and Felicetti R. (2012). "High-temperature behaviour of concrete in tension." *Structural Engineering International*, 22(4), 493–499.

Bamonte P. and Gambarova P. (2014). "Properties of concrete subjected to extreme thermal conditions." *Journal of structural fire engineering*, 5(1), 47–62.

Bamonte P. and Gambarova P. (2015). "High-temperature behavior of SCC in compression: Comparative study on recent experimental campaigns." *Journal of Materials in Civil Engineering*, 28(3), 1–10.

Bamonte P. and Gambarova P. (2016). "High-Temperature Behavior of SCC in Compression: Comparative Study on Recent Experimental Campaigns." *ASCE Journal of Materials in Civil Engineering*, 28(3).

Bamonte P., Gambarova P. and Cangiano S. (2008). "Mechanical and Thermal Properties of NSC and HPCs Exposed to High Temperature: Cement and Aggregate Roles." *Proceedings of the International Conference*, University of Dundee, Scotland, UK. 103–114.

Bamonte P., Kalaba N. and Felicetti R. (2018). "Computational study on prestressed concrete members exposed to natural fires." *Fire Safety Journal*, 97, 54–65.

Bamonte P. and Monte F. L. (2015). "Reinforced Concrete Columns Exposed to Standard Fire: Comparison among Different Constitutive Models for Concrete at High Temperature." *Fire Safety Journal*, 71, 310–323.

Bamonte P. and Pisani M. (2015). "Creep analysis of compact cross-sections cast in consecutive stages - Part 2: Algebraic methods." *Engineering Structures*, 96, 176–189.

Bingol A. and Gul R. (2009). "Effect of Elevated Temperature and Tooling Regimes on Normal Strength Concrete." *Fire and Materials*, 33, 79–88.

Botte W. and Caspeele R. (2017). "Post-cooling propoerties of concrete exposed to fire." *Fire Safety Journal*, 92, 142–150.

Bratina S., Planinc I., Saje M. and Turk G. (2003). "Non-linear Fire-Resistance Analysis of Reinforced Concrete Beams." *Structural Engineering and Mechanics*, 16(6), 695–712.

Buchanan A. H. (2001). *Structural Design for Fire Safety*. John Wiley & Sons.

Burnier O. (2016). "Shear breaking of columns subjected to localized fires." *The 9th International Conference on Structures in Fire*, SiF, Princeton (NJ, USA). 885–892.

Capua D. D. and Mari A. (2007). "Nonlinear Analysis f Reinforced Concrete Cross-Sections Exposed to Fire." *Fire Safety Journal*, 42, 139–149.

Carstensen J. V. (2011). "Material Modelling of Reinforced Concrete at Elevated Temperature. Master's thesis, Technical University of Denmark, Denmark.

Cervenka V., Pukl R. and Eligehausen R. (1990). *Computer Simulation of Anchoring Technique in Reinforced Concrete Beams*. Pineridge Press.

Chan Y., Peng G. and Anson M. (1999). "Residual strength and pore structure of high-strength concrete and normal strength concrete after exposure to high temperature." *Cement and Concrete Composites*, 21, 23–27.

Colina H. and Sercombe J. (2004). "Transient thermal creep of concrete in service conditions at temperatures up to 300C." *Magazine of Concrete Research*, 56, 559–574.

Collins M. P. and Mitchell D. (1997). *Prestressed Concrete Structures*. Response Publications.

Comite Euro-International du Beton (1977). *Buckling and Instability - Bulletin d'Information N. 123*. Paris (France).

Dotreppe J. (1997). "Mechanical properties of quenched and self-tempered reinforcing steel at elevated temperatures compared with recommendations of Eurocode 2 - Part 1-2." *Materials and Structures*, 30, 430–438.

Dwaikat M. B. and Kodur V. (2009). "Response of restrained concrete beams under design fire exposure." *Journal of Structural Fire Engineering*, 135(11), 1408–1417.

Ehm C. and Schneider U. (1985). "The High Temperature Behaviour of Concrete under Biaxial Load." *Cement and Concrete Research*, 25, 27–34.

Elghazouli A., K.A. K. C. and Izzuddin B. (2009). "Experimental evaluation of the mechanical properties of steel reinforcement at elevated temperaturel." *Fire Safety Journal*, 44, 909–919.

Elingwood B. and Lin T. (1988). "Flexure and Shear Behaviour of Concrete Beams during Fires." *Journal of structural fire engineering*, 117(2), 440–458.

Ellobody E. and Bailey C. (2008). "Fire Tests on Bonded Post-tensioned Concrete Slabs." *Engineering Structures*, 31, 686–696.

European Committee for Standardization (2004a). *Eurocode 1: Actions on Structures - Part 1.2: General Actions - Actions on Structures Exposed to Fire*. Bruxelles (Belgium).

European Committee for Standardization (2004b). *Eurocode 2: Design of Concrete Structures - Part 1.1: General Rules and Rules for Buildings*. Bruxelles (Belgium).

European Committee for Standardization (2005a). *Eurocode 2: Design of Composite Steel and Concrete Structures - Part 1.2: General Rules - Structural Fire Design*. Bruxelles (Belgium).

European Committee for Standardization (2005b). *Eurocode 2: Design of Concrete Structures - Part 1.2: General Rules - Structural Fire Design*. Bruxelles (Belgium).

Feasey R. and Buchanan A. (2002). "Post-Flashover fires for structural design." *Fire Safety Journal*, 37(1), 83–105.

Feenstra P. and deBorst R. (1995). "Constitutive model for Reinforced Concrete." *Journal of Engineering Mechanics*, 121(5), 587–595.

Felicetti R., Gambarova P. and Meda A. (2009). "Residual behavior of steel rebars and R/C sections after a fire." *Construction and Building materials*, 23, 3546–3555.

Fellinger J. (2005). "Shear and anchorage behaviour of fire exposed hollow core slabs." *Structural Concrete*, 6(4), 172–179.

Ferretti D., Iori I. and Morini M. (2002). *Stability of Structures - The Case of Structures in Reinforced Concrete (in italian)*. McGraw-Hill, Italy.

fib (2013). *Model Code for Concrete Structures 2010*.

Franssen J. M. (1993). "Thermal elongation of concrete during heating up to 700Â°C and cooling; Stress-strain relationship of Tempcore steel after heating up to 650Â°C and cooling." *Report*, University of LiÃ¨ge, LiÃ¨ge (Belgium).

Gales J., Hartin K. and Bisby L. (2016). *Structural Fire Performance of Contemporary Post-tensioned Concrete Construction*. SpringerBriefs in Fire.

Galvez F., Atienza J. M. and Elices M. (2011). "Behavior of steel prestressing wires under extreme conditions of strain rate and temperature." *Structural Concrete*, 12(4), 255–261.

Gao W., Dai J. and Teng J. (2017). "Fire Resistance of RC Beams under design fire exposure." *Magazine of Concrete Research*, 69(8), 402–423.

Gao W., Dai J., Teng J. and Chen G. (2013). "Finite Element Modeling of Reinforced Concrete Beams Exposed to Fire." *Engineering Structures*, 52, 488–501.

Gardner L., Bu Y., Francis P., Baddoo N. R., Cashell K. A. and McCann F. (2016). "Elevated temperature material properties of stainless-steel reinforcing bar." *Construction and Building Materials*, 114, 977–997.

Gernay T. (2019). "Fire resistance and burnout resistance of reinforced concrete columns." *Fire Safety Journal*, 104, 67–78.

Gernay T. and Dimia M. S. (2012). "Structural behaviour of concrete columns under natural fires." *Engineering computations*, 30(6), 854–872.

Gernay T. and Franssen J. (2012). "A Formulation of the Eurocode 2 Concrete Model at Elevated Temperature That Includes an Explicit Term for Transient Creep." *Fire Safety Journal*, 51, 1–9.

Gernay T. and Franssen J. (2015). "A performance indicator for structures under natural fire." *Engineering Structures*, 100, 94–103.

Ghali A. and Favre R. (1994). *Concrete Structures: Stresses and Deformations*. E & FN Spon, second edition.

Guo Z. and Shi X., eds. (2011). Butterworth-Heinemann, Boston.

Gustaferro A. (1973). "Design of Prestressed Concrete for Fire Resistance." *Journal of Prestressed Concrete Institute*, 18(6), 102–116.

Gustaferro A. and Martin L. (1989). *Design for Fire Resistance of Precast Prestressed Concrete*. Prestressed Concrete Institute, second edition.

Harmathy T. (1993). *Fire safety design and concrete*. Concrete design and construction series. UK: Longman.

Harmathy T. Z. (1968). "Determining the Temperature History of Concrete Constructions Following Fire Exposure." *Journal of the American Concrete Institute*, 65(11), 959–964.

Harmathy T. Z. and Allen L. W. (1973). "Thermal Properties of Selected Masonry Unit Concretes." *Journal of the American Concrete Institute*, 70(2), 132–142.

Hass R. (1986). "Practical Rules for the Design of Reinforced Concrete and Composite Columns Submitted to Fire." *Technical report*.

Hassen S. and Colina H. (2006). "Transient thermal creep of concrete in accidental conditions at temperatures up to 400C." *Magazine of Concrete Research*, 58, 201–208.

He Z. and Song Y. (2009). "Mechanical Behavior of Normal Concrete under Triaxial Compression after High Temperature." *Engineering Mechanics*, 26(10).

He Z. and Song Y. (2010). "Multiaxial tensile-compressive strengths and failure criterion of plain high-performance concrete before and after high temperatures." *Construction and Building Materials*, 24, 498–504.

He Z. and Song Y. (2016). "Failure Mode and Constituve Model of Plain High-Strength High-Performance Concrete under Biaxial Compression after Exposure to High Temperature." *Acta Mechanica Solida Sinica*, 21(2), 149–159.

Hertz K. "Analyses of prestressed concrete structures exposed to fire." *Report 174*, Institute of Building Design.

Hou X., Kodur V. and Zheng W. (2014). "Factors Governing the Fire Response of Bonded Prestressed Concrete Continuous Beams." *Materials and Structures*, 48(9), 2885–2900.

Huang S. and Burgess I. (2012). "Effect of transient strain on strength of concrete and CFT columns in fire - Part II: Simplified and numerical modelling." *Engineering Structures*, 44, 389–399.

Huang Z., Burgess I. and Plank R. (2009). "Three-Dimensional Analysis of Reinforced ConcreteBeam-Column Structures in Fire." *Journal of Structural Engineering*, 135(10), 1201–1212.

Im S., Nishiyama M. and Tani M. (2010). "Mechanical properties of prestressing steel at high temperature." *3rd fib International Congress*. 1–12.

Kalaba N., Kodur V., Agrawal A. and Bamonte P. (2018). "Structural Behaviour of R/C Structures in Fire." *10th International Conference of Structures in Fire*, Belfast (UK). 139–146.

Khoury G. A., Grainger B. N. and Sullivan P. J. E. (1985). "Transient Thermal Strain of Concrete: Literature Review, Conditions within Specimen and Behaviour of Individual Constituents." *Magazine of Concrete Research*, 37(132), 131–144.

Khoury G. A., Grainger B. N. and Sullivan P. J. E. (1986). "Strain of Concrete during First Cooling from 600C under Load." *Magazine of Concrete Research*, 38(134), 3–12.

Klingsch E., Frangi A. and Fontana M. (2009). "Experimental Analysis of Concrete Strength at High Temperatures and after Cooling." *Acta Polytecnica*, 49(1), 34–38.

Kodur V. and Agrawal A. (2016). "Critical factors governing the residual response of reinforced concrete beams exposed to fire." *Fire Technology*, 52(4), 967–993.

Kodur V. and Dwaikat M. (2007). "Performance-based fire safety design of reinforced concrete beams." *Journal of Fire Protection Engineering*, 17(4), 293–320.

Kodur V. and Dwaikat M. (2008). "A numerical model for predicting the fire resistance of reinforced concrete beams." *Cement and Concrete Composites*, 30, 431–443.

Kodur V., Dwaikat M. and Fike R. (2003). "An Approach for Evaluating the Residual Strengthof Fire-Exposed RC Beams." *Structural Engineering and Mechanics*, 16(6), 695–712.

Kodur V., Hibner D. and Agrawal A. (2017). "Residual response of reinforced concrete columns exposed to design fires." *Proceedings of the 6th International Workshop on Performance, Protection and Strengthening of Structures under Extreme Loading*, Guangzhou (Canton), China. 574–581.

Kodur V., Raut N., Mao X. and Khaliq W. (2013). "Simplified approach for evaluating residual strength of fire-exposed reinforced concrete columns." *Materials and Structures*, 46, 2059–2075.

Kodur V. and Shakya A. (2014). "Modeling the Response of Precast, Prestressed Concrete Hollow-Core Slabs Exposed to Fire." *Prestressed Concrete Institute Journal*, 59(3), 78–94.

Kordina K., Ehm C. and Schneider U. (1986). "Effects of Biaxial Loading on the High Temperature Behaviour of Concrete." *Fire Safety Science Proceedings of the First International Symposium*.

Kowalski R. (2010). "Mechanical Properties of Concrete Subjected to High Temperature." *Architecture Civil Engineering Environment*.

Kumar A. and Kumar V. (2003). "Behavior of RCC Beams after Exposure to Elevated Temperatures." *IE Journal*, 84, 165–170.

Lee J. and Fenves G. (1998). "Plastic-damage model for Cyclic Loading of Concrete Structures." *Journal of Engineering Mechanics*, 124(8), 892–900.

Lie T. and Irwin R. (1988). "Evaluation of fire resistance of reinforced concrete columns with rectangular cross-sections." *Internal report 601*, National Research Council Canada. Institute for Research in Construction.

Lie T. and Irwin R. (1990). "Evaliation of fire resistance of einforced cncrete columns with rectangular cross-sections." *Materials and Structures*, 21, 21–32.

LoMonte F., Kalaba N. and Bamonte P. (2017). "On the extension of a plastic-damage model to high temperature and fire." *Proceedings of IFireSS, Ed. Nigro E. and Bilotta A.- 2nd International Fire Safety Symposium*. 703–710.

Lu L., Yuan Y., Caspeele R. and Taerwe L. (2015). "Influencing Factors for Fire performance of simply supported RC beams with implicit and explicit transient creep strain material models." *Fire Safety Journal*, 73, 29–36.

Lubliner J., Oliver J., Oller S. and Onate E. (1989). "A plastic-damage model for Concrete." *International Journal of Solids and Structures*, 25, 299–329.

MacLean J. (2018). "The Structural Response of Reinforced Concrete Columns During and After Exposure to Non-Uniform Heating and Cooling Regimes," PhD thesis, University of Edinburgh.

Malerba P. (1998). *Analisi limite e non lineare di strutture in calcestruzzo armato: techniche di calcolo manuale ed automatico*. International Centre for Mechanical Sciences CISM, Udine, Italy.

Malhotra H. L. (1956). "The Effect of Temperature on the Compressive Strength of Concrete." *Magazine of Concrete Research*, 8(23), 85–94.

Mindeguia J. C., Hager I., Pimienta P., CarrÃ© H. and LaBorderie C. (2013). "Parametric Study of Transient thermal strain of ordinary and high-performance concrete." *Cement and Concrete Research*, 48, 40–52.

Moetaz M. E., Ahmed R., Ahmed A. and Shadia E. (1996). "Effect of Fire on Flexural Behaviour f RC Beams." *Construction and Building Materials*, 10(2), 147–150.

Mohamed G. and Salah M. (2012). "Analysis of Collapse for Concrete Columns During and After the Cooling Phase of a Fire." *XXXe Recontres AUGC-IBPSA*, Chambery, Savoie (France),.

Mohandes F. E. and Vecchio F. (2016). "Reliability of Temperature-Dependent Models for Analysis of Reinforced Concrete Members Subjected to Fire." *ACI Structural Journal*, 113(3), 481–490.

Naus D. (2005). "The Effect of Elevated Temperature on Concrete Materials and Structures." *Report No. NRC Fin No. Y6741*, U.S. Nuclear Commision, Oak Ridge, TN, USA.

Neves I. C., Rodrigues J. P. C. and Padua L. A. D. (1996). "Mechanical Properties of Reinforcing and Prestressing Steel After Heating." *Journal of Materials in Civil Engineering*, 8(4), 189–194.

Nielsen C., Pearce C. J. and Bicanic N. (2002). "Theoretical model of high temperature effects on uniaxial concrete member under elastic restraint." *Magazine of Concrete Research*, 54, 239–249.

Ozbolt J., Bosnjak J., Periskic G. and Sharma A. (2014). "3D numerical analysis of reinforced concrete beams exposed to elevated temperatures." *Engineering Structures*, 58, 166–174.

Pankaj P. (1990). "Finite Element Analysis in Strain Softening and Localisation Problem," PhD thesis, University of Wales.

Raut N. and Kodur V. (2011). "Response of High-Strength Concrete Columns under Design Fire Exposure." *Journal of Structural Fire Engineering*, 137(1), 69–79.

RILEM (1985). *Properties of Materials at High Temperatures: Concrete*. Department of Civil Engineering, University of Kassel, Kassel (Germany).

RILEM T. (1998). "129-MHT: test methods for mechanical properties of concrete at high temperature. Part 7: Transient creep for service and accident conditions." *Materials and Structures*, 31, 290–295.

RILEM T. (2000). "129-MHT: test methods for mechanical properties of concrete at high temperature. Part 8: Steady-state creep and creep recovery for service and accident conditions." *Materials and Structures*, 33, 6–13.

Sarshar R. and Khoury G. A. (1993). "Material and environmental factors influencing the compressive strength of unsealed cement paste and concrete at high telperatures." *Magazine of Concrete Research*, 45, 51–61.

Schneider U. (1988). "Concrete et high temperature - a general review." *Fire Safety Journal*, 13(1), 55–68.

Schneider U., Schneider M. and Franssen J. (2008). "Consideration of nonlinear creep strain of siliceous concrete on calculation of mechanical strain under transient temperature as a function of load history." *Proceedings of the 5th International Conference on Structures in Fire*, Singapore. 463–476.

Stefan R., Sura J., Prochazka J., Kohoutkova A. and Wald F. (2019). "Numerical Investigation of Slender Reinforced Concrete and Steel-Concrete Composite Columns at Normal Temperatures Using Sectional Analysis and Moment-Curvature Approach." *Engineering Structures*, 190, 285–305.

Stern-Gottfried J., Rein G., Bisby L. and Torero J. (2010). "Experimental review of homogeneous temperature assumption in post-flashover compartment fires." *Fire Safety Journal*, 45(4), 249–261.

Terro M. J. (1998). "Numerical Modeling of the Behavior of Concrete Structures in Fire." *ACI Structural Journal*, 95(2), 183–193.

Thienel K. C. and Rostasy F. (1995). "Strength of concrete subjected to high temperature and biaxial stress: Experiments and modeling." *Materials and Structures*, 28, 575 – 581.

Torelli G., Mandal P., Gillie M. and Tran V. X. (2016). "Concrete strains under transient thermal conditions: A state-of-the-art review." *Engineering Structures*, 127, 172–188.

Toric N., Boko I., Juradin S. and Baloevic G. (2014). "Post-fire Reduction of Concrete's Mechanical Properties and its Impact on Residual Load Capacity." *Proceedings of the 8th International Conference on Structures in Fire*, Shanghai (China). 1171–1178.

Troxell G. (1962). "Fire Resistance of Prestressed Concrete." *ACI Special Publication*, 5, 59–86.

Venanzi I., Breccolotti M., D'Alessandro A. and Materazzi A. (2014). "Fire Performance Assessment of HPLWC Hollow-Core Slabs through Full-Scale Furnace Testing." *Fire Safety Journal*, 69, 12–22.

Wickstrom U. (1986). *A very simple method for estimating temperatures, Fire-Exposed Structures: a New Technology to Reduce Fire Losses and Costs*. Elsevier Applied Science, London (UK).

Wu B., Li Y.-H. and Chen S.-L. (2010). "Effect of Heating and Cooling on Axially Restrained RC Columns with Special-Shaped Cross Section." *Fire Technology*, 46, 231–249.

Wu B. and Lu J. (2009). "A numerical Study on the Behaviour of Restrained RC Beams at Elevated Temperatures." *Fire Safety Journal*, 44, 522–531.

Zhang L., Au F. T. K., Wei Y. and Li J. (2015). "Mechanical properties of prestressing steel and after fire." *Magazine of Concrete Research*, 1–10.